NOT FOR PUBLICATION

See note overleaf

AAEC/PR40-P

INDC(AUL)-22/G

AAEC/PR40-P

INDC(AUL)-22/G

XA04N2774

INIS-XA-N--162

AUSTRALIAN ATOMIC ENERGY COMMISSION

RESEARCH ESTABLISHMENT

LUCAS HEIGHTS

PROGRESS REPORT OF PHYSICS DIVISION

1st JANUARY 1974 - 31st JULY 1974

ACTING DIVISION CHIEF - MR. W. GEMMELL

NOT FOR PUBLICATION

CONTENTS

CONTENTS

CONTENTS

CONTENTS

1.1 INTRODUCTION

Details are given on the analysis of the neutron cross section data taken with the Oak Ridge Electron Linac Facility in 1972. Various codes have been developed for this analysis. In several instances interim conclusions are drawn and the basis of the analysis or the experimental method has been questioned. The detail given is greater than in previous reports as it is anticipated that final publication is still some time away. It is hoped that the detail given will prove adequate for criticism and feedback to occur. Of note are the conclusions that the 89 keV ^{40}Ca resonance is a doublet, the apparent asymmetry of several resonances as a result of multiple scattering events, the strong valence contributions to capture in silicon and zirconium and the higher values of Γ_γ for ^{27}Al, than quoted in BNL325. In general, this work confirms earlier studies, but provides both the increased detail and higher resolution necessary for a better understanding of neutron capture and more accurate data for both cross sections and resonance parameters.

The study of capture gamma rays following capture of keV neutrons in the 111 and 113 isotopes of cadmium has enabled partial p-wave capture cross section shapes to be obtained which are in acceptable agreement with calculations.

Preliminary analysis of the anisotropy of the ^{235}U fission fragment distribution casts doubts on earlier measurements which indicated anisotropies <1 and provides support for the $\nu(E)$ conclusions concerning changes in the height of the Strutinsky barrier. Effort continues to parameterise fission product yields using three modes and to finding systematic relationships between the modes and the energy above the fission barrier.

A reactor study of MOATA type cores on the Critical Facility is now complete. A study of a variety of core couplings provided by varying the spacing between the two subcritical cores should be available soon.

The decay of neutron pulses in heavy metal assemblies had previously been found to be sensitive to changes in cross sections much less than present uncertainties in the data. The use of different source energy conditions has been used to explore this feature using the limited timescale of the experiment and the slowing down process. The inclusion of the initial source conditions of energy and time in calculations has proved difficult and some oscillations in the decay constant at long times have been neither eliminated nor resolved.

The use of the $^{7}Li(p,n)$ reaction as a source of neutrons in the above had led to an examination of its angular and angle averaged neutron spectrum using a proton recoil spectrometer. These have been compared with calculations. Very little information appears in the literature.

2.1 MOATA OPERATIONS (T. Wall)

Major use of the reactor has embraced the following:

Uranium analysis	Neutron radiography
Neutron activation analysis	Moisture content of soils
Student training	Radiation damage in transistors
Reactor noise measurements	Molecular decomposition by neutron bombardment

An operational integrated power of 17 MWh was recorded. This compares with a total reactor burnup since commissioning in 1961 of 95 MWh, of which 53 MWh have been recorded since routine 100 kW operation commenced in January 1973.

Uranium Ore Analysis

The uranium analysis service has now a fully operational rig capable of fast assay of uranium ores. A sample of 10 mℓ can be assayed to an accuracy of ±20 per cent at the 0.1 ppm U_3O_8 level, improving to ±3 per cent at 1 ppm U_3O_8 or above.

The change in the capacity of the sample bottles from 2 to 10 mℓ increased the radiation and contamination problems associated with an irradiated ore batch. A shielded area was built for ore storage and the air vent at the storage cassette entrance was fitted with a filter. The sample bottles are now also spot welded to provide a reliable containment.

Activation Analysis of Obsidian Glass

Following a request by the Department of Prehistory, ANU, 'fingerprint' neutron activation analysis has been carried out on samples of obsidian volcanic glasses collected from the west and south Pacific regions. After irradiating with a neutron dose of 2×10^{15} cm^{-2}, the samples were analysed using a germanium detector and an on-line computer system. Isotopes detected which aided in identification included ^{46}Sc, ^{59}Fe, ^{233}Pa, ^{86}Rb, ^{181}Hf, ^{182}Ta, ^{152}Eu and ^{141}Ce. The data obtained to date suggest that several of the known volcanic sources of obsidian can be labelled by this type of activation analysis, thus enabling in some instances a particular artifact to be linked back to its original material source. This should be useful in studying the trading habits of the peoples of the region.

Neutron Radiography

Studies in neutron radiography and possible industrial applications of the

technique have continued. Work has concentrated on improving methods of resolving hydrogenous material within a metal bearing objects. Examples of this are studies of the resin/metal bond in aircraft structures and seating of nylon components within automobile fuel injectors.

Isotopic Analysis Facility using Neutron Capture (J. R. Bird, I. F. Bubb, L. H. Russell)

Prompt gamma rays from capture of a thermal neutron beam in~10-100 g samples of wheat have been detected with a 40 cm^3 (7 per cent) Ge(Li) detector. Automated data analysis is used to provide a versatile technique for determination of those elements with sufficiently high capture cross sections and branching ratios. Figure 2.1 shows how the method is used to observe the presence of chlorine in wheat. The sample size was 21.5 g and chlorine concentrations of the order of 50 ppm can be determined.

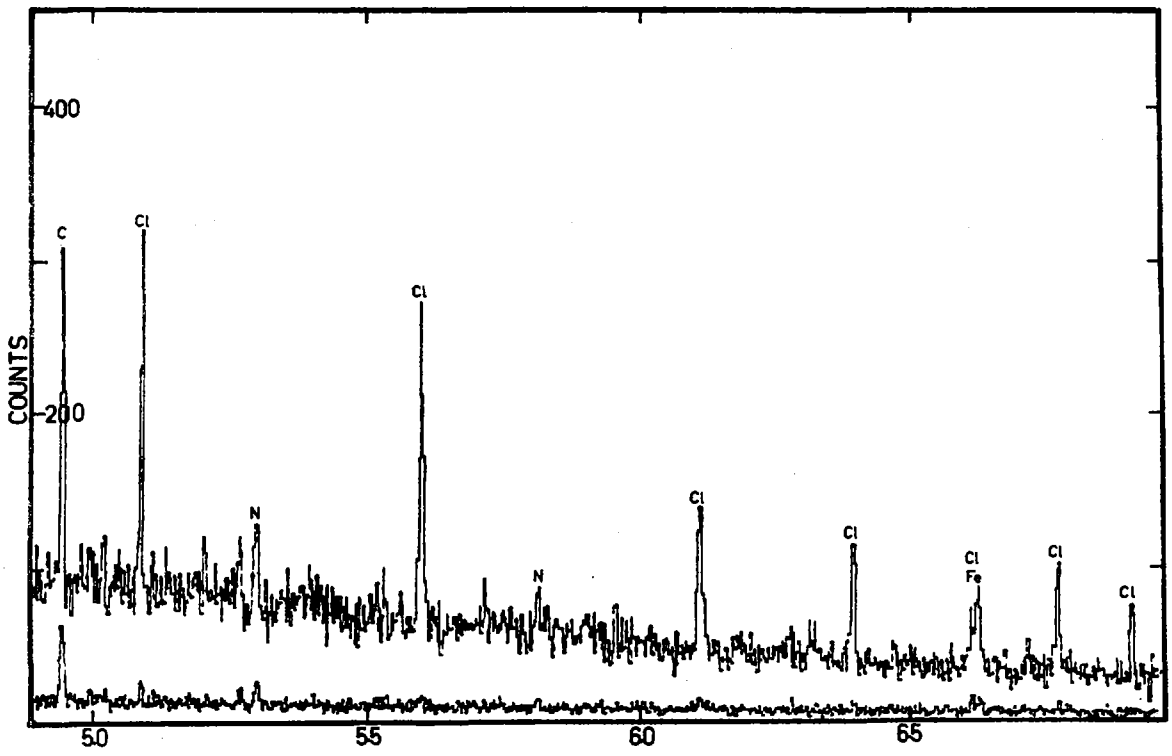

FIGURE 2.1 Prompt gamma ray spectrum from wheat sample showing isotopes identified

2.2 CRITICAL FACILITY OPERATIONS (J. W. Connolly)

The MOATA mockup program ended in June. Four mockup cores were constructed and operated during this program and provided valuable operational experience with the facility. The confidence gained in the reliability of the nucleonics equipment during the program, when very extensive start up checks were performed, has led to the adoption of much simplified start up procedures with a consequent increase in available operational time.

Modifications completed during the period include installation of individual rod scram circuits and alteration of the safety rod drive circuits to permit simultaneous drive of all safety rods to the position of maximum core reactivity. A test rig is in course of construction which will enable the correct functioning of rod drives and rod scram times to be ascertained, prior to mounting on the machine itself.

Considerable effort has been directed to discussion of the Critical Facility Safety Documentation with the Commission's Licensing and Regulatory Bureau.

Critical Facility Experiments (J. R. Harries)

The 'mockup' on MOATA type reactor assemblies was continued to enable measurements of coupled core properties and the prompt neutron decay constants to be made on a range of core geometries. In the original assembly, M1, the core slabs were spaced 450 mm apart; this was increased to 600 mm in the following assembly, M2. Two further critical assemblies have now been constructed; assembly M3 with a spacing of 800 mm, and assembly M4 with a spacing of 450 mm, but with a different fuel arrangement to core M1.

Graphite was used as the coupling material for each assembly, but polythene, lead-cadmium and steel strips were variously used to change the absorption and scattering properties of the coupling region for assembly M4. For each coupling region composition, the prompt neutron decay constant was determined from the correlograms of the neutron noise and the corresponding neutron flux distribution was measured by the activation of manganese foils.

The cross correlogram between the neutron noise in each core slab was measured to determine the coupling between the slabs and the time delays between the two core tanks. Computer programs have been written to fit the data by least squares technique to the difference of two exponentials. Further analysis is proceeding to fit the data to a two node reactor model with a time delay for neutrons travelling between the two slabs and allowing for a

flux tilt across the assembly. Such a model appears to reproduce the main features of the experimental correlograms.

The coupling coefficient of assembly M4 was also measured by observing the flux tilt produced when a rod close to one slab was scrammed. The rod drop experiments are being analysed using the two node model applying a correction for the difference in core neutron flux distributions before and after the scram.

The temperature coefficient of reactivity of the top reflector of assembly M4 has been measured by replacing one quarter of the top polythene reflector with water and determining the changes in critical setting as the water temperature is increased. The temperature coefficient so determined is $\sim+1.3 \times 10^{-6}\ ^{o}C^{-1}$. However, the total worth of this part reflector is only 10^{-3} $\delta k/k$, whereas for a fully water reflected system the reflector is worth $\sim 10^{-1}$ $\delta k/k$. If the magnitude of the temperature coefficient of the reflector is presumed proportional to the worth of the reflector, a totally water reflected system would have a temperature coefficient of $\sim+13 \times 10^{-5}\ ^{o}C^{-1}$, not inconsistent with values calculated for the SPERT studies.

Further discussion of the mockup program must await resolution of difficulties associated with trying to represent the reactor in two dimensional calculations.

Critical Facility - Future Experiments (D. B. McCulloch)

It is intended that the next assembly (FC1) will be a simple ^{235}U-graphite configuration with the 'hardest' neutron spectrum which can be achieved and a reasonable central volume with the fuel currently available. It will be used to enable fast reactor core physics measurement techniques to be explored and developed.

The fuel is in the form of 93 $^{w}/o$ enriched ^{235}U metal strips, each 0.076 x 50.8 x 400 mm. These will be inserted in slots machined in one surface of graphite blocks each 50 x 100 x 800 mm. The resulting core region will approximate a cube of 800 mm side, and be fully graphite reflected. Preliminary calculations indicate that 5 fuel strips per slot ($C:^{235}U \simeq 450:1$) in such an assembly will give a critical configuration within the limits of the available fuel.

Detailed calculations, using the AUS code with the GYMEA cross section library, have been performed to obtain estimates of the critical mass, temperature coefficients, mean neutron lifetime, worth of the control rods and their associated 'channels', flux and reaction rate distributions, etc. An appropriate graphite structure for the assembly is now being constructed on the critical facility tables.

2.3 PULSED NEUTRON AND SPECTRUM MEASUREMENTS (I. Ritchie, M. Rainbow, S. Whittlestone, A. Rose)

An earlier series of experiments and calculations has shown that the decay parameters measured in pulsed neutron experiments in heavy metal assemblies (e.g. Th, U) are sensitive to changes in neutron cross sections smaller than the present level of uncertainty in these cross sections, thus providing an alternative method of evaluating the accuracy of data for fast reactor calculations. Such alternative integral methods are useful in view of the long-standing systematic errors which persist in the measurement of microscopic data.

The first series of experiments was carried out using a high energy source (~2 MeV) and because of the time range covered and the slowing down process of the neutrons as a function of time, probed effectively the energy range from about 2 MeV to 500 keV. By using different source conditions these experiments have been extended to cover most of the energy range of interest in fast reactors.

Attention has also been given to extending the integral measurements to measurements of the neutron energy spectrum in the pulsed assembly. Work has also continued on the more general problem of assessing methods of measuring neutron energy spectra in a fast reactor environment.

Pulsed Integral Experiments in Thorium

An extensive series of time and space dependent ^{239}Pu and ^{235}U reaction rates were made with the following source conditions.

(i) A thick lithium target using the Li(p,n) reaction at 2.3 MeV with a pulse width of ~10 ns; source energy ~100 to 400 keV.

(ii) A thick lithium target using the Li(p,n) reaction at 2.8 MeV with a pulse width of ~10 ns; source energy 300 to 700 keV.

(iii) A thick beryllium target using the Be(d,n) reaction at 2.8 MeV with a pulse width of ~200 ns; source energy ~2 keV.

Analysis of the data obtained with source conditions (i) and (ii) is well advanced and some interesting results have been produced. The 'instantaneous decay constants' of the ^{239}Pu and ^{235}U reaction rates measured with source (ii) (figure 2.2) vary quite markedly with time. This behaviour is unusual, but may be related to the small oscillations noted at long times after the pulse in previous experiments with a more energetic source. Possible but speculative explanations relate this result to the effect of the inelastic levels in thorium on the slowing down spectrum or to the higher proportion than previously

thought of low energy neutrons (~100 keV) from the thick target Li(p,n) neutron source.

Comparison with Multigroup Calculations

The time dependent diffusion theory codes TENDS and TIMEX, essentially unchanged since 1968, have been updated to take advantage of the improved central computer and Dataway facilities. Both codes can now handle a source which is quite arbitrarily distributed in time. This enables the experimental neutron pulse profile to be accurately represented in the calculations.

Work has begun on a comprehensive study of the sensitivity of parameters measured in pulsed neutron experiments in ^{232}Th and ^{238}U assemblies to nuclear data for these materials.

Particular attention will be given to the inelastic scattering cross sections and the use of tailored source spectra available from the Li(p,n) and Be(d,n) reactions. Experimental results are being compared with diffusion theory calculations utilising a revised data set which takes account of resonance self shielding in the unresolved resonance region. Unlike the previous experiments with a high energy source (~2 MeV), where so few neutrons reached the unresolved resonance region (~5 to 50 keV) in the time interval covered by the experiments that accurate data for this region was unnecessary, the softer spectra used in the present series of experiments meant that a significant number of neutrons reached the unresolved resonance region and that more accurate data is required in the calculations. The calculations also require a knowledge of the neutron energy spectrum of the thick target Li(p,n) source. This has been calculated from a combination of theoretical and measured angular distributions for the $^{6}Li(p,n)^{7}Be$ and $^{6}Li(p,n)^{7}B^{*}$ reactions. The angle integrated spectrum for a proton energy of 2.38 MeV is shown in figure 2.3.

Inelastic Scattering in Time Dependent Slowing Down

When a neutron with energy just greater than an inelastic level is inelastically scattered, it is left with an energy small compared with its initial energy. The closer its initial energy is to that of the inelastic level, the lower will be its final energy. Since its velocity will also be reduced, it follows that its contribution to the flux will be reduced, although its contribution to the neutron density will remain the same. It then seems reasonable to expect a rapid decrease in the flux and an increase in the decay rate of the flux as the average neutron energy approaches that of an inelastic level. The magnitude of the change will clearly depend on the magnitude of the

inelastic cross sections in the region of the inelastic level and the magnitude of other competing processes. It is of interest to see whether the marked change in the measured decay rate noted when using the low energy Li(p,n) source can be ascribed to this and to estimate the dependence of the effect on the inelastic cross section.

A simple model has been constructed to describe the time dependent slowing down spectrum in the presence of elastic and inelastic scattering. Increased decay rates of the form found in the experiment can be achieved by judicious choice of scattering cross sections, but it would appear at this stage that the effect would require scattering properties which are unreasonably different from those of thorium. More sophisticated calculations are required to complete the investigation.

Energy Spectrum Measurements in Heavy Metal Assemblies

The high efficiency, fast timing resolution and good gamma ray discrimination properties of the organic scintillator NE213, give prospects of a small detector that would permit measurement of time dependent spectra inside heavy metal assemblies, using a proton recoil technique. This method would augment the classical pulsed time of flight technique for spectrum measurement which measures the steady state spectrum, but contains less information than the time dependent spectrum. Major effort has been directed towards developing the detector and the relevant computer codes required to convert the measured pulse height spectra to neutron energy spectra.

Detector Development

Some scintillators have the property that neutrons excite a higher proportion of slowly decaying (~0.5 μs) molecular energy levels than gamma rays. NE213 is one of these. Measurement of the scintillation decay time of a pulse indicates whether the initiating event was a neutron or a gamma. Any impurities, especially electron donors such as oxygen, shorten the lifetimes of the slow component, reducing neutron-gamma discrimination.

The system designed to fill the liquid scintillation chamber easily without contaminating the liquid with oxygen, has proved successful as may be gathered from the pulse shape discrimination performance shown in figure 2.4. Careful optimisation of photomultiplier operating conditions has permitted observation of neutrons in the range 10 keV to 10 MeV.

Experience with large (5 cm diameter) scintillation chambers has led to a design for a prototype miniature (~1 cm diameter) detector for insertion into the heavy metal assembly.

Pulse Height Spectrum Analysis Code

Specifications have been worked out for a code which accepts pulse height data from the detector and uses pulse height profiles for monoenergetic neutrons to generate the neutron energy spectrum. A code developed for analysing pulse height spectra from gas proportional proton recoil counters has been modified by D. Lang to do this. Experimental data is available for testing the code.

Determination of Pulse Height Profiles for Monoenergetic Neutrons

Given sufficient data on neutron cross sections, scintillator response to charged particles and photomultipliers, it is possible to calculate the pulse height profile corresponding to monoenergetic neutrons. Alternatively, it is possible to measure these responses experimentally using neutron beams of known energy. However, in practice, since there are gaps in the data required for the calculation and measurement requires a knowledge of the relative intensity of the neutron beams, it is better to employ a combination of calculation and experiment.

The response functions for monoenergetic neutrons can be calculated from a local code which requires as input, data on the photomultiplier performance and the response of the scintillator to charged particles of different energies. The resolution of the photomultiplier used has been shown to be a well defined function of light pulse input, and the response of the scintillator to gamma rays can be used to calibrate a scale of light output as a function of electron energy. It remains to measure the response of the scintillator to protons and carbon nuclei. An extensive review of the literature on scintillator responses to protons and carbon nuclei has revealed poor accuracy and disagreement between different authors. Experimental data has been collected for NE102 and NE213 detectors using a pulsed time of flight technique to produce neutrons of well defined energy. The data will provide a test for the code and, if the code is satisfactory, allow calculation of responses over the range 10 keV to 1 MeV.

Time of Flight Analysis Code

A code has been commissioned which converts time of flight spectra to neutron energy spectra. An essential part of this code is the manipulation of the experimental neutron and beam pulse time distribution to extract the neutron time of flight distribution corresponding to an infinitely narrow pulsed source.

Figure 2.5 shows an input time distribution and the time of flight spectrum obtained from it.

Proton Recoil Spectrometry

The neutron energy spectrum from a thick lithium target bombarded with 2.9 MeV protons covers the range 0 to 1.2 MeV which is very close to the effective range of gas proportional proton recoil spectrometers used to measure neutron energy spectra in fast reactors. The source has few gamma rays and none of the high energy neutrons present in reactor spectra so that measurements of the source provide a good and straightforward test to assess the accuracy and reliability of the proton recoil method.

Angular measurements of the distribution of neutrons from Li(p,n) reaction in thick lithium metal were made. A new target assembly was installed on the elevated facility beam line which made it possible to combine angular measurements (with thick metal target) and calibration and response function measurements (with thin metal target) without the problems of changing beam lines, etc.

With this thick target, repeat measurements were made of angular distributions from the Li(p,n) reaction under the following conditions.

$0.04 \text{ MeV} \leq E_n \leq 0.2 \text{ MeV}$ with filling of 1 atm H_2

$0.1 \text{ MeV} \leq E_n \leq 0.6 \text{ MeV}$ with filling of 3 atm H_2

$0.4 \text{ MeV} \leq E_n \leq 1.2 \text{ MeV}$ with filling of 3 atm CH_4

It would have been preferable to use hydrogen fillings only for these measurements, but to cover the energy range to 1.2 MeV required filling the detector to a pressure of 10 atm. This was done, but problems with high voltage leakage made it simpler to use a filling of ~3 atm of CH_4.

Analysis of the data has largely been completed using the SPEC-IV code.

An intercomparison analysis reveals that repeated measurements are consistent within individual sets. Data obtained from different sets have been compared at 0° and consistency is reasonable. The different detector fillings were chosen to cover the necessary energy range with sufficient overlap between the ranges to allow normalising of the spectrum. Initial analyses indicate good agreement in the overlap region.

Calibration of the detectors has been done using either monoenergetic neutrons or small amounts (5 per cent) of nitrogen in the filling gas. The use of ^3He rather than N for calibration is preferred as only trace amounts of ^3He are required. To this end a new gas filling system has been built incorporating a mass spectrometer head. This should allow greater control in gas filling.

Detector Efficiency Calculations (E. Clayton)

One difficulty in calculating the efficiency of a neutron detector is the accurate estimation of the output pulse height for low energy protons. A survey of all available data was undertaken and has now been incorporated into the program. The code produces a resultant output spectrum and efficiency from an initial neutron beam of known energy incident on the detector. Before this can be compared directly with experimental measurements the spectrum must be folded with a function representing the photomultiplier resolution and statistics. Following J. R. Prescott (NIM 22, 1963, 256) the following resolution function has been tested.

$$R(y,y') = \left(\frac{y}{y'}\right)^{\frac{1}{2}} e^{-(y'+y)} I_1\left(2(yy')^{\frac{1}{2}}\right) \qquad \ldots(1)$$

where I_1 is a modified Bessel function of the first kind.

This relates the probability of a resultant output pulse y' given an input pulse y. The resultant spectrum is then defined by

$$c(y') = \int T(y)R(yy')dy \qquad \ldots(2)$$

where T(y) is the theoretical spectrum from the Monte Carlo calculation. The resolution function R needs a parameter relating deposited electron energy to the number of photoelectrons at the first dynode. This is measured for each photomultiplier.

Resolution folding has now been included in the code allowing direct comparison with experiment. It is anticipated that experimental measurements using an NE103 detector will be analysed shortly.

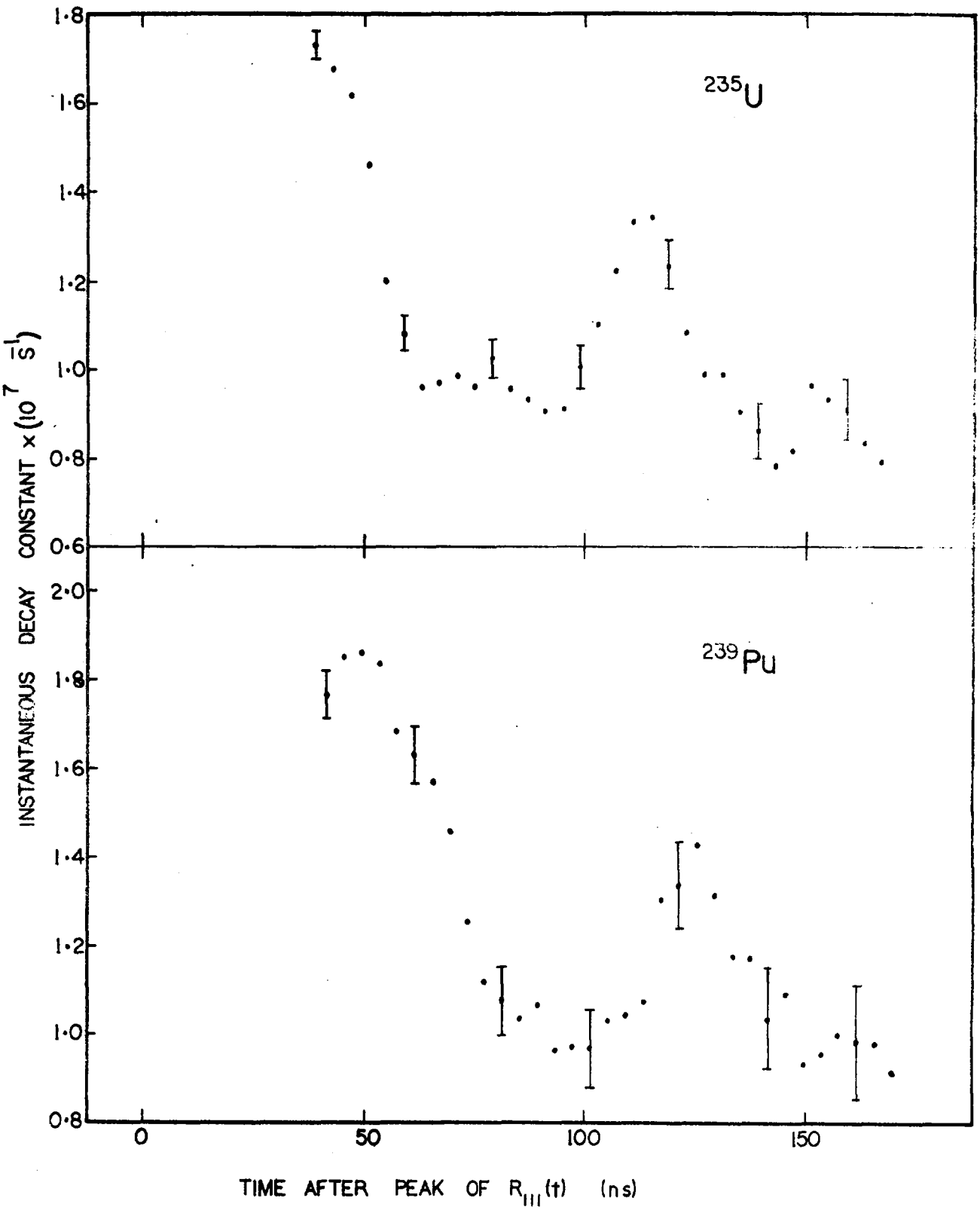

FIGURE 2.2 Instantaneous fission rate (^{235}U and ^{239}Pu) decay constants in pulsed thorium assemblies

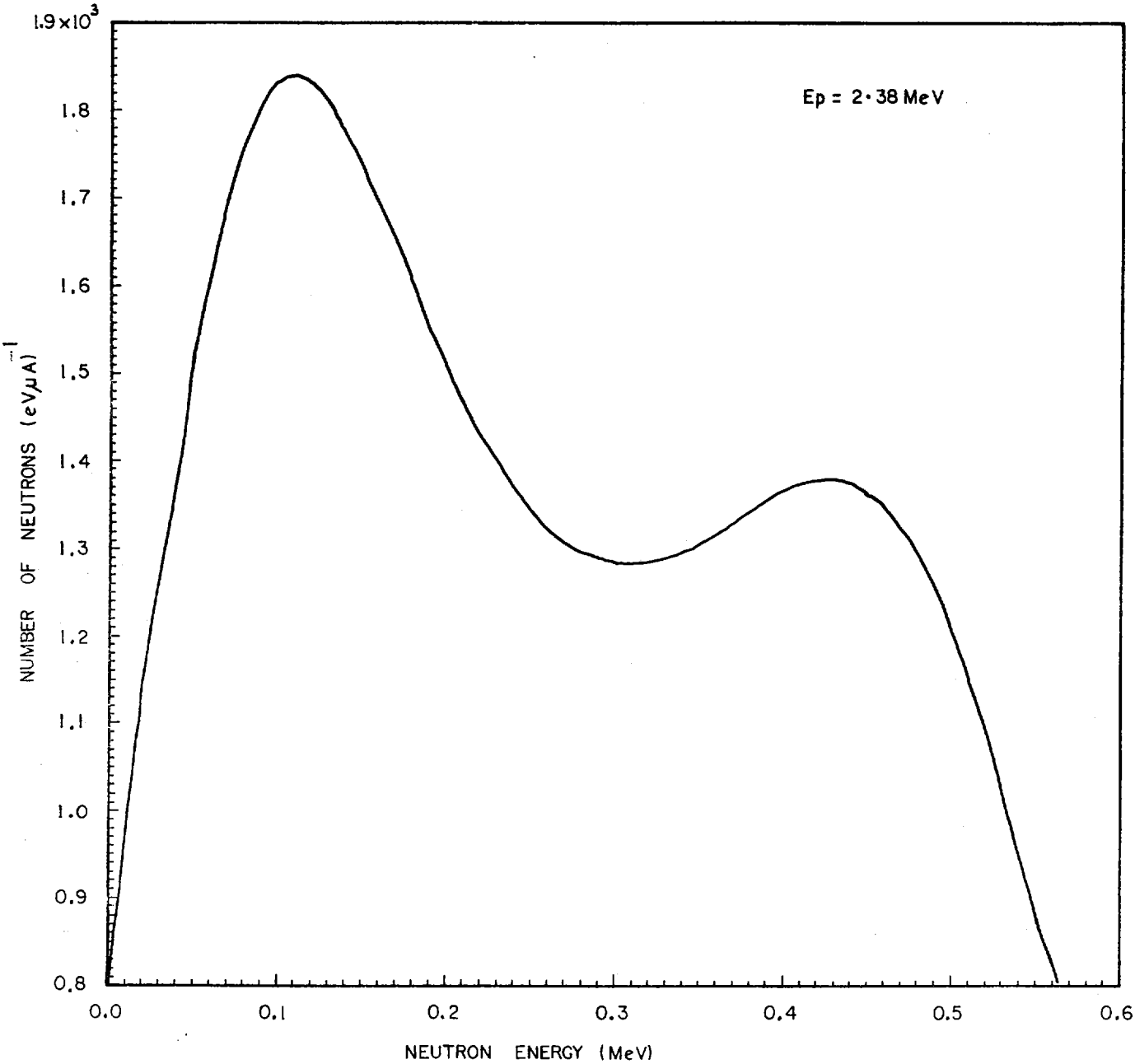

FIGURE 2.3 Angle integrated neutron spectrum from thick $^{7}Li(p,n)$ reaction at E_p = 2.38 meV

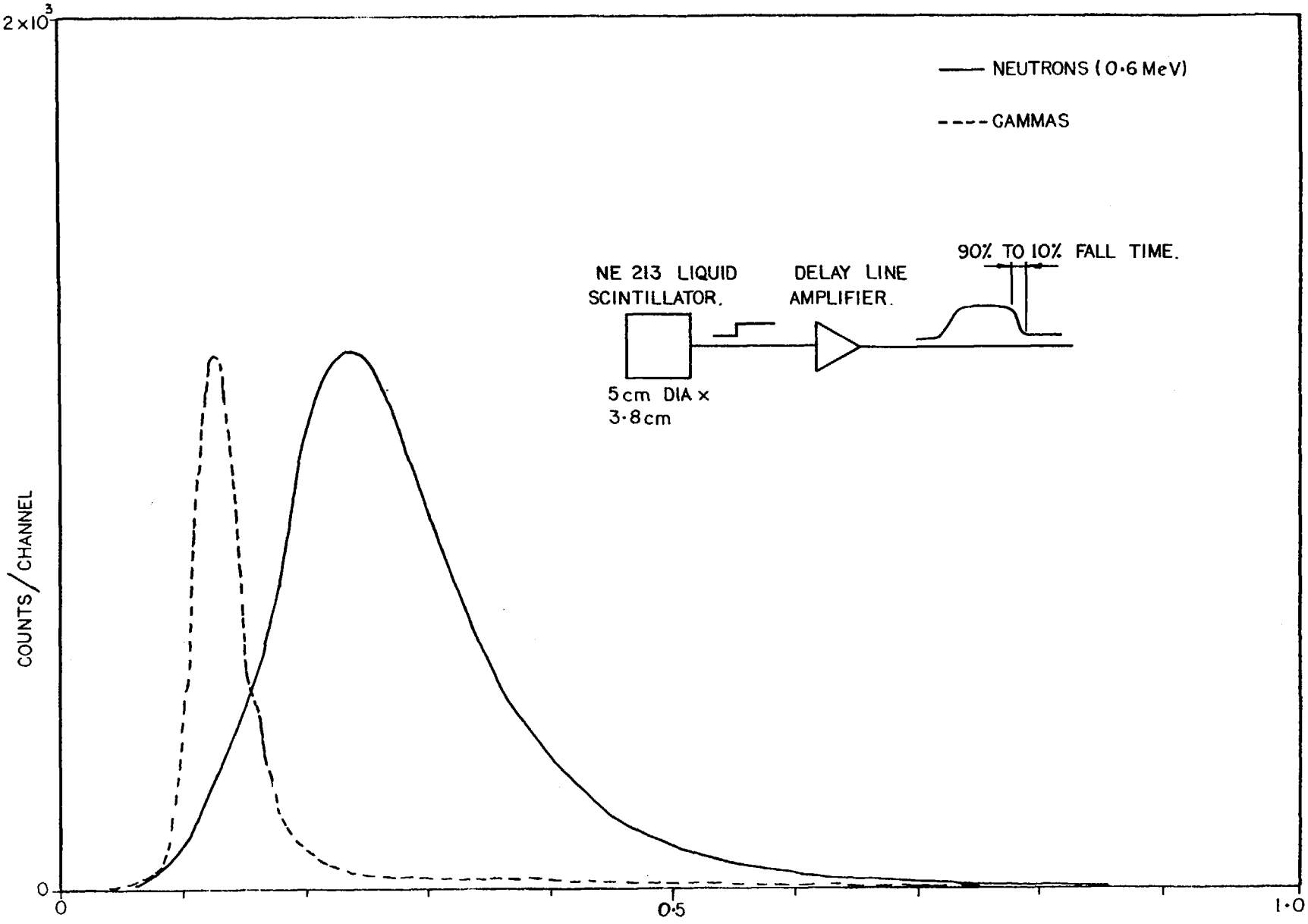

FIGURE 2.4 Distribution of decay times (90-10% pulse height) for neutrons and gamma rays in NE213 liquid scintillator

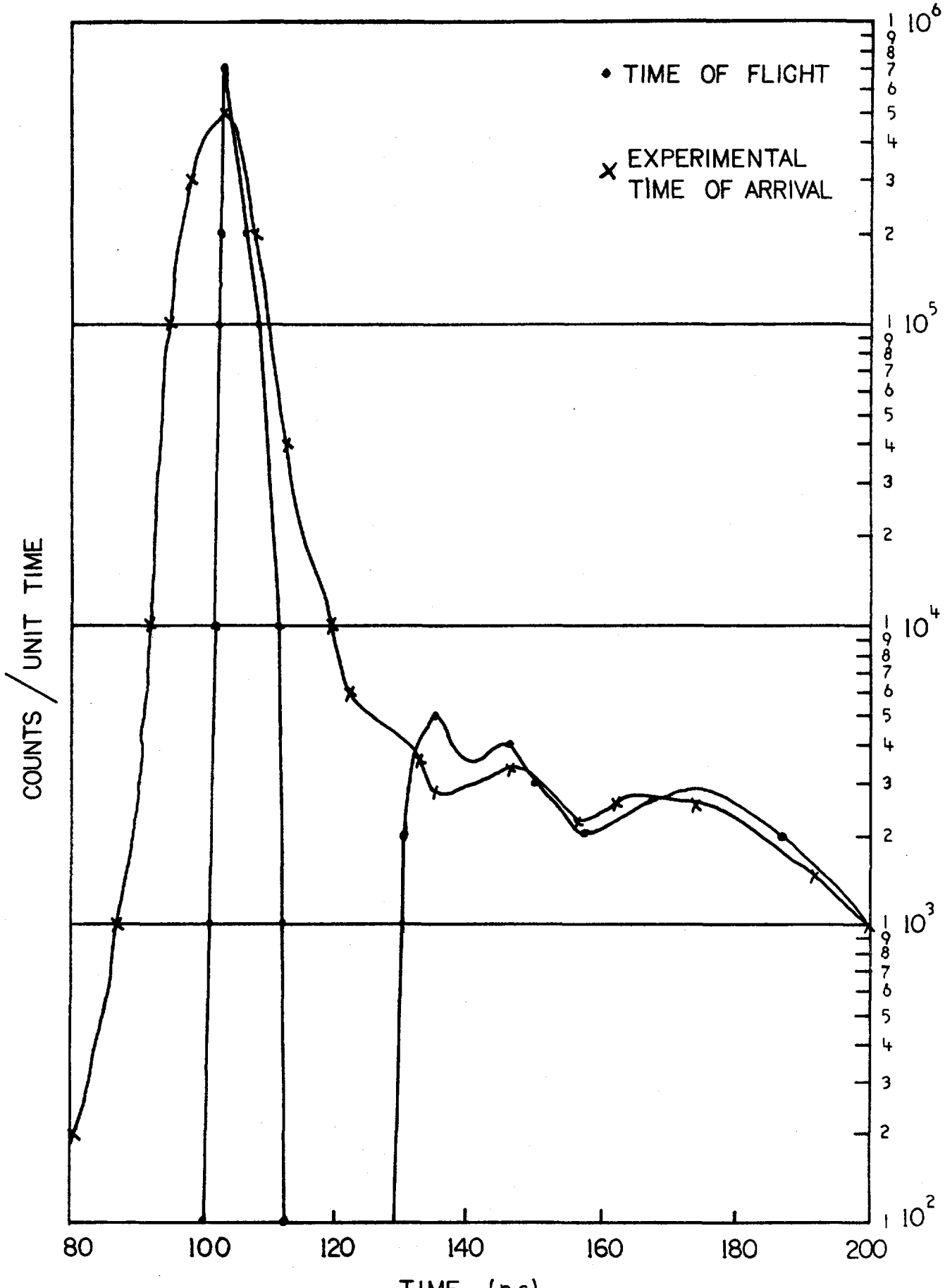

FIGURE 2.5 Neutron time and time of flight distributions for $^{7}Li(p,n)$ reaction. E_p = 2.24 MeV

2.4 SAFETY STUDIES

Blowdown (W. J. Turner, G. Trimble)

The critical flow model using Jones' slip described in the last progress report (AAEC/PR39-P) has been used to calculate the critical flow rates for the conditions of the Fauske* critical flow experiments. Good agreement was obtained as shown in figure 2.6 and the model has now been incorporated in both the OWEN-1 and NAIAD codes.

A report of this work on critical flow models is to be presented in a paper at the 5th Australasian Fluid Mechanics Conference.

The new loss of coolant code NAIAD has been extended in a number of ways:

1. The above new critical flow model has been incorporated. This has been done in the form of tables so that only insignificant extra computing time is required for problems involving critical discharge.

2. Multiflow path problems may now be solved provided no more than 9 pipes connecting at up to 10 points are involved.

3. Slip correlations, which specify the relation between the speeds of the steam and water phases in two phase flow, have been included in a new way such that it is now a relatively simple matter to add new slip relations. Four slip relations are now available to the code user: Jones, homogeneous, CISE and Beattie.**

4. The properties of water required are now obtained from tables generated from the ASTEM4A code, thus no 'fitting' of steam tables is involved. The subdivision in the present tables should be sufficient for most problems, however new tables with arbitrarily small subdivision can easily be generated if required. A similar modification has also been made to OWEN-1.

---

*Fauske, H. K. (1962) - Contribution to the theory of two-phase, one-component critical flow. ANL6633.

**Beattie, D. R. H. (1974) - Drag reduction phenomena in gas-liquid systems. Int. Conf. on Drag Reduction, Cambridge.

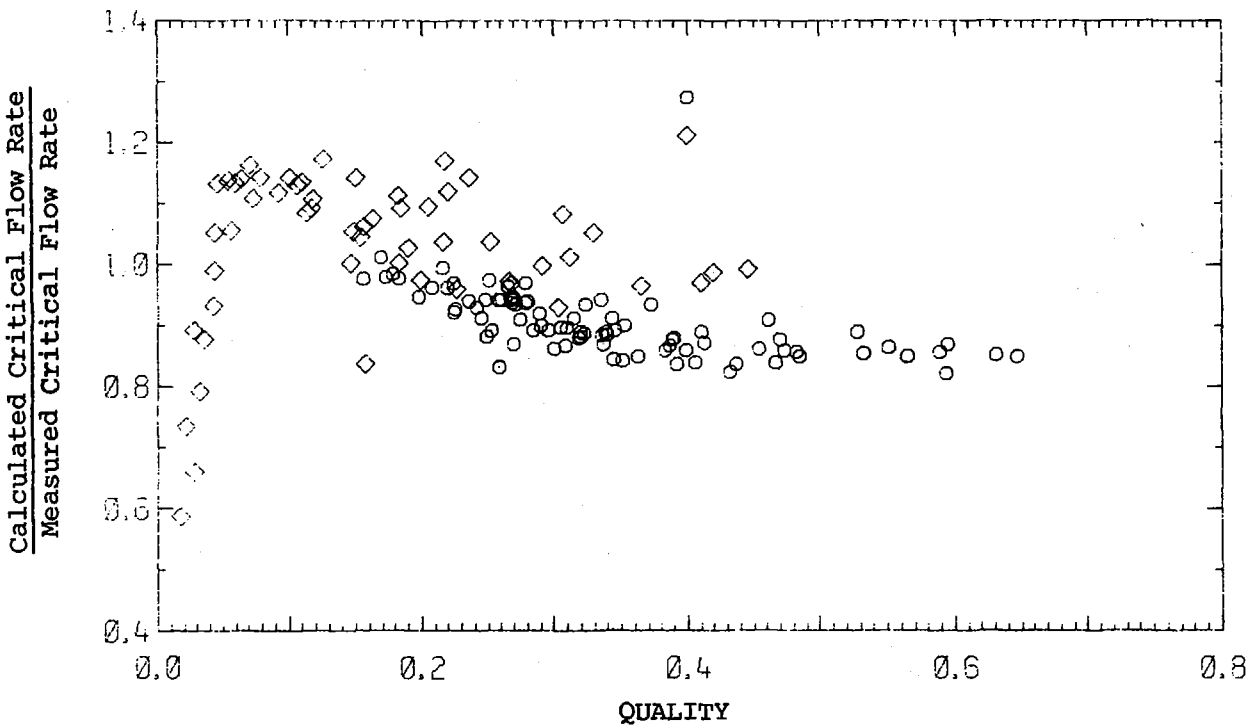

FIGURE 2.6 Comparison of measured and calculated critical flow rate as a function of water quality

5. The pipe temperature calculation and the hydraulic calculation are coupled by the surface heat transfer calculation. NAIAD, in common with all other codes, used an explicit method to calculate the surface heat transfer. This can lead to numerical instability in some problems. An implicit method has been developed and included in NAIAD. No significant additional computing is involved.

All 16 CISE (Premoli 1969) experiments have now been analysed with NAIAD, including the experiment initiated by a burst at the feeder inlet. Previously we were unable to analyse this experiment with OWEN-1 because of flow reversal at the inlet, but no problem was found using NAIAD. The agreement with experiment is only fair and further information is being obtained from Premoli about the experiments.

SPERT (J. W. Connolly)

Analysis of SPERT power transients using the ZAPP code has been extended to cases where fuel plate cladding temperatures exceed the saturation temperature of light water. The model on which this analysis is based neglects steam void formation, shutdown being produced by the collapse of the temperature distribution established in the coolant prior to boiling. This collapse is attributed to a high conductivity 'boiling' zone propagating from the clad into the coolant. Although the neglect of steam voids would not be expected to be valid at later stages of power bursts, the ZAPP calculations have reproduced the experimental data very well, which suggests steam voids may be formed after most of the energy in the burst has been released.

Figures 2.7 and 2.8 show the calculated and measured burst properties of SPERT cores B24/32 (under-moderated) and B12/64 (over-moderated). Improvements in the running time of ZAPP have permitted the analysis of very slow transients (initial inverse period $\alpha_o < 1$) which previously required a prohibitive amount of computer time. The arrows shown on some temperature data for core B24/32 indicate the magnitude of the corrections made to experimental data obtained at locations other than the core centre.

The level of agreement obtained between calculation and experiment is very pleasing, particularly since no normalisation of any kind is involved. The input to the calculations consists solely of nuclear data input to the code AUS, which generates reactivity feedback terms; these, together with material properties, then form the input to ZAPP.

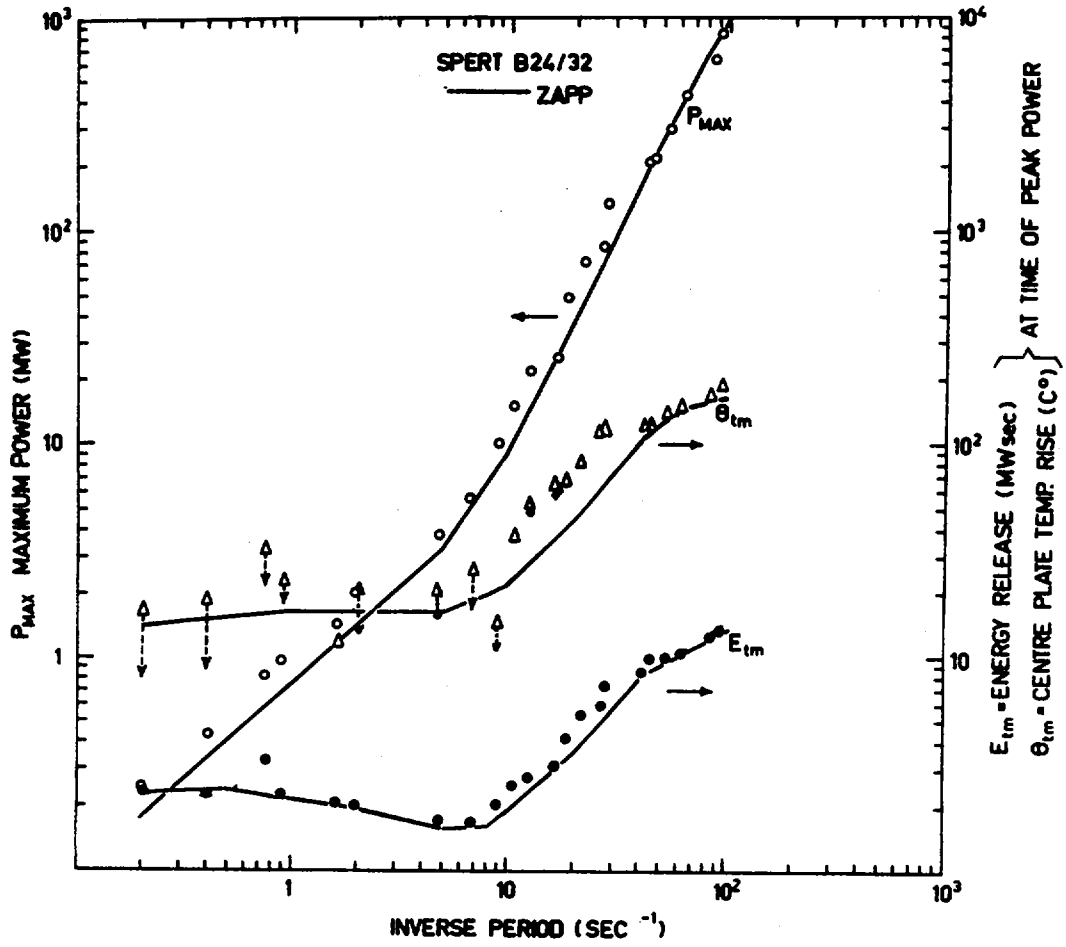

FIGURE 2.7 Maximum power, maximum energy release and fuel plate temperature of the SPERT B24/32 core for various transient inverse periods

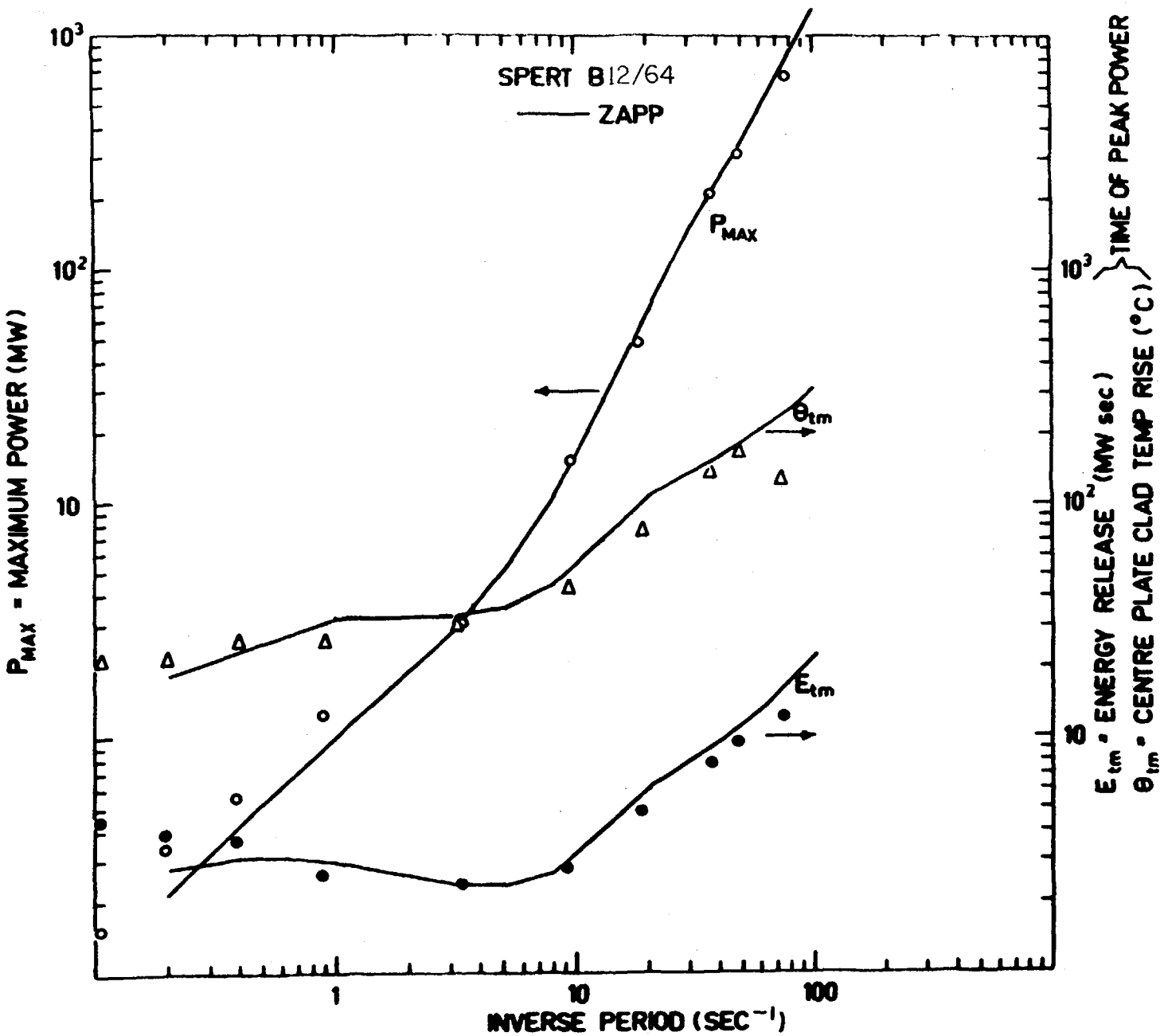

FIGURE 2.8 Maximum power, maximum energy release and fuel plate temperature of the SPERT B12/64 core for various transient inverse periods

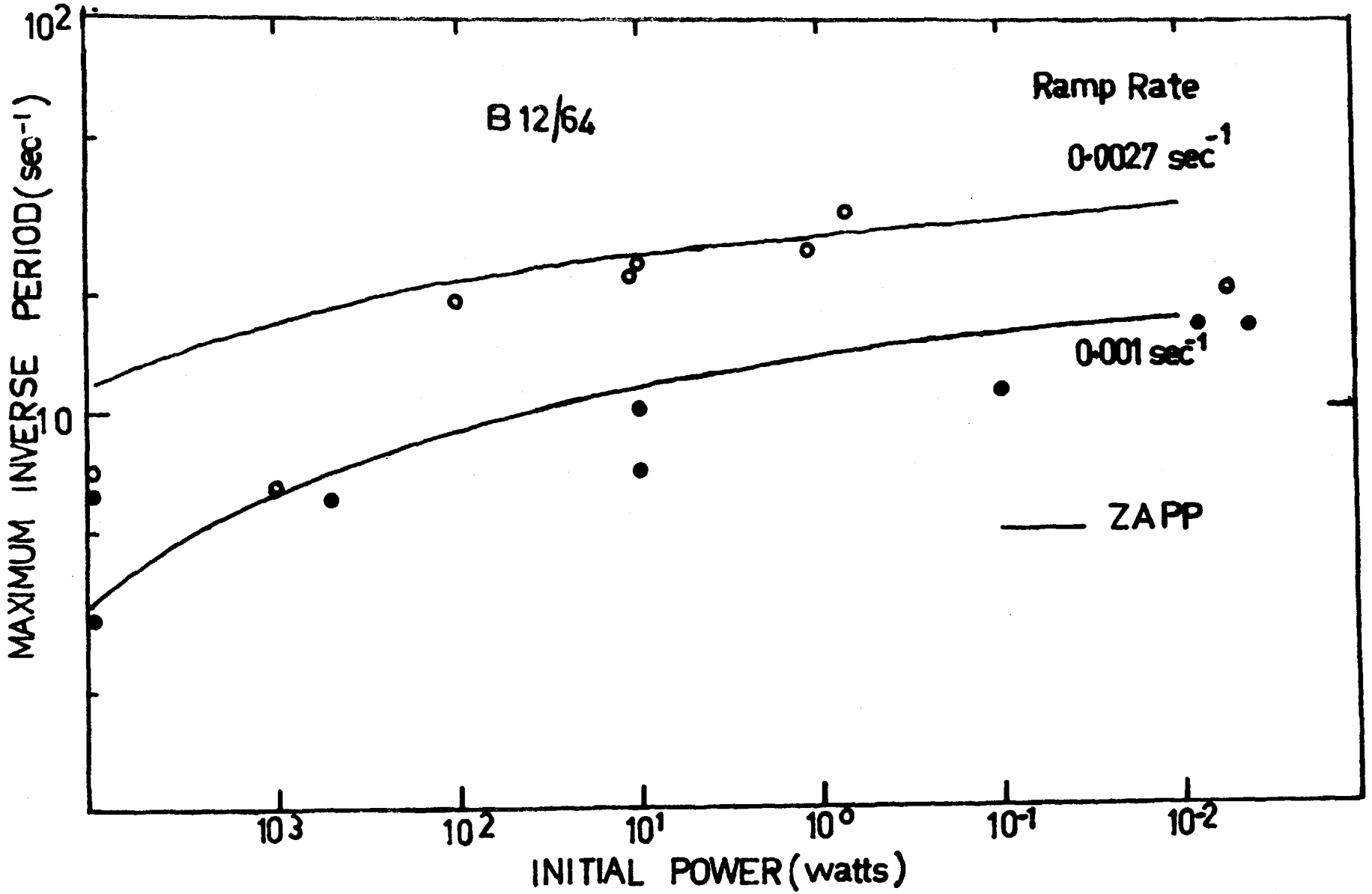

FIGURE 2.9 Maximum inverse period of SPERT B12/64 core as a function of initial power

ZAPP calculations have also been completed for the SPERT D12/25 core, which was finally destroyed by a transient of initial period 3.2 ms. For the transient periods between 7 and 3.2 ms structural damage of increasing severity was caused to the core. ZAPP (which cannot allow for such damage) increasingly overpredicts both peak power and energy release for initial periods less than ~14 ms.

Ramp tests on core B12/64 have also been calculated by ZAPP and are shown as a function of reactor power at the time of ramp initiation in figure 2.9. Agreement with experiment is again good, although the experimental data contain some widely scattered results.

The ZAPP transient analysis is currently being used to examine transients in the SPERT D_2O moderated reactors. Consideration is being given to the extension of the code to handle forced coolant flow situations.

Fuel-Coolant Interactions (A. W. Dalton)

Work was begun with a comprehensive literature search for pertinent material. Interest in fuel-coolant interactions in the reactor context stems from the destructive fast transients in the BORAX I (1954) and SPERT I (1962) test series, in which unexpectedly large explosive energy releases approaching the thermodynamic limit were observed. There appeared to be general similarities with the Al/H_2O vapour explosion at the Reynolds Aluminium Plant, Illinois, USA, which rocked a 25 mile area, causing a total of 40 deaths and casualties and property damage around $\$10^6$ (Witt et al. 1970).

Analysis of these incidents showed that:

1. Chemical reactions did not play an important role.
2. Pressures up to 1.5 kWh were produced.
3. Energy transfer took place in ~100 μs.
4. Extensive fragmentation occurred.
5. Work done approached the thermodynamic limit.

An understanding of the mechanisms of such processes is clearly of vital importance in the safety analysis for liquid moderated reactors.

Reactions of this type in the reactor fuel/coolant context are being actively investigated both theoretically and experimentally in a number of countries and many theories concerning the nature of the explosive trigger have been suggested. However, the model of Buchanan and Dallforce (1973),

Culham Laboratory, UK, appears to be emerging as the most acceptable. It is relatively simple, contains few ad hoc assumptions and appears to explain most of the accumulated observations, including the results of small scale experiments at Culham. This model considers that the energy source is the excess heat in the fuel and that the interaction is divided into five stages:

(i) the initial perturbation triggers the interaction and causes a vapour bubble to form at the fuel-coolant interface;

(ii) bubble expansion and collapse with jetting;

(iii) penetration of the fuel by the liquid jet;

(iv) heat transfer from the fuel to the jet;

(v) the formation of a new bubble.

The process repeats itself cyclically from stage (ii). The most important result from the safety aspect is that the strength of the interaction is reduced as the external pressure is increased and can be inhibited entirely if the pressure is large enough.

We are now examining this model in detail, particularly with regard to its basic physical principles; this may result in our attempting to obtain the corresponding computer code to carry out some actual calculations.

2.5 FISSION PRODUCT DISPOSAL (J. R. Harries)

The feasibility of transmuting the hazardous longlived radioactive isotopes present in reactor waste has been examined. Even to transmute only the most hazardous fission product electrons or gamma ray bombardment was found, as shown in Table 2.1, to require more energy than the fission reactor yields in their formation (~100 MeV electrical per nucleus). For protons, even with the most favourable assumptions, the energy requirement is still more than half the original fission yield, so cannot be considered a practical possibility.

Neutron transmutation of these fission products would be possible with the high neutron fluxes that might be produced by future controlled thermonuclear reactors or by using spallation targets. However, the benefits of so transmuting the fission product cesium-132 and the strontium-90 would probably still be outweighed by the costs of the energy requirements and separation processes and by the consequent potential combination accidents.

The neutron transmutation of the transuranic component of the waste was found to be feasible by recycling in currently operating reactors, although future fast reactors will be even more suitable. Neutron absorption in the transuranic actinides has a reasonable probability of causing fission, so that the waste is both converted to a smaller quantity of shorter lifetime fission products and yields fission energy for utilisation. The main difficulty is the lack of a process yielding a sufficiently high separation of actinides from fission products.

TABLE 2.1

Energy for Accelerator Transmutation of Strontium-90 and Cesium-132 Fission Products

	Beam Energy	Electrical Energy*
Proton	200 MeV	400 MeV
Gamma	1 GeV	2 GeV
Electron	80 GeV	160 GeV
Neutron:		
U target	25 MeV	50 MeV
Pb target	50 MeV	100 MeV

*Assuming accelerator efficiencies for conversion of electrical energy into beam energy could reach 50%

2.6 DENSE PLASMA FOCUS NEUTRON SOURCE (G. R. Hogg, J. Tendys, J. A. Daniel)

Measurements of the spectrum of the X-ray emission from the dense plasma focus device have been made using a four channel X-ray spectrometer (AAEC/PR39-P, p.35). The plasma electron temperature can be derived from such measurements if a thermal (Maxwellian) electron distribution is assumed and furthermore, if the bremsstrahlung spectrum is pure and not contaminated with line radiation arising from impurities in the filling gas.

Initial measurements were made with a coaxial gun whose centre electrode was capped with tungsten which prevented rapid erosion of the centre electrode. After several hundred firings of the gun, the entire vacuum system and gun electrodes were contaminated with tungsten and hence the X-ray spectrum was also heavily contaminated with the tungsten K, L and M line radiation. It was not possible to derive a definitive plasma electron temperature from these measurements. However, by an iterative process the spectrum of the X-ray output was determined over the energy range 1 to 10 keV.

Further measurements were made with a hollow centre electrode (to reduce metal evaporation) and a clean vacuum system. Operation of the gun with pure hydrogen gas fillings resulted in very erratic focusing with a consequent large shot to shot variation of several orders of magnitude in the X-ray output. It was necessary to operate the gun with gas fillings containing 1 per cent argon to provide satisfactory focusing. Although the addition of argon produced K line contamination of the bremsstrahlung spectrum, it was possible to compensate for this and determine a plasma electron temperature. At a capacitor bank voltage of 18 kV (stored energy 13 kJ) and a gas filling of 5 torr H_2 + 1% A, a plasma electron temperature of 0.3 ± 0.1 keV has been derived.

The construction of a small coaxial gun designed to operate at 1 kJ has commenced. This gun will be used to determine the relationship between neutron output, electron dimensions and stored energy.

3. 3 MeV ACCELERATOR

(H. Broe, A. van Heugten, J. Copland, P. Lloyd, S. Kanard, M. J. Kenny)

During the past year the installation of thermo-mechanical pumps in all beam legs was completed. All our vacuum requirements are now provided by this type of pump, resulting in a much cleaner vacuum and the minimum of maintenance. The main turbo pump has now completed 56 000 hours service, requiring routine maintenance only.

To overcome small changes in beam direction caused by wear in the ion source canal, two sets of electrostatic deflection plates have been installed in the case end of the accelerating tube. They are controlled from the control room and work quite satisfactorily.

Interaction between the main and auxiliary amplifiers of the nanosecond pulser was finally overcome by complete shielding of the auxiliary drive shaft. Tuning and stability have been greatly improved. The present accelerating tube and charging belt have now been in service for 11 000 hours.

The power supplies for the magnet motor generator sets had a history of troubles; they have been replaced by locally made solid state devices which are operating satisfactorily.

The accelerator was used for 1721 hours during the period 1st January to 30th June, 1974, distributed as in Table 3.1. Maintenance accounted for an additional 835 hours.

TABLE 3.1

ACCELERATOR TIME ALLOCATION - JANUARY 1 TO JUNE 30, 1974

Topic	Expt. No.	Title	Personnel	Origin	Running Time (hours)
Fission	11	$\bar{\nu}$ vs E_n	Boldeman, Walsh	Physics	462
	15	Fragment Angular Dist.	Caruana	Wollongong	152
	16	Californium Spectra	Culley	Physics	4
Neutron Capture	21	Ge(Li) Capture Spectra	Kenny, Allen, Pe	Physics/UNSW	63
	23	Capture Mechanisms	Allen, Kenny, Barrett Bray	Physics/Melb/ANU	128
Neutron Transport	32	Pulsed Spectra - Th	Whittlestone	Physics	159
	33	Spectra - Fast Assemblies	Rose	Physics	48
Nuclear Analysis	41	Oxygen Analysis	Russell, Murch	Physics/Flinders	72
	42	Applications	Bird, Russell	Physics	147
	43	Dosimetry	Cripps	Health Physics	38
Atomic Physics	51	Channelling	Szpitalak	UNSW	17
Charged Particle	61	(p,γ) Spectroscopy	Solomon, Read, Mya, Hain	Melbourne	166
	62	(p,γ) Spectroscopy	Higbie, Hart	Queensland	54

Tests:	73 hours
Total operating time:	1721 hours
Maintenance:	835 hours
Development:	491 hours

3.1 FISSION MEASUREMENTS (J. W. Boldeman, R. L. Walsh, J. Caruana)

Energy Dependence of $\bar{\nu}_p$ for ^{233}U

A minimum in $\bar{\nu}_p$, the average number of prompt neutrons emitted per fission, for ^{233}U is expected at $E_n \sim 150$ keV from our previous results for the energy dependence of the ^{233}U fission fragment average kinetic energy $\bar{E}_K(E_n)$, wherein $\bar{E}_K(E_n)$ was found to increase by 300 keV when E_n increased from zero to 150 keV. For $E_n > 150$ keV, $\bar{E}_K$ flattens out and remains independent of E_n up to 1 MeV at least. The size of the kinetic energy increase implies a dip in $\bar{\nu}_p(E_n)$ of about 0.035 neutrons. Our earlier ^{233}U $\bar{\nu}_p$ measurements between 300 keV and 2 MeV are being extended to search for this dip at 150 keV.

The jump in $\bar{E}_K(E_n)$ and substantial dip in $\bar{\nu}_p(E_n)$ are a direct result of the discrete nature of the low lying collective rotational energy bands at the second hump in the fission potential barrier and of the changeover from predominantly s-wave to p-wave fission in the region E_n = 0-150 keV.

Fission Fragment Mass Distribution Studies

A new collimator has been installed in the thermal column of MOATA in preparation for mass distribution studies in the thermal neutron fission of ^{233}U, ^{235}U and ^{239}Pu. The studies will include measurements of the number of neutrons emitted by fragments of specific mass for a number of ranges of the total fission fragment kinetic energy.

Neutron Emission from Specific Fission Fragments

A computer program now exists which allows on-line analysis of 1024 channels of X-ray spectra on the PDP-11/10. However, no measurements have been taken as hardware problems have arisen in the interfacing of the PDP-11/10 to the PI1200 magnetic tape deck.

A stronger ^{252}Cf source is to be inserted in the system (2.2×10^5 fission min^{-1} compared to 7×10^4 fission min^{-1} used previously).

Angular Distribution of Fission Fragments from $^{235}U(n,f)$ and $^{233}U(n,f)$

The experimental program is now complete with data obtained for incident neutron energies between 0 and 2 MeV. The $^{3}T(p,n)^{3}He$ reaction was used for the higher energy data.

The ^{235}U anisotropy data are shown in figure 3.1. There is no evidence of anisotropies $W(0^\circ)/W(90^\circ) < 1$ in the low energy region as has been reported

by Specht et al.* and Nesterov et al.** and was interpreted as suppression of the $K = 0^+$ collective band and enhancement of channels with $K \geq 2$.

The ^{233}U anisotropy data (figure 3.2) show a very rapid increase in $W(0^o)/W(90^o)$ between $E_n = 0$ and 100 keV, with a subsequent levelling off above 100 keV. This behaviour is a direct result of the changeover from s to p-wave fission for $^{233}U(n,f)$ in this energy region and is in agreement with our previous finding of a rapid increase in $\bar{E}_K(E_n)$, the total kinetic energy of the ^{233}U fragments, from $E_n = 0$ to 150 keV†.

The presence of collective channel effects in the ^{233}U angular distribution data and its absence in the ^{235}U data parallels our $\bar{\nu}_p(E_n)$ results for the same nuclides and reinforces our conclusions as to the change in Strutinsky barrier heights in the mass region††.

Californium Time of Flight Measurement (D. Culley)

An experiment has been designed to measure with high precision the prompt fission neutron spectrum arising from the spontaneous fission of ^{252}Cf. A long standing discrepancy exists between previous measurements and ^{252}Cf is important because its spectrum has now been defined as the standard neutron spectrum. The time of flight technique will be used for the energy range 0.5 to 15 MeV. For energies below 0.5 MeV ^6Li scintillators will be used.

Construction and assembly of equipment has begun with the erection of a support structure 4.5 m high, with provision for neutron flight paths up to 5 m. The plastic scintillators, of which two will be used, have been assembled and the response of these detectors to gamma rays of known energy investigated. The response to neutrons of known energy has also been investigated using the Van de Graaff and time of flight gating methods.

The manufacture of the gas scintillator chamber to detect ^{252}Cf fission has been completed and the deposition of the ^{252}Cf source is under way.

A proton telescope, the efficiency of which may be calculated from its geometry, is currently being manufactured and will be used to make some direct experimental determinations of detector efficiencies.

---

*Specht, H. J. et al. (1966) - Phys. Rev. Lett., 17, 1187.

**Nesterov, V. G. et al. (1967) - Sov. J. Nucl. Phys, 4, 713.

†Boldeman, J. W. and Walsh, R. L. (1973) - Soviet National Conference on Neutron Physics, Kiev.

††Walsh, R. L. and Boldeman, J. W. (1971) - J. Nucl. Energy, 25, 321.

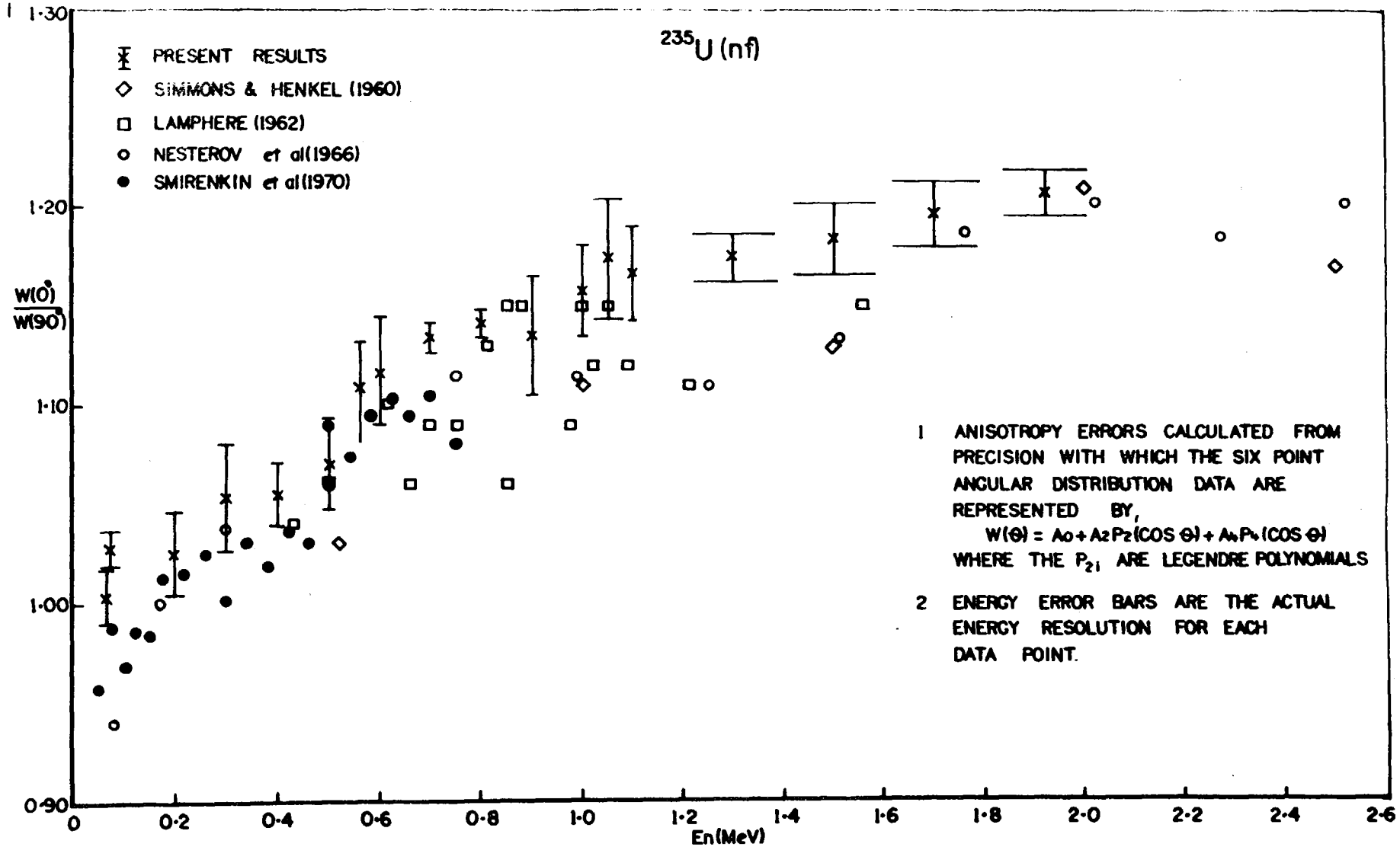

FIGURE 3.1 Anisotropy of the ^{235}U fission fragment distribution versus incident neutron energy

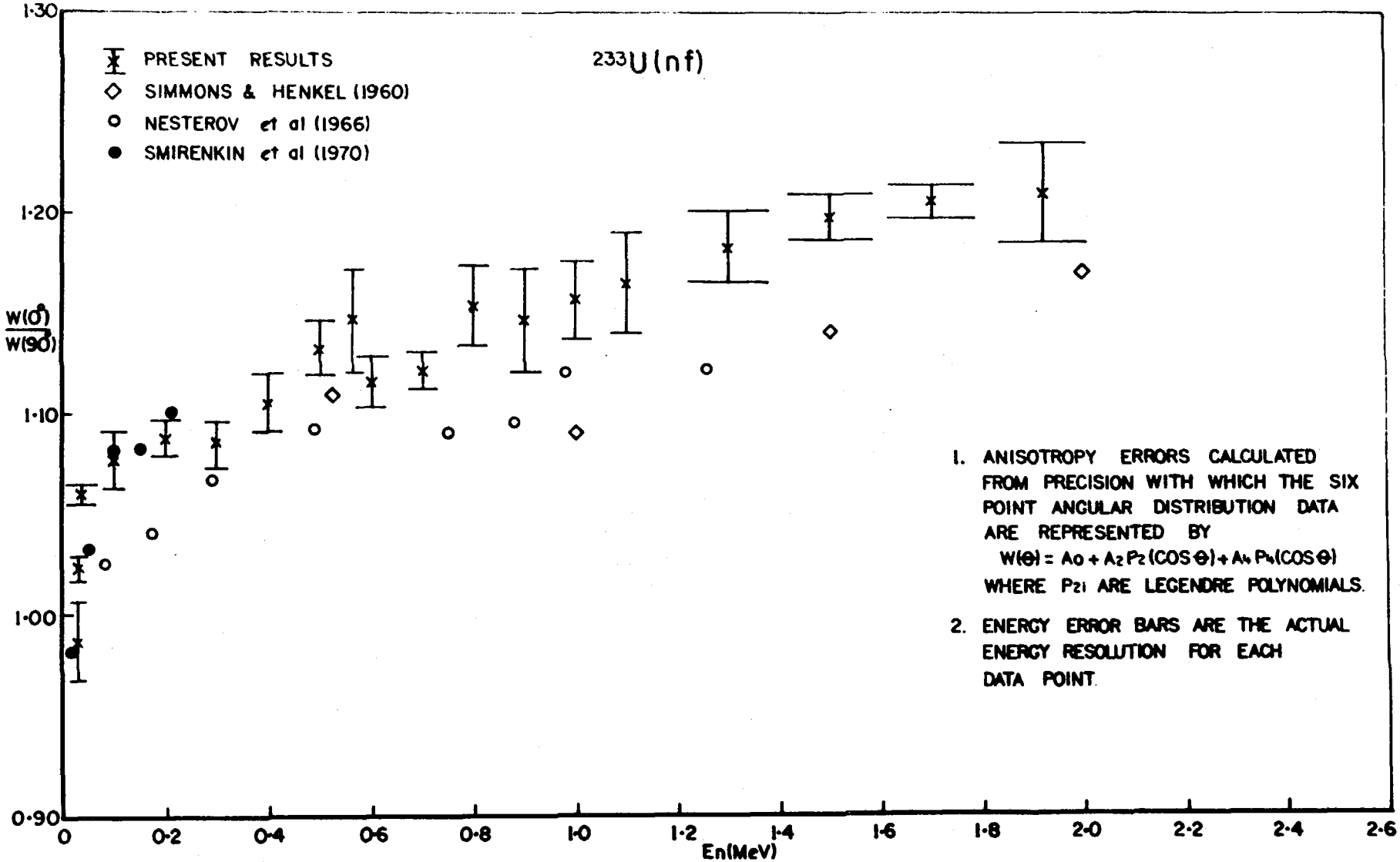

FIGURE 3.2 Anisotropy of the ^{233}U fission fragment distribution versus incident neutron energy

3.2 NUCLEAR REACTIONS

Energy Dependence of Partial p-wave Capture Cross Sections

(Hla Pe, B. J. Allen, M. J. Kenny, J. R. Bird)

The energy dependence of partial p-wave capture cross sections has been measured for capture by the odd isotopes of cadmium, ^{111}Cd and ^{113}Cd. This has been achieved by observing intensities of transitions to positive parity states in ^{112}Cd and ^{114}Cd. These states are not populated after thermal capture, but are populated by electric dipole transitions after p-wave capture. Figure 3.3 shows the relative partial p-wave capture cross section for the composite results of ^{111}Cd and ^{113}Cd. For comparison purposes, data obtained by Kompe* is also shown.

Fast Neutron Capture Gamma Ray Spectra in Fe

(B. J. Allen, M. J. Kenny, R. F. Barrett, K. H. Bray)

Gamma ray spectra have been measured for neutron capture in iron for neutron energies up to 1 MeV. Analysis of the spectra has been in terms of both the statistical and valence capture models. In the case of the 27.7 keV resonance where the parameters are well known, the valence model predicts a transition strength to the ground state doublet about one half of the observed value. This leads to the consideration of the neutron capture process being semidirect in which the incoming neutron scatters in the target nucleus creating a two particle, one hole state.

Single Particle States in Neutron Capture

(J. R. Bird, R. F. Hille)

The systematics of the strongest transitions in thermal and resonance neutron capture for nuclei with $20 < A < 140$ have been investigated and show evidence for the position of single neutron states. Results for (n,γ) and (d,p) experiments have been compared and the resulting systematic trends have been used to predict results for capture by nuclei which have not been studied, such as ^{24}Mg, ^{26}Mg, ^{36}S and ^{318}Ar.

---

*Kompe, D. (1969) - Nucl. Phys. A133, 513.

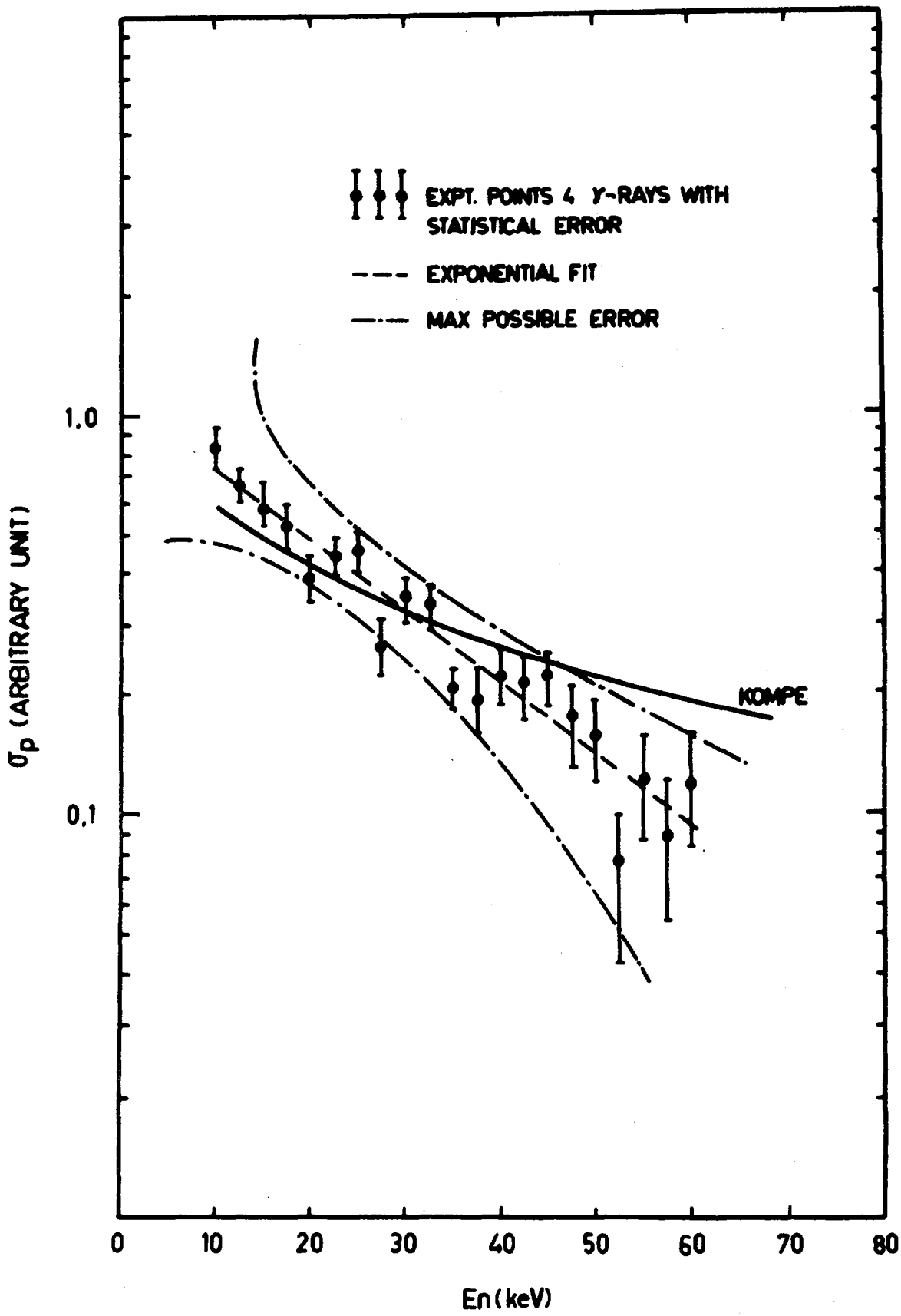

FIGURE 3.3 Partial p-wave capture cross section (arbitrary units) for ^{111}Cd and ^{113}Cd versus neutron energy

3.3 NEUTRON CAPTURE CROSS SECTIONS (B. J. Allen, W. K. Bertram, J. R. Bird, J. W. Boldeman, M. J. Kenny, A. R. Musgrove, Hla Pe, R. L. Walsh)

High resolution neutron capture cross section data have been obtained for a large number of isotopes on the Oak Ridge Electron Linear Accelerator in collaboration with R. L. Macklin at ORNL*. Analysis of this data has proceeded and present progress with respect to a number of isotopes is considered in the following sections. During the period under consideration, a neutron capture symposium was held at Lucas Heights. The symposium covered experimental problems associated with collaborative capture cross section measurements at ORELA, valence effects in gamma ray spectra and cross sections, valence and doorway theory, interference effects and systematic properties of capture reactions across the periodic table.

Informal proceedings of the symposium will be available shortly.

Analysis of Data

A new approach has been adopted for the analysis of resonance data. Monte Carlo fits are now made for each resonance using a modified version of the RPI code† operating directly on the capture cross section data and its variance. s, p and d wave resonances are included and a multi-level option is also available when resonance-resonance interference is significant.

The mass and energy dependence of the detector neutron sensitivity (as per R. R. Winters) has been included as a correction to the capture data.

A detailed description of the application of the Monte Carlo code to the analysis of ORELA data is as follows.

A Monte Carlo area analysis program has been written to fit resonance parameters to the capture yield data provided by ORELA. The code is a considerably modified version of the RPI/ORNL code described by Sullivan et al.† One hundred channel segments (or multiples thereof) are fed through MCFIT in a search for peaks with FWHM > resolution width Γ_R.

Figure 3.4 shows a segment of the $^{40}Ca(n,\gamma)$ yield data near 125 keV where a linear background fit is some 2 mb (10%) above the ambient background level (as determined in windows to the left and right of the window shown in the figure). Since there appears to be evidence of a peak near 125.7 keV, we

---

*Research sponsored by the USAEC under contract with Union Carbide Corporation

†Sullivan, J. G., Warner, G. G., Block, R. C. and Hockenbury, R. W. (1969) - RPI-328-155; plus later errata.

attempt an area fit in figure 3.5. The quantity required is $\kappa = g\Gamma_n\Gamma_\gamma/\Gamma$. The program adjusts whichever of Γ_n, Γ_γ is the smaller, in order to fit the experimental yield. At 125 keV we expect to find that $\Gamma_n >> \Gamma_\gamma$ and since this is a very small resonance (if not spurious) we assume (for the purpose of fitting) that $\Gamma_n = 1$ eV. We further assume this to be a d-wave level. As shown on the figure, the self shielding correction (C1) is found to be 0.93 while the radiative width giving the correct experimental area is found to be about 33 meV. More correctly, if our original assumption that $\Gamma_n >> \Gamma_\gamma$ was correct, this resonance has $g\Gamma_\gamma \simeq$ 100 meV. As described later (section 3.3.6), we feel confident that Γ_γ (d-wave) is probably closer to 600 meV and hence if this level is d-wave, we have in this case $\Gamma_\gamma >> \Gamma_n$ and hence $\kappa \simeq g\Gamma_n = 100$ meV.

Where counting statistics are good, it is possible to resolve resonances having $\Gamma_n > 0.4\ \Gamma_R$ (i.e. by performing shape analysis to determine Γ_n). An example illustrating this point is given in figure 3.6 where we fit to the 20 keV ^{40}Ca resonance. Although $\Gamma_R = 33$ eV for this ^{40}Ca resonance, noticeably poorer fits are obtained with $\Gamma \geq 11$ eV as compared with our best estimate $\Gamma_n = 5 \pm 3$ eV. Although not shown, a fit with $\Gamma_n = 1$ eV does not converge (i.e. is non-physical). Our final estimate is in excellent agreement with the value recommended in the latest BNL-325* ($\Gamma_n = 6 \pm 2$). We can perform analysis to these tolerances only because our resolution FWHM is very accurately determined from a careful fit to widths of many unresolved resonances in several isotopes.

To exemplify a case with $\Gamma_n > \Gamma_R$ where a visual shape fit is performed along with the usual area analysis, we give in figure 3.7(a) an analysis of the 89 keV resonance in ^{40}Ca. Γ_R here is 175 eV and clearly a good fit is obtained with $\Gamma_n = 300$ eV. By comparing a number of fits with Γ_n varying from 100 to 500 eV we can give the approximate errors on this value as $\Gamma_n = 300 \pm 50$ eV. The only cause for alarm here is that about three authors have seen this level in (n,total), and all agree that the neutron width of this resonance is $\Gamma_n \simeq 150$ eV. Since it appears unlikely that the early authors have all erred, we can be quite sure that this resonance is a doublet (a result anticipated in the new BNL-325* from an unknown source).

---

*Mughabghab, S. F. and Garber, D. I. (1973) - BNL-325, 3rd Ed.

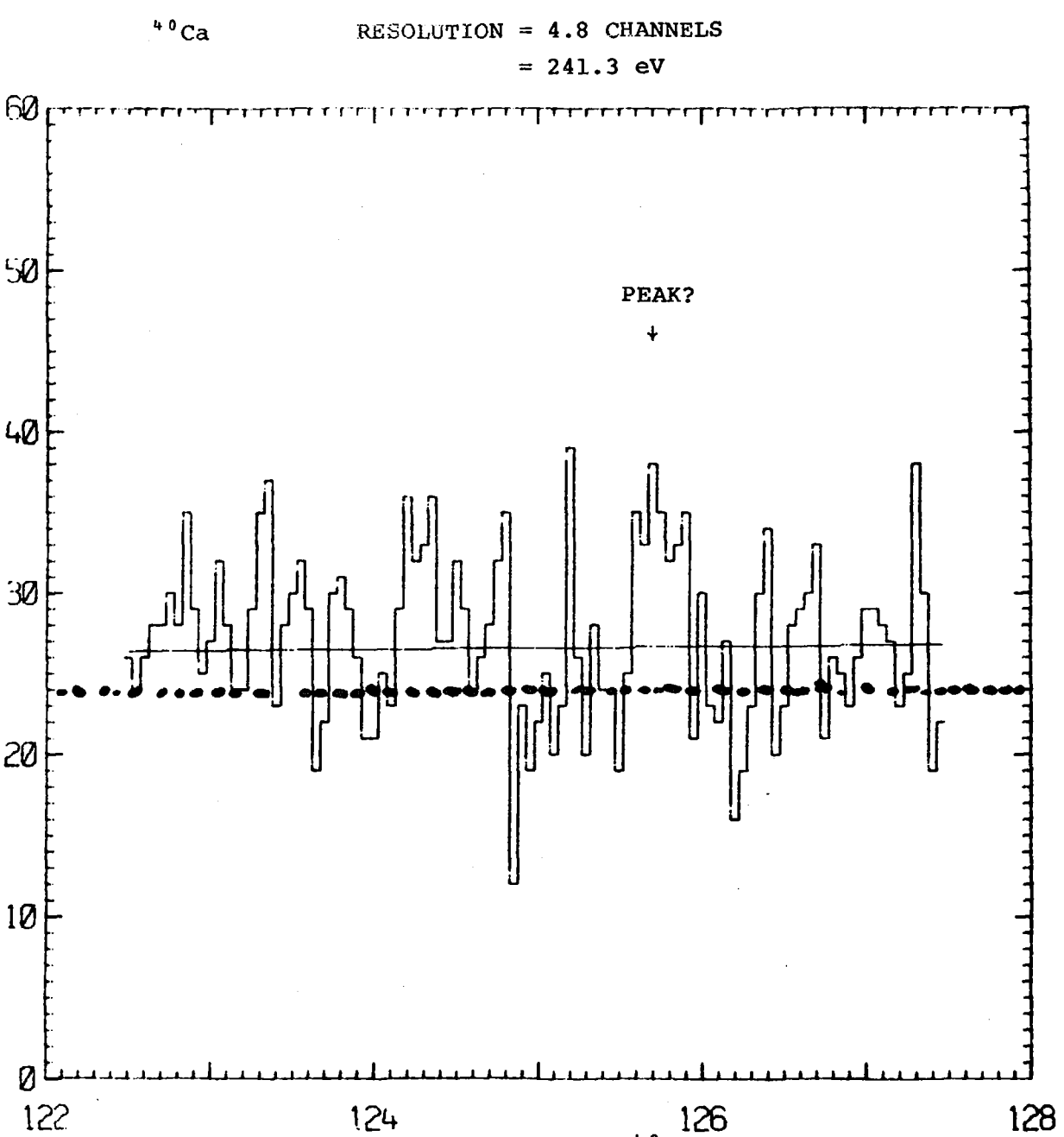

FIGURE 3.4 Background fit to ^{40}Ca data at ~125 keV indicating possible peak at 125.7 keV

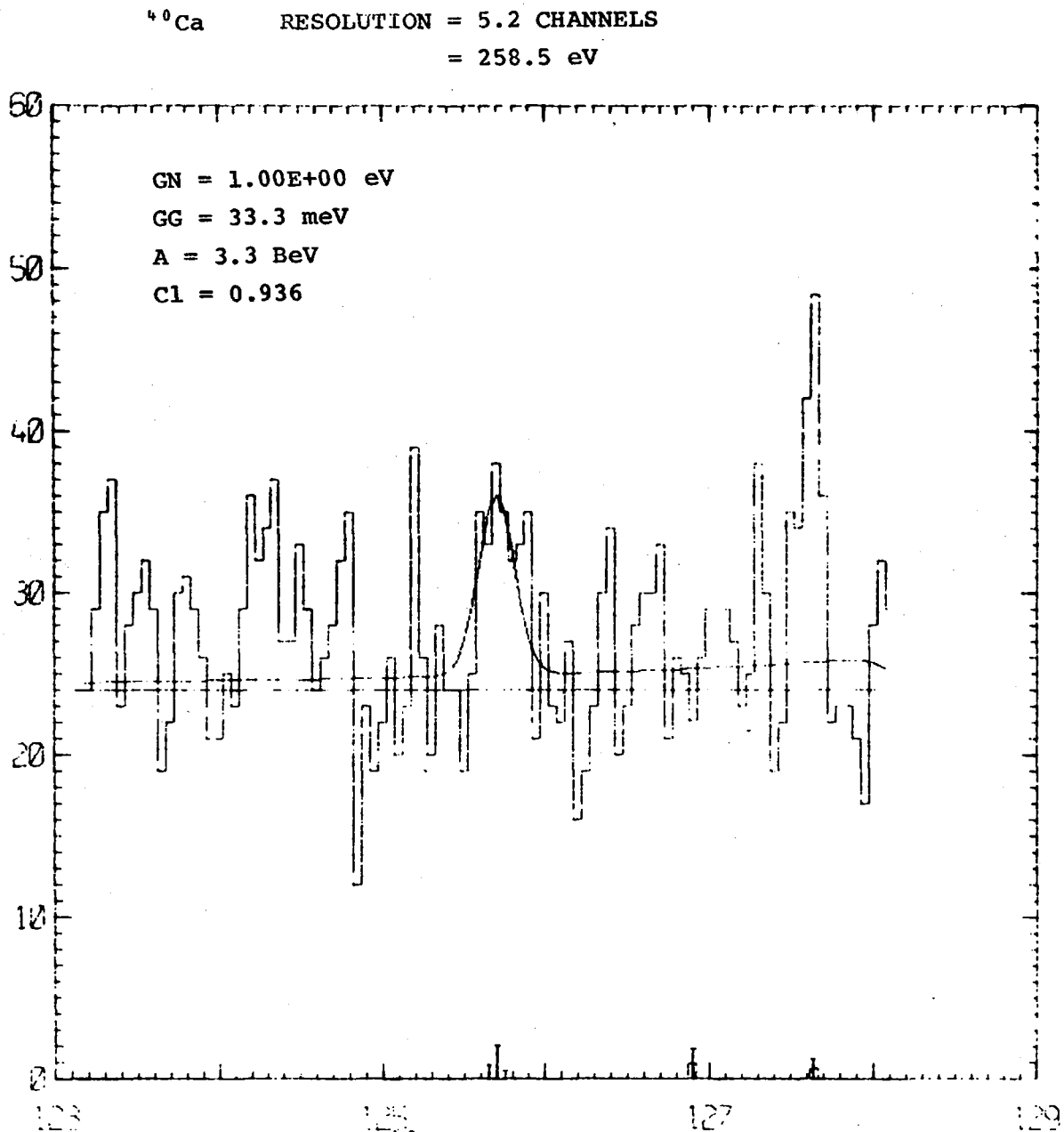

FIGURE 3.5 Fits to the ^{40}Ca s-wave resonance at 125.7 keV.
(Γ_n 1 eV; Γ_γ = 33.3 meV)

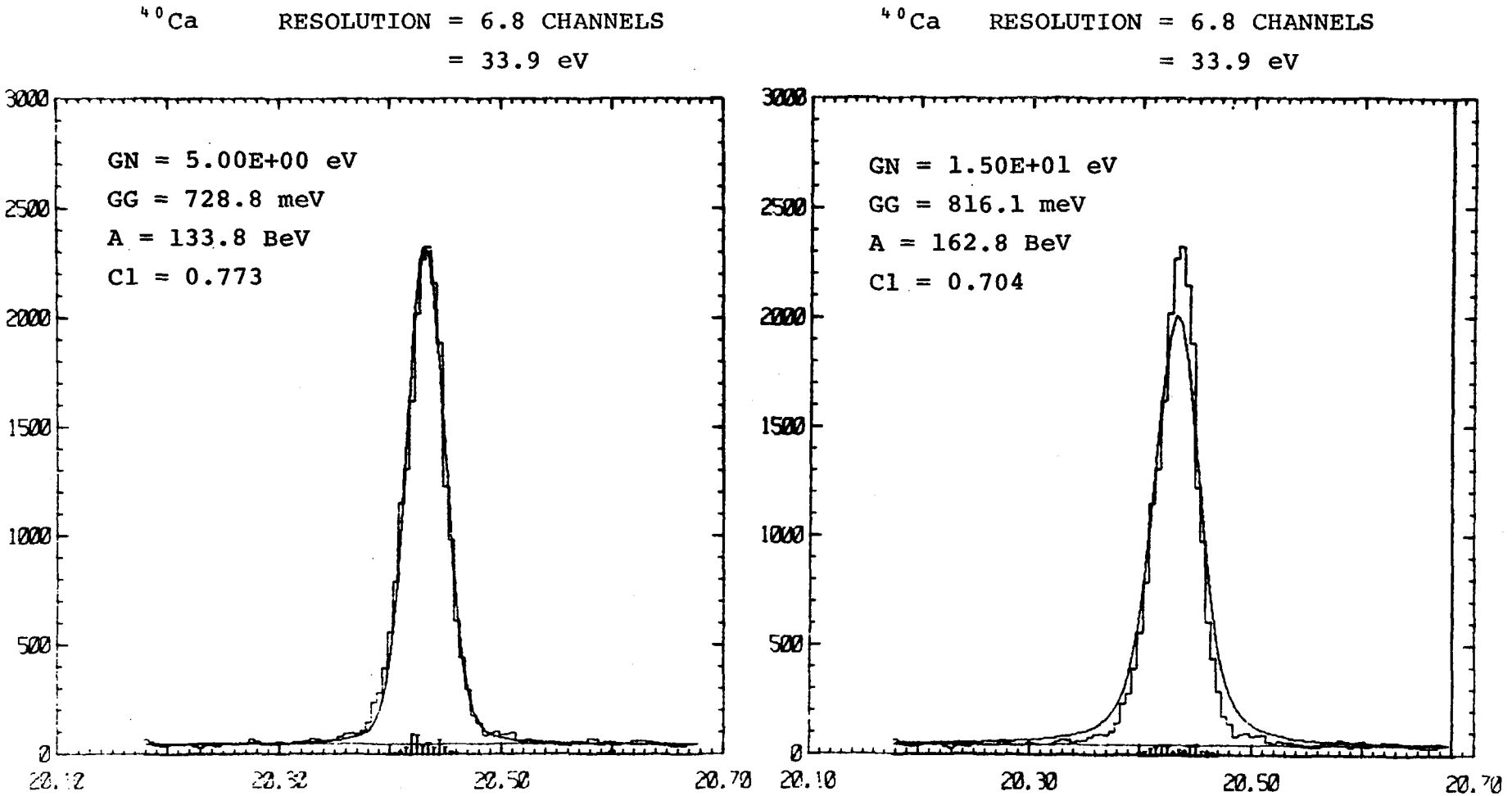

FIGURE 3.6 Fits to the ^{40}Ca s-wave resonance at 20.4 keV.
(FWHM resolution = 34 eV; Γ_n = 5 eV)

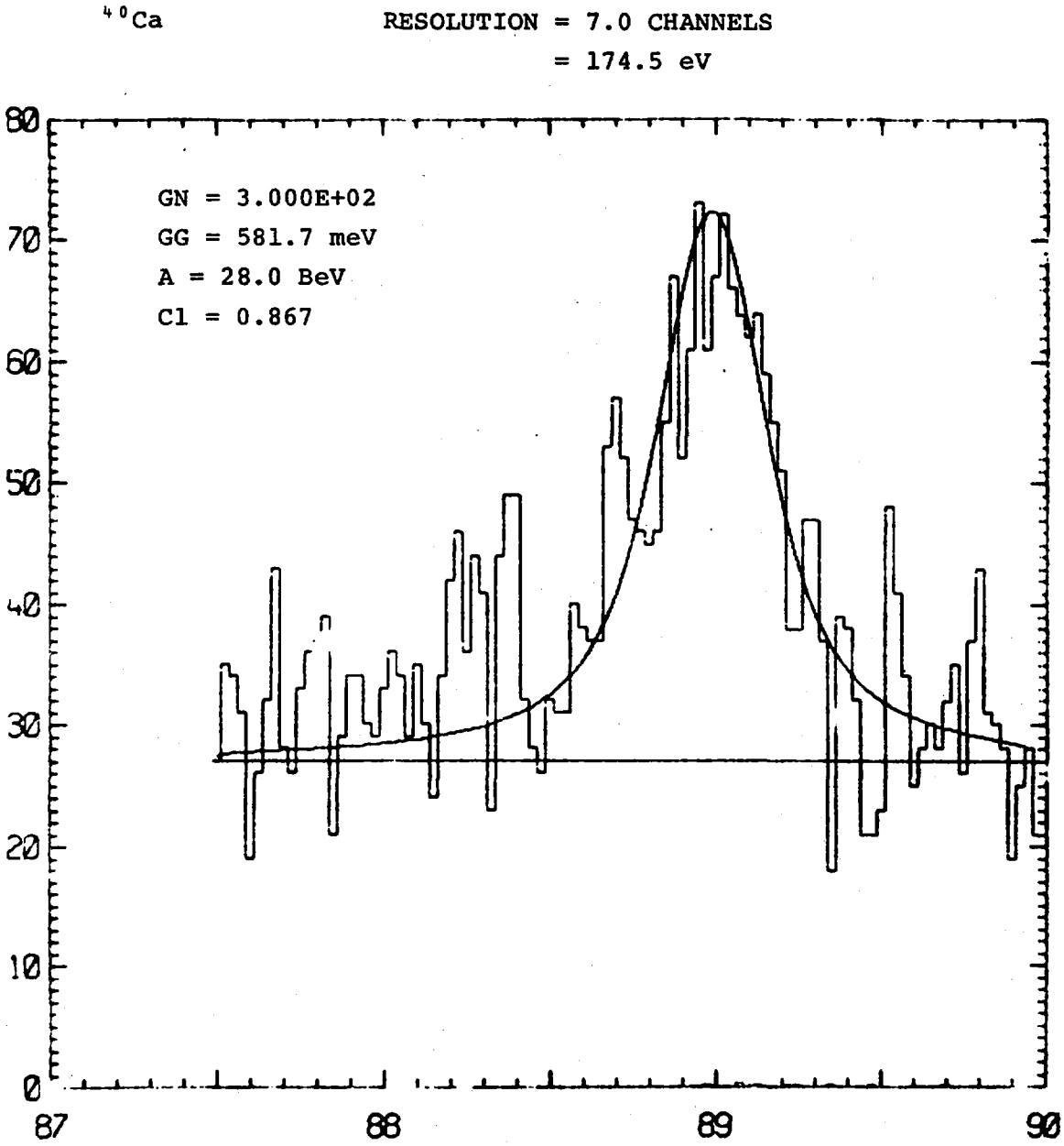

FIGURE 3.7a ^{40}Ca resonance at 89 keV fitted by Γ_n = 300 eV

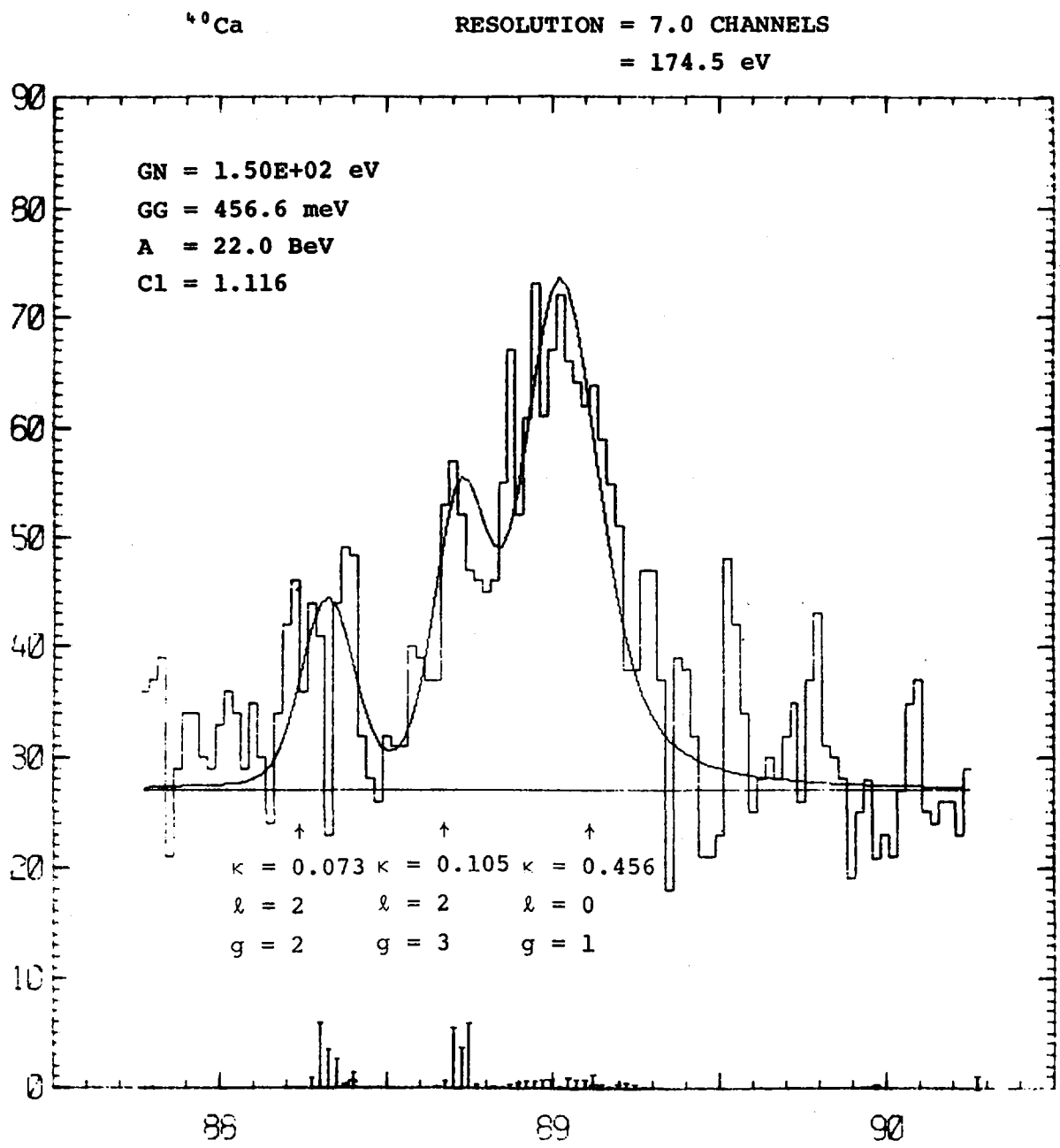

FIGURE 3.7b ^{40}Ca resonance at 89 keV fitted by Γ_n = 150 eV

Strong ground state transitions were reported* for neutron bombarding energies near 90 keV, which leads us to presume that the other member of this doublet could be a d-wave resonance with g = 3 giving E1 transitions to the ground state of ^{41}Ca ($7/2^-$). With no other evidence to guide us, we have proceeded to fit the right hand side of this resonance with an s-wave level having the generally agreed value for Γ_n = 150 eV (figure 3.7(b)). This resonance turns out to have κ = 0.46 and hence Γ_γ = 460 meV. The leftover part has κ = 0.10, while for good measure a third resonance has been included at 88.3 keV.

Interference Effects in Neutron Capture

Because of the assumption of random phases of the partial radiative amplitudes in the statistical model, interference effects are not expected to be observed in total capture.

However, in specific cases when a partial capture cross section (i.e. (γ_o,n)) is measured, when $\Gamma_\gamma \simeq \Gamma_{\gamma o}$ (as in $^{207}Pb(n,\gamma)$ or where partial capture cross sections $\sigma(n,\gamma_i)$ are measured, then interference effects may be present.

The experimental problem in capture is that for large neutron width resonances, multiple scattering can cause an apparent asymmetry and this must be adequately taken into account.

In the 41 keV $^{207}Pb(n,\gamma)$ study, the multiple scattering was calculated from resonant parameters and subtracted and the net primary yield fitted with the appropriate form to obtain the non-resonant cross section.

We are now able to incorporate the interference formalism into the Monte Carlo calculation itself, thereby obtaining a consistent analysis for both primary and multiple yields.

The last (γ,n) results of Jackson still suggest a significant non-resonant component and it is planned to reanalyse the high bias capture result in the above manner.

In the case of Pb resonance-resonance effects are suspected to be small, but according to Shaken and Weiss, can account for the observed asymmetry.

---

*Chan, D. M. H. and Bird, J. R. (1971) - Aust. J. Phys. 24, 671.

In ^{48}Ti there are four large s-wave resonances below 60 keV, two of which overlap. As the γ-ray spectra are well known from Lucas Heights measurements and show only one or two dominating transitions, a three channel (γ-ray) multilevel calculation of the capture cross section has been used to analyse the observed cross section (figure 3.8). Certainly it is not possible to reproduce the data by a single level calculation, and when the signs of $\Gamma_n^{\frac{1}{2}}$, $\Gamma_{\gamma i}^{\frac{1}{2}}$ are not equal, for example, a complete correlation between the signs of the neutron and radiative amplitudes is required.

Unfortunately, the 17 keV resonance (Γ_n = 8.7 keV) generates a large amount of multiple scattering which must, however, fit the observed interference minimum. A satisfactory fit to the data not only yields a consistent set of resonance parameters in fair agreement with σ_T, but provides for the first time confirmation of multilevel theory in neutron capture at keV energies. Relative measurements at eV energies of $I_{\gamma i}/\Sigma_i I_\gamma$ with Ge(Li) detectors have shown the effects of resonance-resonance interference, but it does not appear that an absolute capture cross section measurement has been analysed in this manner before.

Formalism

For widely spaced resonances with many capture channels, the single level s-wave Breit-Wigner formula can be used

$$\sqrt{E}\sigma_\gamma = \frac{\pi}{k^2} g_J \sum \frac{\Gamma^o_{\lambda n} \Gamma_{\lambda\gamma}}{(E_\lambda - E)^2 + \Gamma_\gamma^2/4} \qquad \ldots(1)$$

When D ~ Γ and the number of capture channels is small, multilevel theory is required to account for asymmetries due to resonance-resonance interference.

A. The capture cross section for $C \to C^1$ is given in terms of the collision matrix

$$\sigma_{cc'} = \frac{\pi}{k^2} g_J \left|\delta_{cc'} - U_{cc'}\right|^2 \qquad \ldots(2)$$

where

$$U_{cc'} = f(R_{cc'}) \qquad \ldots(3)$$

and the R matrix is

$$R_{cc'} = \sum_\lambda \frac{\gamma_{\lambda c}\, \gamma_{\lambda c'}}{E_\lambda - E} \qquad \text{at energy E} \qquad \ldots(4)$$

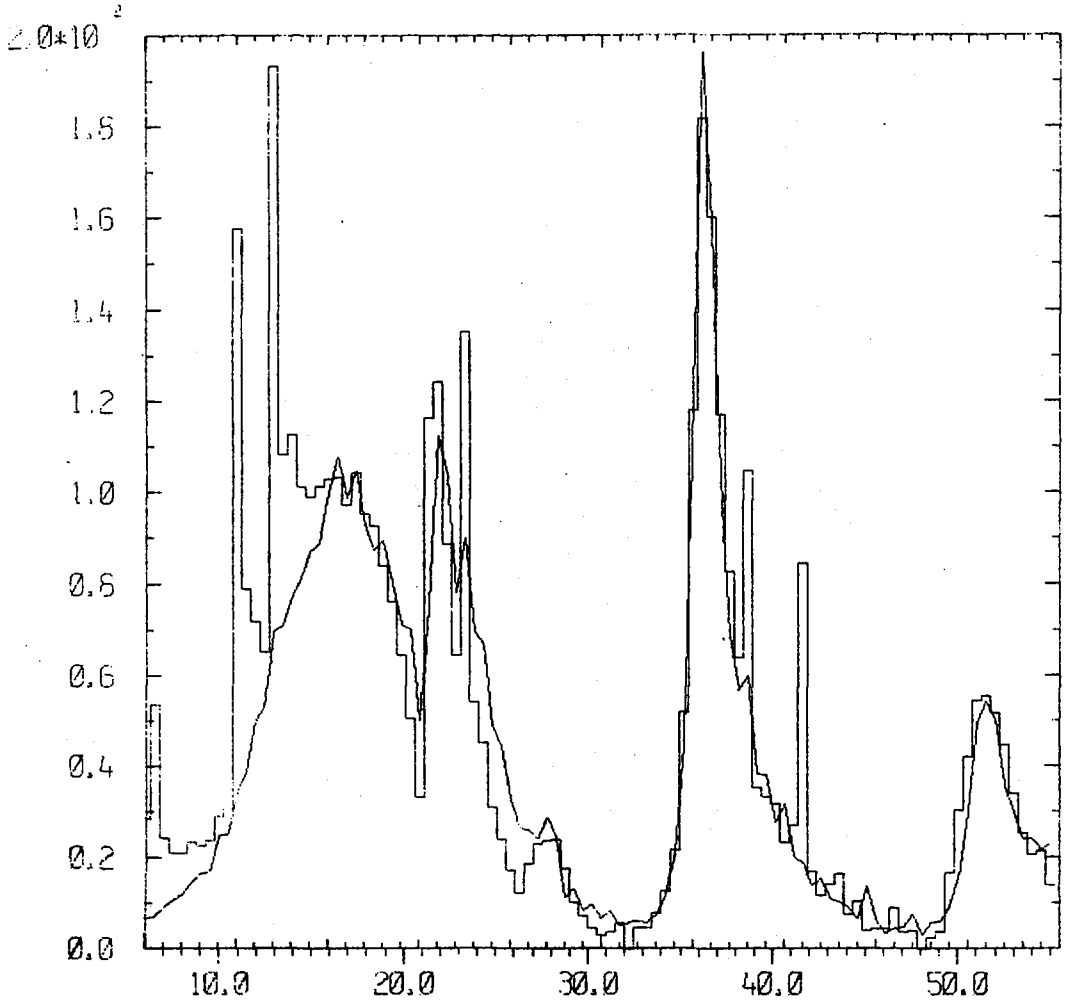

FIGURE 3.8 Multilevel fit to the ^{48}Ti neutron capture data in energy range 10-50 keV

The solution of this equation is difficult for more than two channels.

B. The collision matrix can also be expressed in terms of the level matrix H (normally called A)

i.e. $$U_{cc'} = f(H) \qquad \ldots(5)$$

$$H = (C - E)^{-1} \qquad \ldots(6)$$

and C has matrix elements

$$C_{\lambda\mu} = E_\lambda \delta_{\lambda\mu} - i/2\ \Gamma_{\lambda\mu} \qquad \ldots(7)$$

$$\Gamma_{\lambda\mu} = \sum_i \sqrt{\Gamma_{\lambda c}}\ \sqrt{\Gamma_{\mu c}} \qquad \ldots(8)$$

The disadvantage of this method is that the matrix (C - E) must be inverted at each energy.

C. An improved computational procedure can be achieved with the following method.

Diagonalise C by finding the orthogonal matrix U such that

$$UCU^T = E^1$$

with $$UU^T = 1$$

The complex diagonal matrix E^1 has elements

$$E^1_\lambda = \Sigma_\lambda - i/2y_\lambda \qquad \ldots(9)$$

as $$C = U^T E^1 U$$

$$H = (C - E)^{-1} = U^T (E^1 - E)^{-1} U \qquad \text{from (6)}$$

and $$H_{\mu\nu} = \sum_\lambda \frac{U_{\lambda\mu}\ U_\lambda}{\bar{E}_\lambda - E} \qquad ..(10)$$

Substituting for $H_{\mu\nu}$ in (5)

$$U_{cc'} = f(g_{\lambda c}, \Sigma_\lambda, y_\lambda, E) \qquad ..(11)$$

where

$$g_{\lambda c} = \sum_\nu U_{\lambda\nu} \sqrt{\Gamma_{\nu c}} \qquad ..(12)$$

Using (11) to calculate the cross section given by (2) and using

$$A_\lambda^{cc'} + iB_\lambda^{cc'} = ig_{\lambda c}^{(o)} g_{\lambda c'} \sum_\mu \frac{g_{\mu c}^{(o)*} g_{\mu c'}^*}{(\Sigma_\mu - \Sigma_\lambda) + i/2(y_\mu + y_\lambda)} \quad \ldots(13)$$

we obtain the final result

$$\sqrt{E}\,\sigma_{cc'} = \frac{\pi}{k^2} \frac{A_\lambda^{cc'} + (\Sigma_\lambda - E) B_\lambda^{cc'}}{(\Sigma_\lambda - E)^2 + \frac{1}{4} y_\lambda^2}$$

(for $c \neq c'$).

This cross section can be evaluated in much the same way as the single level formula. All parameters are (approximately) energy independent.

Sodium (^{23}Na)

Thirteen levels between 3 keV and 306 keV have been identified. Seven of these levels correspond in energy (to within 0.5 per cent) to established levels*. Three other levels at 117.5, 132.1 and 143.3 keV are respectively 3, 3 and 4 keV higher in energy than those of the RPI group**.

A further level seen at 243.3 keV verifies a 242.5 keV resonance (reported by the Columbia group)†, but not listed in BNL-325.

The remaining two levels, at 190 and 305.8 keV, have not been reported before.

It is unfortunate that the 3 keV low energy limit of the data is too high to fully include the important 2.85 keV level.

Some doubt exists as to the validity of the experimental normalisation as values of $g\Gamma_n\Gamma_\gamma/(\Gamma_n+\Gamma_\gamma)$ are consistently higher than expected from previous data*, even for those cases where the present Γ_n values are in good agreement.

Natural Silicon

The earlier analysis of the thin natural silicon data has been revised following the availability of better total cross section data. The total cross section data, in addition to providing more accurate input data for self shielding and multiple scattering corrections, has also allowed a better assignment

---

*BNL-325, June 1973, Vol. 1.

**Hockenbury et al, Phys. Rev. 178 (1969) 1746.

†Slagowitz, et al. Phys. Rev. C 8 (1973) 1827.

of specific resonances amongst the isotopes of silicon. The capture data for ^{28}Si appear to show very strong valence effects in agreement with the conclusion of Toohey and Jackson from the inverse $^{29}Si(\gamma,n)$ reaction.

Analysis of thick sample (0.105 atom barn^{-1}) measurements indicate new features in the data not observed in the earlier analysis of the thin Si (0.027 atom barn^{-1}) data.

Possible asymmetry is seen for resonances at 55 and 180 keV with the lower energy sides having the sharper fall off. On closer examination, this asymmetry is found to be present in the thin sample data.

^{27}Al

The measured neutron capture cross section of Al shows 56 resonances in the energy range 2.5 to 1100 keV, of which 23 are resolved width resonances. Many new resonances are recorded with widths less than the experimental resolution, especially in the higher energy region. Fifteen resonances have been observed between 310 and 600 keV and 19 resonances between 600 and 1100 keV. The preliminary resonance parameters for these resonances are listed in Table 3.2.

For the resonances at 5.904 keV the agreement with BNL-325 is 0.02 per cent in resonance energy and 7.1 per cent in Γ_γ. The agreement with BNL data for the 34.882 keV resonance is 5.3 per cent in resonance energy and about 4.4 per cent for Γ_n, whereas the value obtained for Γ_γ in this analysis is 6.5 eV which is significantly larger than the value in BNL-325 ($\Gamma_\gamma = 2 \pm 0.3$ eV). The present value of Γ_γ however, is comparable to Singh's* result ($\Gamma_\gamma = 8.30$ eV) obtained by fitting the thermal capture cross section assigning $J^\pi = 2^+$.

The resolved resonances are shown as R in the table. Monte Carlo analyses will be made for all resonances.

An apparent asymmetry is observed for the 35 keV resonance (figure 3.9). It is possible that the asymmetry may result from the capture of scattered neutrons in the aluminium body of the capture detector.

---

*Singh, U. N. and Garg, J. B. (1972) - High Resolution Neutron Resonance Spectroscopy in Natural Fluorine, Aluminium, Chlorine and Potassium. Statistical Properties of Nuclei. Plenum Press, New York-London.

TABLE 3.2

ALUMINIUM RESONANCE

APB = 0.01868; TEDEFF = 1.54; $I^{\pi} = 5/2^{+}$; $S_n = 7725.4 \pm 0.05$ keV

Resonance No.	E_n (keV)	Respar $g\Gamma_\gamma\Gamma_n/\Gamma$ (eV)		g	Monte Carlo Γ_n (eV)	Monte Carlo Γ_γ (eV)
1	5.904	0.217	R	0.25	16.0	0.883
2	24.293	0.004				
3	34.882	3.576	R	0.42	3100	6.5
4	85.943	2.192				
5	91.106	0.091				
6	91.967	0.027				
7	99.609	0.442				
8	103.716	0.156				
9	119.707	3.178	R			
10	143.077	3.533	R			
11	145.932	0.037				
12	158.225	1.001	R			
13	203.517	0.373				
14	204.466					
15	205.802	10.182	R			
16	220.144	0.064				
17	223.685	0.278	R			
18	256.813	0.125				
19	260.329	0.603				
20	268.126	0.323				
21	279.981	1.841	R			
22	289.500					
23	312.930	0.585	R			
24	313.822	0.076				
25	344.569	0.302				
26	359.954	0.611				
27	366.444	2.551	R			
28	385.699	0.507	R			

TABLE 3.2 (cont'd)

Resonance No.	E_n (keV)	Respar $g\Gamma_\gamma\Gamma_n/\Gamma$ (eV)		g	Monte Carlo Γ_n (eV)	Monte Carlo Γ_γ (eV)
29	410.204	1.336	R			
30	419.659	0.945				
31	420.500					
32	476.454	0.653	R			
33	489.085	0.326				
34	525.052	1.151	R			
35	545.497	0.867				
36	568.085	0.180				
37	585.622	0.948				
38	590.369	0.424				
39	597.000					
40	601.545	1.441				
41	648.090	3.288	R			
42	654.664	0.327				
43	703.975	1.271	R			
44	724.703	0.399				
45	760.908	2.120	R			
46	765.113	0.535				
47	774.055	0.578	R			
48	783.250	1.582	R			
49	820.264	1.364				
50	854.828	2.319	R			
51	862.689	0.725				
52	903.545	0.927				
53	915.664	1.939	R			
54	927.664	1.444				
55	938.244	1.819	R			
56	979.113	0.481				
57	1017.863	0.391				
58	1037.943	1.349				

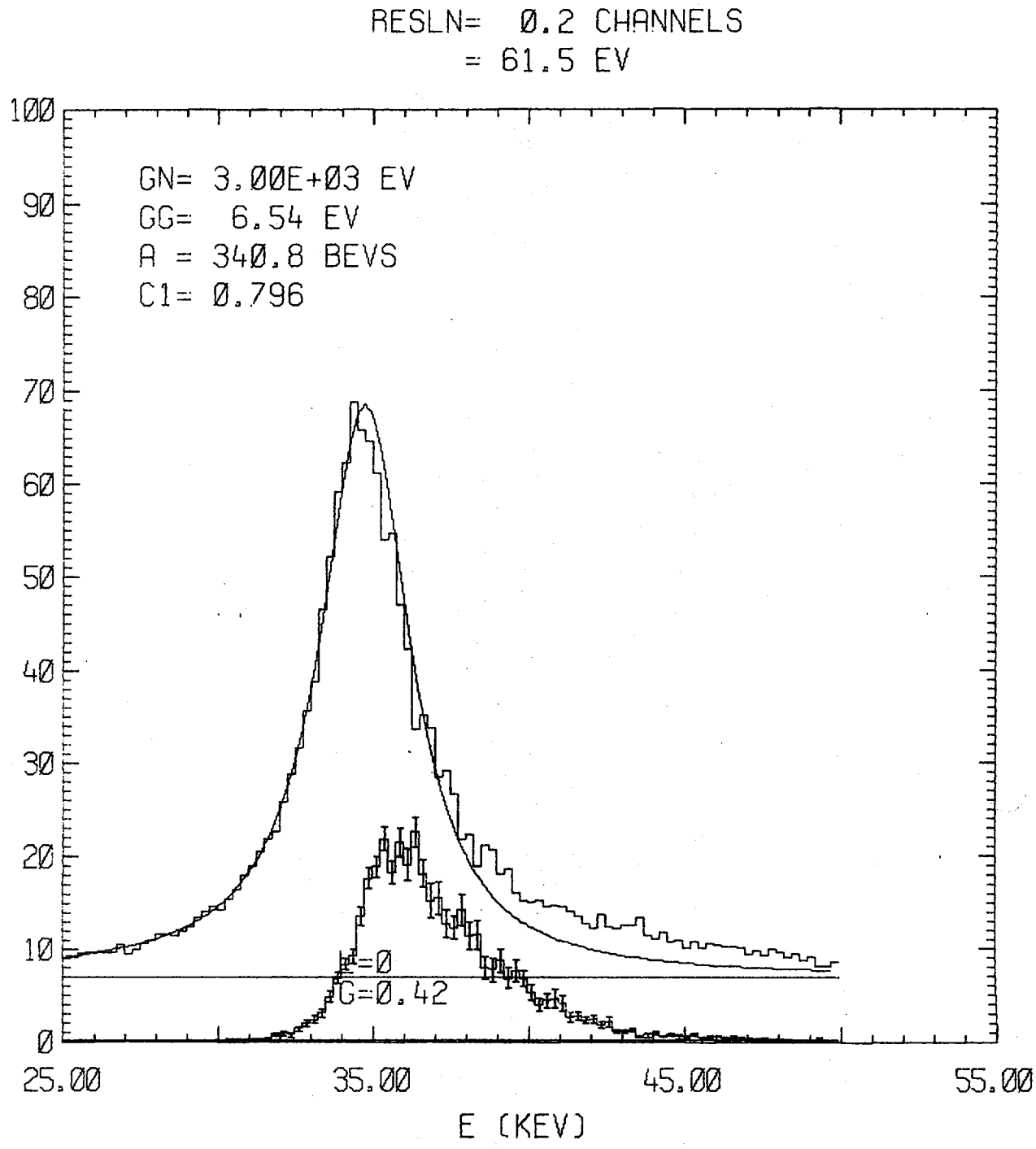

FIGURE 3.9 The ^{27}Al resonance at 35 keV indicating apparent asymmetry. Subtracted multiple scattering component is also shown.

keV Capture Resonances in $^{40}Ca(n,\gamma)$

As mentioned above, a number of d-wave capture resonances have been identified in ^{40}Ca. The argument began with our identification of the 90 keV resonance as a doublet and we assumed that the remnant was d-wave from its known ground state transitions (to $7/2^-$ in ^{41}Ca).

The evidence for this argument is provided by figure 3.10 where the group of points down near 3 keV must assuredly have $\Gamma_n << \Gamma_\gamma$. A standard Bayes' theorem analysis* of the Γ_n values extracted from these levels shows them to be 'almost certainly' d-wave (rather than p-wave). Figure 3.11 shows such an analysis for the 4.6 keV resonance with assumed parameters shown. This level has >90 per cent chance of being d-wave.

Figure 3.10 gives a preliminary plot of the ^{40}Ca values obtained to date. Known s-wave levels at 20, 90, 131, 169, 218, 250, 292, 330 and 356 are shown with large radiation widths of about what one might expect in this mass region. As expected, these are correlated with the reduced neutron widths in accordance with the simple capture mechanism described as the 'valence neutron model' where the incident s-wave neutron scatters from a single particle channel state directly to a final shell model P orbital. This behaviour is also seen in ^{138}Ba and other nuclei discussed in this section.

Of particular interest, however, in ^{40}Ca are resonances near 161, 186, and 290 keV which are seen as minute peaks in the high resolution (200 m station at ORELA) n,total data of Johnson** also taken at ORELA. In his analysis he presumed these to be d-wave and in the capture measurement we find strong evidence to support this conclusion since they have very large capture areas (κ > 1.0 eV). We extract a d-wave radiative width of ~600 meV for these large resonances ($\Gamma_n >> \Gamma_\gamma$) and are able to make some other d-wave assignments on this basis, noteably at 172, 214, 281, 322, 327, 340, 345 keV (not seen in n,total)).

---

*Musgrove, A. R., Allen, B. and Macklin, R. L. - keV Neutron Resonance Capture in ^{135}Ba - AAEC/E327 (in press)

**Johnson, C. - private communication (ORNL-DWG73-8791).

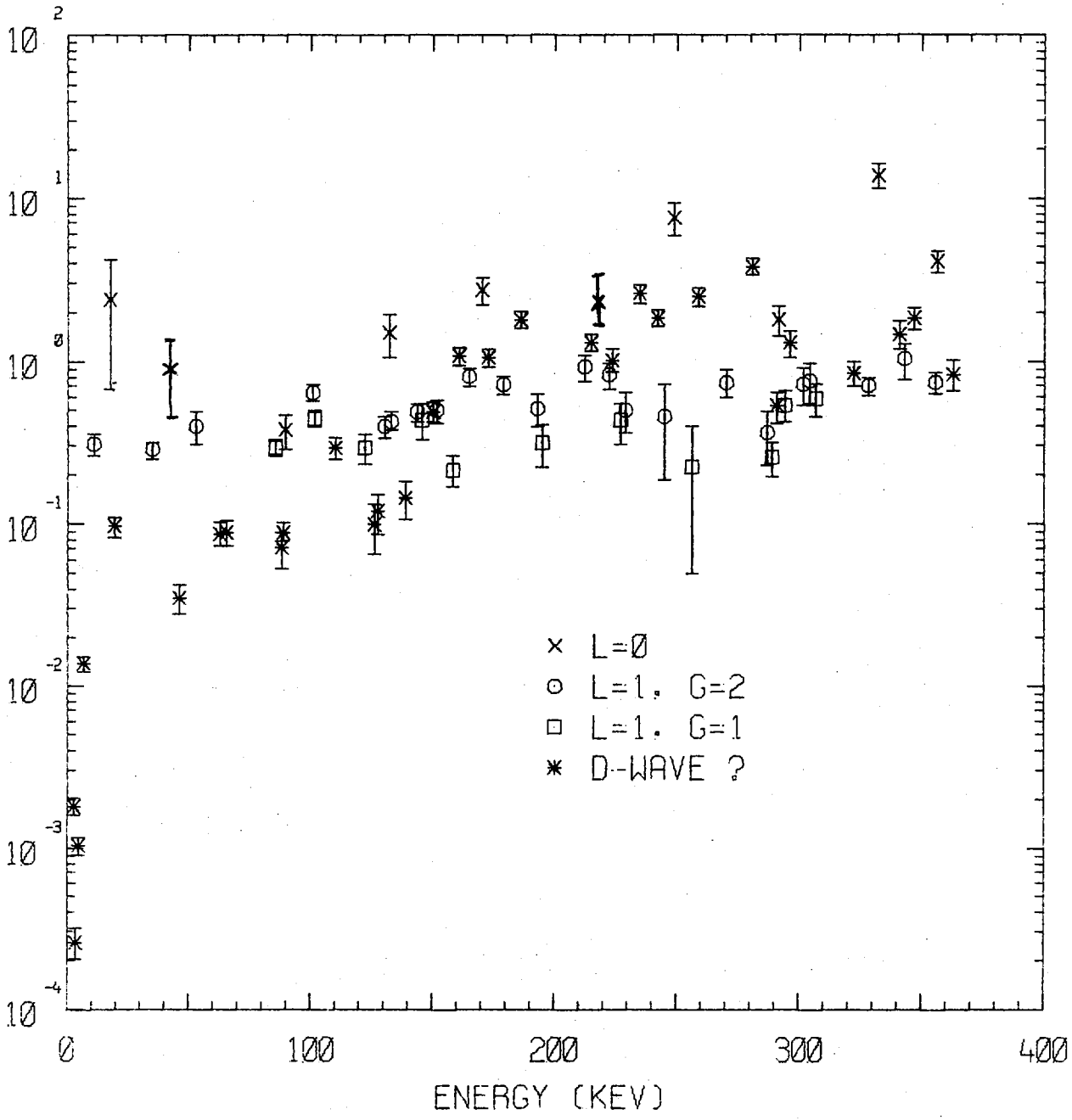

FIGURE 3.10 $g\Gamma_n\Gamma_\gamma/\Gamma$ for ^{40}Ca at energies <400 keV

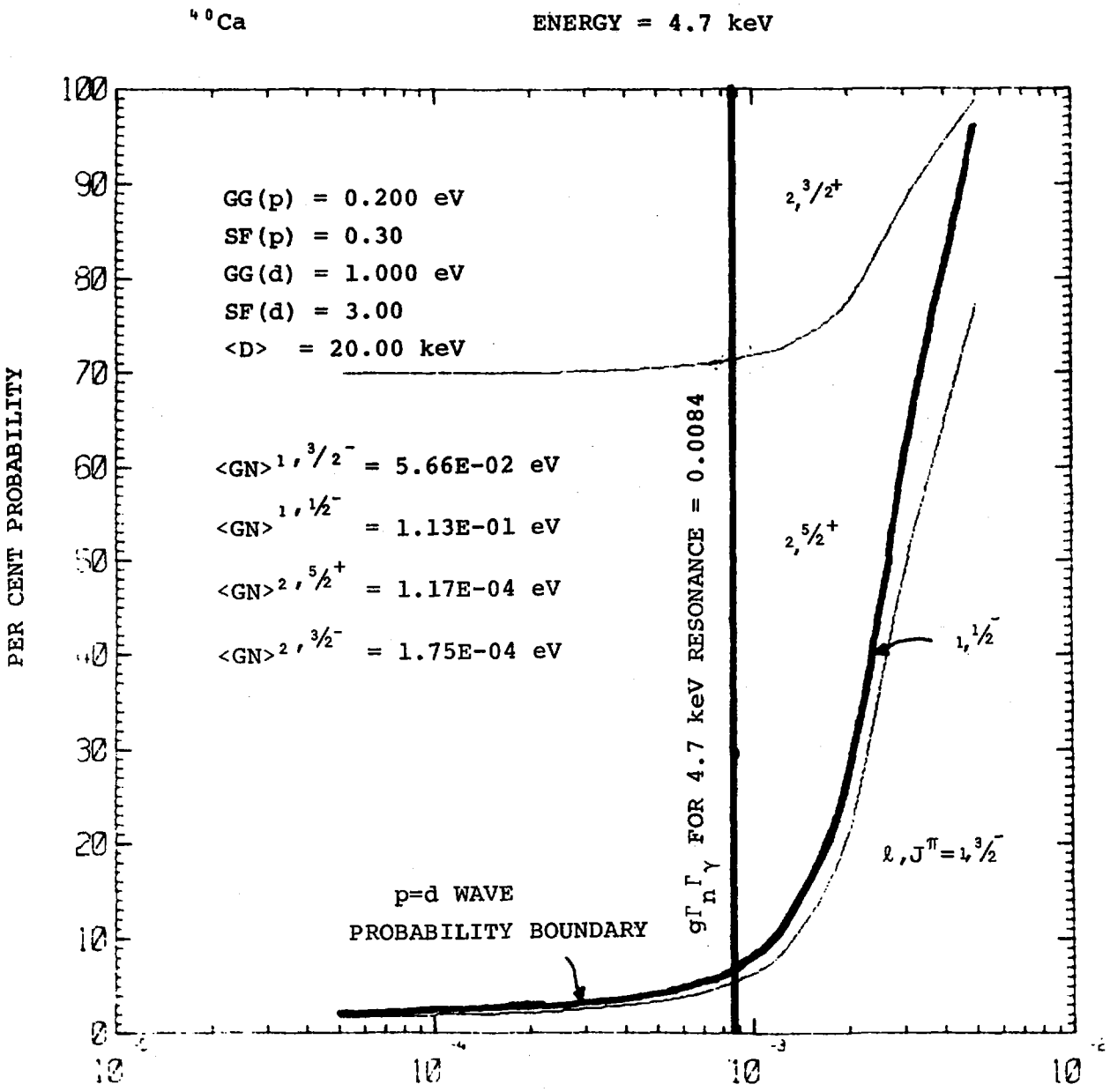

FIGURE 3.11 Analysis of relative a priori probabilities of each (ℓ,J) sequence for 4.7 keV ^{40}Ca resonance

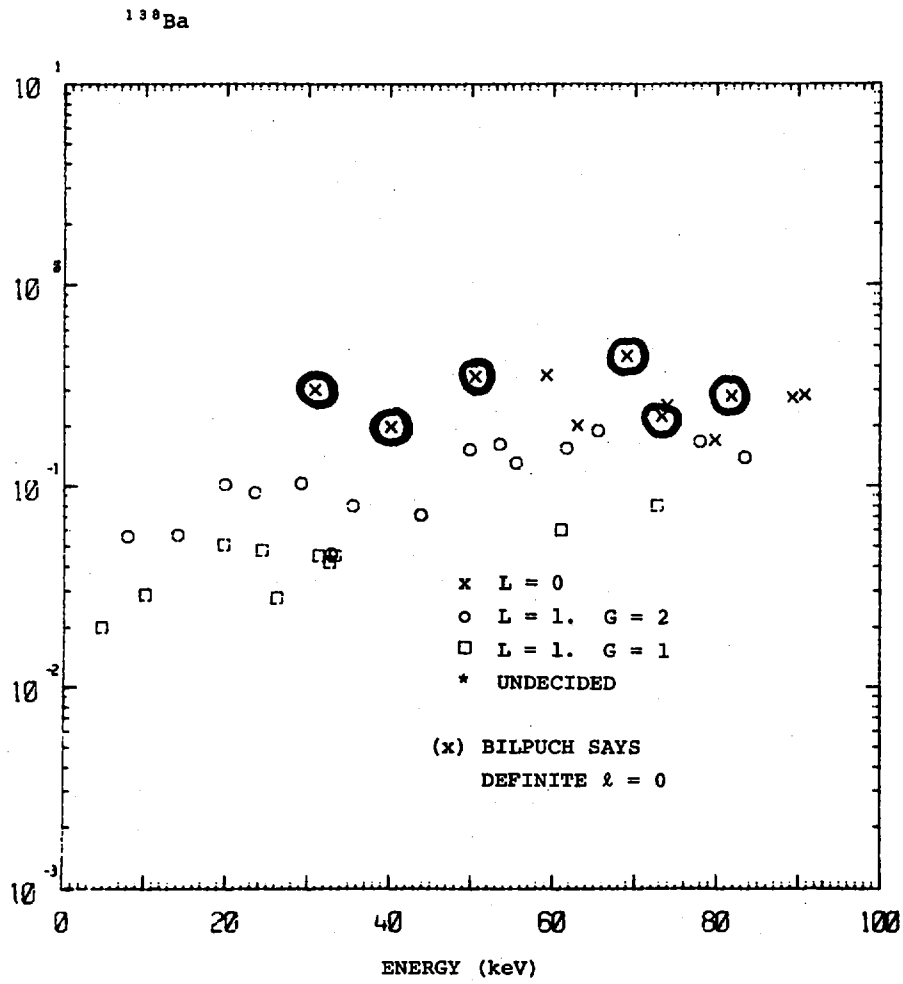

FIGURE 3.12 $g\Gamma_n\Gamma_\gamma/\gamma$ for ^{138}Ba for neutron energies between 3 and 95 keV

Neutron Capture in Chromium (Preliminary Data ^{50}Cr, ^{52}Cr)

The major s-wave resonances of ^{50}Cr occur at 5.603, 28.60 and 38.00 keV. Table 3.3 gives the energies and calculated values of $g\Gamma_n\Gamma_\gamma/\Gamma$ for these resonances and also for 22 p-wave resonances. For comparison purposes, figures obtained at RPI by Stieglitz et al. are also given.

Capture in ^{52}Cr is dominated by s-wave resonances at 50.180 and 98.045 keV. The figures for these two and also for 16 p-wave resonances are included in the second half of Table 3.3.

Although Monte Carlo calculations are not yet complete on most resonances, some preliminary observations can be made concerning agreement between ORELA and RPI data. Resonance energies nearly always agree within the experimental errors. The RPI data must be regarded as less accurate above 100 keV, because of flux fall off as shown by the larger errors quoted. Below 100 keV the systematic difference in energies, if it exists, is less than 50 eV in the direction of ORELA energies being higher.

Values of $g\Gamma_n\Gamma_\gamma/\Gamma$ while showing some fluctuations are generally lower by a factor of 2 to 4 for the ORELA data below 70 keV. Above 70 keV the ORELA figures (^{52}Cr) are high - possibly because of uncertainties in RPI data. In ^{50}Cr, no comparison is available above 70 keV.

Figure 3.13 shows the difference in resonance energy between ORELA and RPI measurements. Error bars are the quoted RPI figures plus 1 channel width for ORELA uncertainty.

Natural Zr Measurement

A comparison of capture data for the Zr isotopes obtained through ORELA measurements with capture data from RPI revealed almost total lack of agreement. In general the RPI results were larger (~factor of 2) although specific variations ranged from 0.5 to 10 for the ratio of the capture areas. Further, there has been some concern in other data about the accuracy of the ORELA Li reaction normalisation. Faced with these problems, the Zr data have been remeasured by R. L. Macklin using a natural Zr metal target. Special care was exercised during this measurement to ensure that all experimental conditions were understood and various efficiencies were repeatable. At this stage, the lower energy prominent resonances in ^{90}Zr have been analysed from the natural data. Table 3.4 presents a comparison of the original ^{90}Zr data and the ^{90}Zr data from the natural cross section. The agreement is particularly good and within 10 per cent. There may be a tendency for the natural data to be

TABLE 3.3

NEUTRON CAPTURE IN CHROMIUM (^{50}Cr, ^{52}Cr)

CHROMIUM-50							CHROMIUM-52						
E_{Res} (keV)		ΔE ORELA-RPI		$g\Gamma_n\Gamma_\gamma/\Gamma$			E_{Res} (keV)		ΔE ORELA-RPI		$g\Gamma_n\Gamma_\gamma/\Gamma$		
ORELA	RPI	keV	Within Error	ORELA	RPI	ORELA/ RPI	ORELA	RPI	ORELA	Within Error	ORELA	RPI	ORELA/ RPI
5.474	5.49±0.02	-0.016	Y	0.017	0.014	1.2	23.001	22.9 ±0.10	+0.1	Y	0.231	0.549	0.42
5.603	5.64±0.03	-0.037	N	1.709	3.10	0.6	27.655	27.6 ±0.11	+0.05	Y	0.261	0.734	0.36
9.325	9.30±0.03	+0.025	Y	0.025	0.053	0.5	31.711	31.6 ±0.12	+0.11	Y	0.118	0.384	0.31
18.675	18.6 ±0.08	+0.075	Y	0.320	0.660	0.5	33.993	33.99±0.13	+0.003	Y	0.139	0.431	0.32
24.94	24.8 ±0.10	+0.14	N	0.180	0.365	0.5	34.388	34.3 ±0.13	+0.088	Y	0.093	0.323	0.28
28.60	28.53±0.10	+0.07	Y	0.206	0		48.359	48.3 ±0.21	+0.059	Y	0.185	0.829	0.23
33.55	33.4 ±0.12	+0.15	N	0.485	0.992	0.5	50.18	50.2 ±0.3	-0.02	Y	1.186	1.16	1.0
35.56	35.3 ±0.13	+0.26	N	0.903	1.650	0.55	57.811	57.8 ±0.28	+0.09	Y	0.432	0.537	0.8
38.00	37.3 ±0.2	+0.7	N	2.368	2.50	0.95	79.25	79.2 ±0.6	+0.05	Y	0.024	0.194	0.1
40.74	40.6 ±0.15	+0.14	N	0.412	0.884	0.5	98.05	97.1 ±0.8	+0.9	N	6.137	4.80	1.3
50.20	50.1 ±0.25	+0.1	Y	0.344	0.596	0.57	106.5	107.0 ±0.8	-0.5	Y	0.545	0.341	1.6
53.75	53.7 ±0.27	+0.05	Y	0.431	0.719	0.60	111.9	111.0 ±0.9	+0.9	Y	0.813	0.241	3.4
55.33	55.3 ±0.3	+0.025	Y	0.178	0.88	0.2	113.2	113.0 ±0.9	+0.16	Y	0.348	0.512	0.7
59.35	59.7 ±0.3	-0.35	N	0.563	1.12	0.5	115.3	116.0 ±1.0	-0.74	Y	0.160	0	
63.48	63.4 ±0.4	+0.075	Y				123.1	123.2 ±1.0	-0.1	Y	1.017	0.504	2.0
64.98	65.1 ±0.4	-0.125	Y				130.8	132.0 ±1.2	-1.2	Y	0.897	0.441	2.0
66.03	66.0 ±0.43	+0.025	Y				139.7						
68.43	69.2 ±0.45	-0.775	N				153.3	155.0 ±1.2	+1.75	N	0.635	0.372	1.7
70.50	70.5 ±0.46	0	Y				165.1	168.0 ±1.3	-2.9	N	0.745		
73.50	73.5 ±0.48	0	Y										
78.00	77.8 ±0.52	+0.2	Y										
79.33	79.4 ±0.53	-0.075	Y										
90.60	90.7 ±0.63	-0.1	Y										
129.8	130.5 ±1.0	-0.7	Y										
187.4	188.8 ±1.5	-1.4	Y										

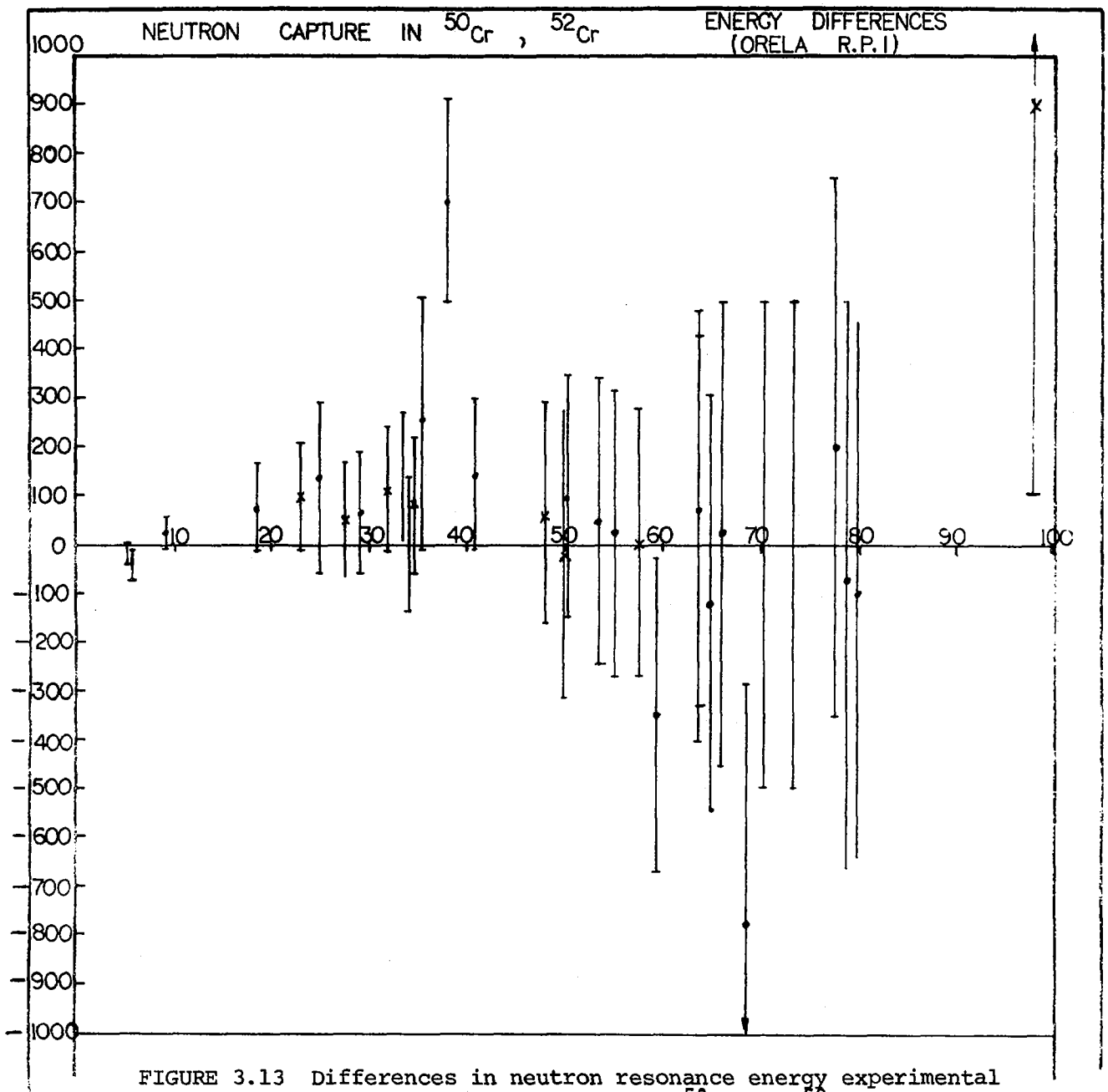

FIGURE 3.13 Differences in neutron resonance energy experimental versus resonance energy for ^{50}Cr and ^{52}Cr

slightly higher by 10 per cent.

It is planned to proceed with the analysis of resonances in the other Zr isotopes which should provide a good check of self shielding and multiple scattering corrections in the analysis procedure.

TABLE 3.4

Resonance Energy (keV) ^{90}Zr data	Γ_γ (eV) ^{90}Zr data	Γ_γ (eV) Nat_{Zr}	Γ_n (eV)	ℓ	g
3.864	0.074	0.084	10.0	0	1
4.014	0.217	overflowed	0.5	1	1
7.271	0.185	0.174	4.0	1	2
8.869	0.242	0.279	6.0	1	1
16.919	0.136	0.138	1.7	1	1
19.123	0.098	0.115	4.5	1	2
19.738	0.327	0.374	22.5	1	1
28.885	0.184	0.181	1.2	1	2
35.394	0.691	0.75	18.0	0	1
41.423	1.413	1.6	260.0	1	2

Evaluation of Resonance Parameters

A program to analyse and evaluate resonance parameter information has been written. It is discussed here with reference to the recently completed analysis of $^{138}Ba(n,\gamma)$.

For $^{138}Ba(n,\gamma)$ some 38 peaks in the region 3 to 95 keV were identified and were compared with an early measurement of the (n,total) cross section by Bilpuch et al.* Table 3.5 gives the final resonance parameters obtained in the analysis, while figure 3.12 shows a plot of $\kappa = g\Gamma_n\Gamma_\gamma/\Gamma$, for the resonances identified. Those resonances assigned as definitely s-wave by Bilpuch are indicated and a consideration of this plot allows further s-wave levels to be assigned on the basis of their having $\Gamma_\gamma \sim 300$ meV. For these peaks Bilpuch was unable to detect an interference dip in the (n,total) cross section.

*Bilpuch, E. G., Seth, K. K., Bowman, C. D., Tabony, R. H., Smith, R. C. and Newson, H. W. - Ann. Phys. 14, 387 (1961).

The remainder are probably p-wave resonances although we have made no concerted effort to prove statistically that they are not $\ell > 1$, as was done in ^{40}Ca. The reason here is simply that we find no evidence of a nice separation of the various $\ell > 1$ waves as was found in ^{40}Ca, and hence assignment to either p or d-wave sequences would be impossible. It is likely that $\Gamma_n > \Gamma_\gamma$ for these levels and if so, they have an average p-wave radiation width of about 45 meV (i.e. also a factor of 7 down on the s-wave Γ_γ). If we examine the (n,total) data more closely, we see a number of small peaks below 30 keV which were not analysed by Bilpuch et al. These appear to correlate in position with some of our p-wave levels and hence we are confident that to have been seen in a low resolution total measurement, they must have $\Gamma_n > 0.05$ eV. We have assumed all the levels in this region similarly have $\Gamma_n > \Gamma_\gamma$. Tentative g assignments have been made somewhat boldly, since the $g\Gamma_\gamma$ values extracted from the area analysis seem to fall into two groups. However, it should be noted that there is a rather quick energy dependent increase in the p-wave widths and at this stage it does not seem possible to rule out instrumental effects entirely.

Figure 3.14 shows a different sort of plot provided by the analysing program. The asterisks represent the Γ_n^o values of the s-wave levels which are correlated with their radiative widths as can be seen. The correlation coefficient between Γ_n^o, Γ_γ is 0.45, which for 12 levels in the sample is just significant. Once again, the magnitudes of the observed s-wave radiation widths are very well explained in terms of the valence neutron model*.

In figures 3.15 and 3.16 we have tested both the s-wave and the p-wave reduced widths against the Porter-Thomas distribution. In figure 3.15 $\langle\Gamma_n^o\rangle$ has been fixed at S_0 x $\langle D\rangle$ since both these quantities are determined separatly from staircase plots. The number of levels present (integer) is fitted and indicates that one level may have been missed in the range. Since our first s-wave level occurs at 31 keV, it may well be that a small s-wave level is misassigned with $E_r < 31$ keV and, if so, the correlation coefficient already discussed would increase somewhat, since all of these levels have small radiation widths and neutron widths. Also, there must be a fairly large s-wave level near thermal energies to account for the thermal (n,γ) cross section of 350 mb. This would also account for the thermal capture spectrum

---

*Lane, A. M. - private communication.

which shows strong lines to final p-wave states*. In figure 3.16 the two p-wave populations are tested with an option which allows a free fit to both $\langle\Gamma_n^\ell\rangle$ and N. It is also possible to fix $\langle\Gamma_n^\ell\rangle$ to some other (read in) value and fit only to N.

Next, a routine test is made for the s and p-wave level spacings against the Wigner distribution. We never find sufficient levels in either population to pursue statistical tests to higher sophistication as the Columbia group does, and we are generally content if a visual inspection of this test does not disclose gross discrepancies.

Finally, the experimental capture cross section is calculated by summing up the resonance capture areas, while errors in the average cross section are added in three separate categories; statistical errors, self-shielding errors and overall normalisation errors. In different energy regions, one or other of these errors may dominate the final cross section error. A comparison of the experimental cross section is then made with the usual statistical model cross section calculation using estimates for the average quantities involved, provided by the program.

This analysis program is currently being improved and can now also deal with fissioning nuclei.

Further calculational options are available and briefly these are:

(a) Bayes' Theorem Analysis

Already described, and see AAEC/E327.

(b) Correlation Analysis

Calculates the correlation coefficient between Γ_n^ℓ and Γ_γ using randomly sampled Γ_n values and by calculating a valence contribution to Γ_γ. The compound nucleus part is allowed to have a Gaussian distribution and up to three separate valence contributions can be considered. The effect of missing levels can also be studied.

(c) Valence Capture Statistical Capture Cross Sections

This calculates the effect of having a

---

*Groshev, L. V. Dvoretskii, V. N., Demidov, A. M. and Al'vash, M. S. - Sov. Nuc. Phys. 10, 392 (1970).

**Musgrove, A. R., Allen, B. J. and Macklin, R. L. - AAEC/E327 (1974).

$$\sqrt{\Gamma_\gamma} = a\,\Gamma_n^o + b$$

rather than the usual

$$\langle\Gamma_\gamma\rangle = b$$

on the statistical model capture cross section. The calculation is Monte Carlo in nature and will eventually assist in updating the AAEC data library.

(d) Wald-Wolfowitz Statistical Test

This is used to test for energy dependent structure in Γ_n^ℓ or Γ_γ obtained in our analyses. This test is particularly simple to apply and can be found described in application in AERE-R6633.

Valence Component in the Neutron Capture Cross Section of ^{90}Zr

A total of 102 resonances have been identified in the capture cross section of ^{90}Zr between 3 and 200 keV. By comparison of the present data with the total cross section and inverse $^{91}Zr(\gamma,n)$ data from Toohey and Jackson*, complete resonance parameters have been extracted for 40 $p^3/_2$, 9 $p_{\frac{1}{2}}$ and 16 s-wave resonances. The relevant neutron strength functions extracted from the resonance parameters are $S_0 = 0.55 \times 10^{-4}$, $S_1 = 2.5 \times 10^{-4}$, $S_1\ (p^3/2) = 3.55 \times 10^{-4}$ and $S_1\ (p_{\frac{1}{2}}) = 1.25 \times 10^{-4}$. It is noteworthy that strength function is significantly larger than the $S_1\ (p_{\frac{1}{2}})$ strength function in agreement with early theoretical predictions. From Porter Thomas fits to the reduced neutron widths it is observed that there is an excess of $p3/_2$ levels and less $p_{\frac{1}{2}}$ levels than expected from statistical theory.

A significant correlation (p = 0.59) exists between the reduced neutron widths and the radiative widths for the 40 $p^3/_2$ resonances. The data are therefore a very strong confirmation of the Valence Neutron Model (e.g. Lynn 1968). With standard valence theory all radiative widths can be calculated approximately from the associated reduced neutron width. To explain the measured correlation coefficient, it has been necessary to include with the valence component an enhanced ground state transition uncorrelated with the valence neutron width. These enhanced ground state transitions have been

---

*Toohey, R. E. and Jackson, H. E. (1974) - Phys. Rev. C 9, 346.

observed in other capture studies, notably the resonance capture gamma ray spectra from ^{56}Fe. A possible theoretical explanation for the enhanced compound nucleus transition is presented.

The average capture gamma ray spectron for neutron capture in ^{90}Zr between 2 to 80 keV has been calculated from the Valence Model and the present data and found to be in very close agreement with experimental data taken by Pattenden (Bird et al.*)

---

*Bird, J. R., Allen, B. J., Bergqvist, J. and Biggerstaff, J. A. (1973) - Nuclear Data Tables, Vol. 1, No. 6.

TABLE 3.5

RESONANCE PARAMETERS FOR ^{138}Ba

^{138}Ba: Radius = 5.80f, Target Spin = 0: E = 3-91 keV

Resonance	Energy (keV)	$g\Gamma_n\Gamma_\gamma/\Gamma$ (eV)	Capture Area (beV)	Error % (self shielding statistical)	ℓ	g_J	Γ_n (eV)	Γ_γ (meV)	Γ_n^0 (eV)	Γ_n^1 (eV)	Bilpuch et al.(1961) E (keV)	Bilpuch et al.(1961) Γ_n (eV)	Comments
1	4.714	0.020	17.8	(30,2)	1	(1)	-0.5	21± 5		-0.96			Γ_n = 1 looks too wide
2	7.867	0.056	29.2	(10,3)	1	(2)	5 ± 2	28±3		-4.5			
3	9.956	0.033	13.9	(10,4)	1	(1)	2 ± 2	34±3		-1.3			
4	14.04	0.067	19.7	(10,4)	1	(2)	≤5 (3)	34±3		-1.0			
5	19.70	0.042	8.8	(10,7)	1	(1)	(1) ≤10	43±3		-0.3	peak seen here in Bilpuch data		∴we assume $\Gamma_n \gg \Gamma_\gamma$
6	19.90	0.099	20.7	(5,5)	1	(2)	(7.5)	50±2		-1.7			(Γ_n) values used are estimates only
7	23.44	0.092	16.4	(6,6)	1	(2)	(10)	46±3		-1.8	3 peaks seen in this region and not analysed by Bilpuch		Γ_n and g values estimated only
8	24.30	0.045	7.7	(6,13)	1	(1)	(5)	46±3		-0.8			
9	26.24	0.028	4.4	(5,17)	1	(1)	(1)	28		-0.1			
10	29.25	0.100	14.2	(5,9)	1	(2)	(5)	50		-0.6	Slight evidence of this peak in Bilpuch data		
11	30.91	0.349	46.8	R(7,5)	0	1	225±50	350±25	1.28		31.7S	190±20	
12	31.31	0.050	6.6	(5,16)	1	(1)	(5)	50		-0.6			

TABLE 3.5

Resonance	Energy (keV)	$g\Gamma_n\Gamma_\gamma/\Gamma$ (eV)	Capture Area (beV)	Error % (self shielding statistical)	ℓ	g_J	Γ_n (eV)	Γ_γ (meV)	Γ_n^0 (eV)	Γ_n^1 (eV)	Bilpuch et al. (1961) E (keV)	Bilpuch et al. (1961) Γ_n (eV)	Comments
13	32.63	0.042	5.3	(5,20)	1	(1)	(1)	44		0.1	32.5?	28±12	Bilpuch Γ_n value for assumed ℓ=0. g=1. This pair presumably have different g values (Wigner spacing law)
14	32.83	0.041	5.2	(5,20)	1	(2)	(10)	20		1.0			
15	33.35	0.044	5.4	(5,25)	1	(1)	(1)	44		-0.1			Resonances 12-15 all have approx. equal $g\Gamma_n\Gamma_\gamma/\Gamma$ but are surely not all g=1
16	35.42	0.083	9.7	(5,20)	1	(2)	(10)	41		-1.0	36.5	28± 12	Either resonance 35.4 or 36.6 may correspond. Almost certainly doublet in our data.
17	36.6		4.9	(,50)									
18	40.25	0.250	25.8	R(5,10)	0	1	150±50	250±10	0.75		39.8S	100±10	
19	43.75	0.077	7.3	(5,25)	1	(2)	(5)	39		-0.4			Marginal trace in Bilpuch data
20	49.86	0.139	11.6	(5,15)	1	(2)	(5)	71		-0.3			
21	50.4	0.322	26.5	R(5,11)	0	1	250±50	325±25	1.11		51S	275±50	
22	51.3	0.069	5.6	(5,31)	1	(1)	(1)	73		-0.05			
23	53.4	0.145	11.3	*(5,21)	1	(2)	10	73		-0.5	53.5	30±25	We prefer ℓ =1, g=2 ∴Γ_n = 10 eV for this

TABLE 3.5 (cont'd)

Resonance	Energy (keV)	$g\Gamma_n\Gamma_\gamma/\Gamma$	Capture Area (beV)	Error % (self shielding statistical)	ℓ	g_J	Γ_n (eV)	Γ_γ (meV)	Γ_n^0	Γ_n^1	Bilpuch et al. (1961) E (keV)	Bilpuch et al. (1961) Γ_n (eV)	Comments
24	55.5	0.157	11.8	*(5,18)	1	(2)	20	79		-1.0	55.5	50±30	As above; Γ_n = 20 eV
25	59.1	0.456	32.1	*(5,10)	0	1	70	460±15	0.29		59.5	70±30	Unresolved. Assumed ℓ=0 because of $g\Gamma_\gamma$ and used Bilpuch value of Γ_n.
26	61.0	0.078	5.3	*(5,32)	1	(1)	(5)	80		-0.6	61	60±40	This is a doublet so have assumed Γ_{n1}=5, Γ_{n2}=20 eV
27	61.6	0.153	10.3	*(5,23)	1	(2)	(20)	76		1.7			
28	63.0	0.181	11.9	R(5,20)	0	1	100±50	180±10	0.40		62.5	130±40	Just resolved
29	65.5	0.180	11.4	(5,14)	1	(2)	(5)	94		-0.2			Seen but not reported by Bilpuch
30	69.0	0.589	35.4	R(2,10)	0	1	400±100	587±80	1.52		68.5S	460±40	
											70 ?	50±40	We do not see this one directly
31	72.9	0.175	10.0	(5,21)	1	(2)	(5)	86		-0.2			Marginal trace in Bilpuch data
32	73.3	0.142	8.0	(5,20)	1	(1)	(10)	138		-0.4	73.5S	130 40	Resolved doublet large $g\Gamma_\gamma$ and .·. we say ℓ=0.
33	74.0	0.247	13.9	S?(5,18)	0	1	100	245±10	-0.04				

TABLE 3.5

Resonance	Energy (keV)	$g\Gamma_\gamma\Gamma_\gamma/\Gamma$ (eV)	Capture Area (beV)	Error % (self shielding statistical)	ℓ	g_J	Γ_n (eV)	Γ_γ (meV)	Γ_n^0 (eV)	Γ_n^1 (eV)	Bilpuch et al. (1961) E (keV)	Bilpuch et al. (1961) Γ_n (eV)	Comments
											76.5	50±30	We do not see this one and too large ΔE to correspond with our 78 keV resonance
34	78.0	0.209	11.1	(5,22)	1	(2)	(10)	103		-0.30			
35	79.8	0.225	11.7	R?(5,24)	0	1	(150±50)	150±10	0.53		79.3S	160±40	
36	81.8	0.315	16.0	S?(2,15)	0	1	20	320±20	0.07		81S?	≤30	Bilpuch not sure of ℓ. We say ℓ =0 from $g\Gamma_\gamma$
37	83.5	0.221	11.0	(5,26)	1	(2)	(10)	.109		-0.3	84S?	<30	We assume ℓ = 1, g = 2 from $g\Gamma_n\Gamma_\gamma/\Gamma$. This gives Γ_n < 10 eV
											86.5S?	<30	We do not see this level
38	89.4	0.332	12.8	S?(5,16)	0	1	~20	338±20	~0.07		88S?	<30	We say ℓ= 0 from $g\Gamma_\gamma$
39	90.9	0.284	13.0	S?(5,20)	0	1	~20	288±10	~0.07		91S?	<30	Bilpuch not sure of ℓ. We say ℓ = 0 from $g\Gamma_\gamma$

We have also tried to see the peaks reported by Bilpuch et al. for E_n > 100, but although some structure is evident, statistical errors and especially background subtraction errors make analysis fruitless.

TABLE 3.5 (cont'd)

NOTES

Reference:

Bilpuch, E. G., Seth, K. K., Bownman, C. D., Tabony, R. H., Smith, R. C. and Newson, H. W. - Ann. Phys. 14, 387, 1961.

S after their resonance energy indicates Bilpuch et al. are definite resonance $\ell = 0$

S? after their resonance energy indicates Bilpuch et al. have analysed the resonance as $\ell = 0$, $g = 1$, but ℓ assignment uncertain.

? after their resonance energy indicates Bilpuch et al. not sure of existence of this peak as separate resonance.

Our Comments

R We resolve this resonance (i.e. we perform shape + area analysis).

R? Getting close to the limit of our resolution.

S? We assign these as $\ell = 0$ because they have $g\Gamma_\gamma$ of order 300 meV (i.e. $>> g\Gamma_\gamma$ (p-wave).

* Unresolved resonances and we use Bilpuch's Γ_n values in area analysis program.

(Γ_n) Γ_n value assumed for our analysis program.

(g_J) g_J value assumed for area analysis program. The p-wave population separates quite nicely into two populations if we assume $\Gamma_\gamma(p)$ independent of J.

Errors

The self shielding and multiple scattering error is due to the error in Γ_n.

Statistical error quoted is derived from measurement.

The error quoted on Γ_γ is due solely to lack of knowledge of Γ_n and therefore the self shielding correction factor.

NO ERRORS IN ABSOLUTE NORMALISATION ARE INCLUDED IN THIS TABLE ANYWHERE

From the normalisation to $^{181}Ta(n,\gamma)$ we estimate the overall normalisation error of our cross section (and therefore of $g\Gamma_n\Gamma_\gamma/\Gamma$) to be about 15%.

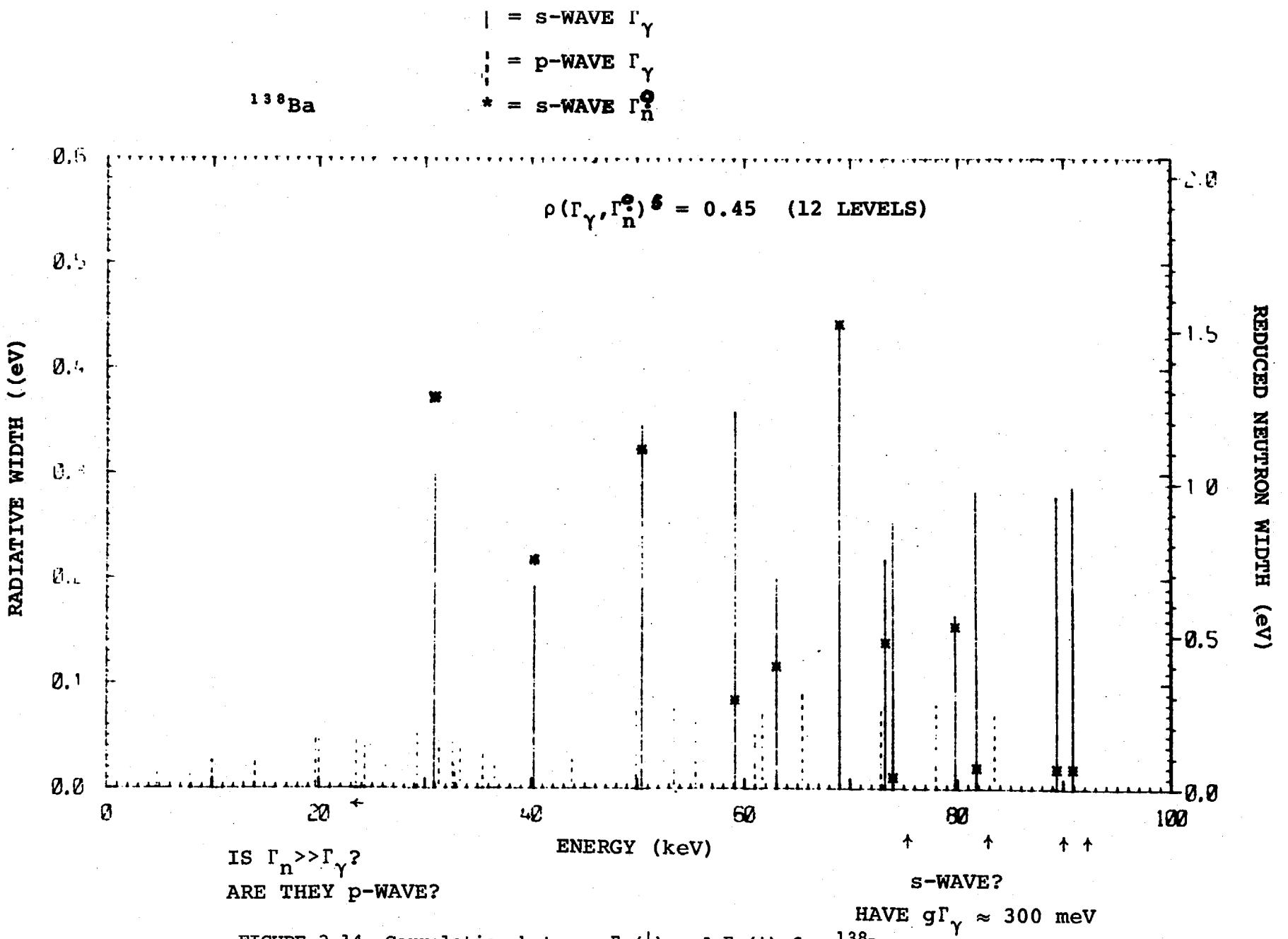

FIGURE 3.14 Correlation between Γ_γ(|) and Γ_γ(*) for ^{138}Ba s-wave resonances

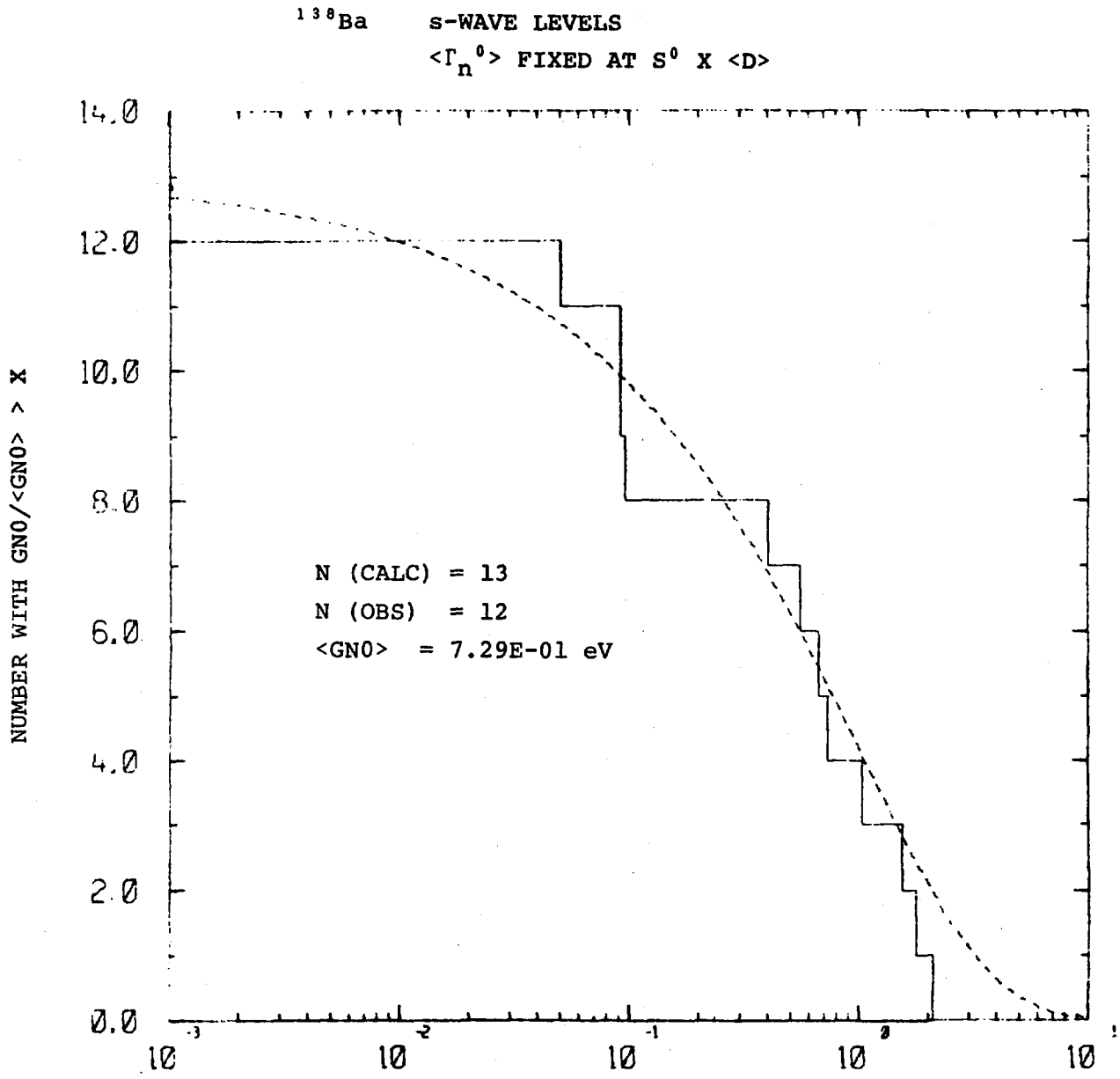

FIGURE 3.15 Porter-Thomas fit to ^{138}Ba s-wave population with $\langle\Gamma_n^0\rangle$ constant and estimated N

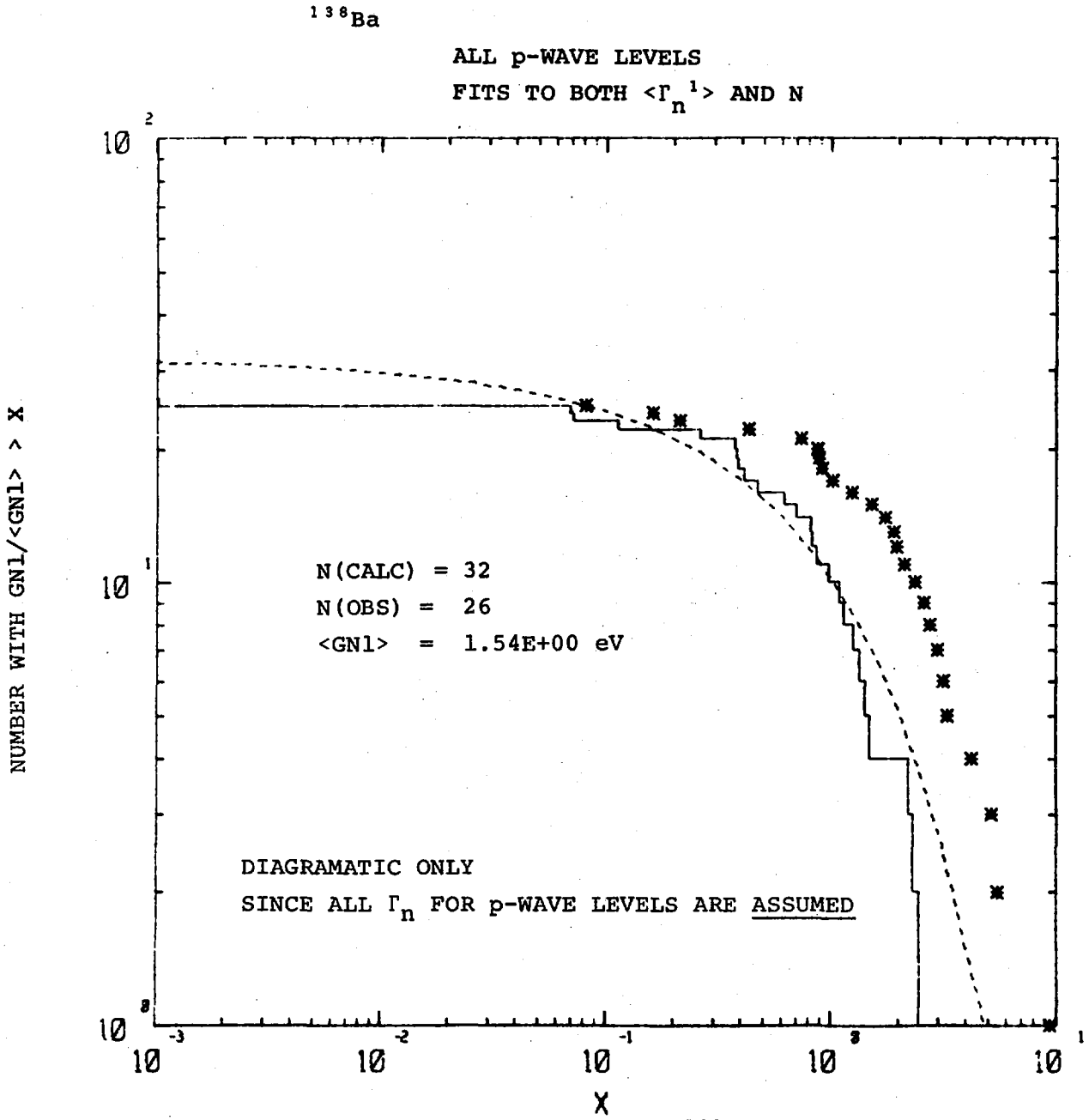

FIGURE 3.16 Porter-Thomas fit to ^{138}Ba p-wave reduced neutron widths $\langle\Gamma_n^1\rangle$ and adjusted N

4.1 THEORETICAL PHYSICS

AUS Modular Scheme (B. Clancy, B. Harrington, J. Pollard, G. Robinson)

The suite of AUS modules used for reactor calculations on the site IBM 360/50 has been continued to be checked out against both benchmark type as well as real reactor type systems. The tedious checking out has resulted in minor improvements to some of the modules.

AUS Module MIRANDA and Cross Section Library

Development of the MIRANDA module has continued. Some minor modifications have been made to the resonance treatment and the preparation of group resonance integrals from homogeneous PEARLS calculations has been improved. The comparison of the numerical slowing down code PEARLS and MIRANDA for ^{238}U captures in simple 2-region cylindrical geometry has therefore been repeated. The results of this comparison are given in Table 4.1. It can be seen that the agreement is excellent with errors exceeding 1 per cent only for the larger 8 cm diameter metal rods.

Some work was begun on the comparison of MIRANDA with integral experiments using the GYMEA cross section library, but this has been postponed until a new ENDFB based library is prepared. The ENDFB based library contains 128 group data which should be suitable for fast as well as thermal reactors. Resonance scatterers such as Na and Fe are represented by subgroup parameters and are treated in MIRANDA in a similar fashion to fuel nuclides. Most of the required modifications to MIRANDA have been made. Non-resonance data has been extracted from the ENDFB data file using the ORNL code SUPERTOG, but resonance data requires a special treatment. The general approach adopted for resonance data is to generate point cross sections, run a series of PEARLS calculations and fit the resulting group resonance integrals with subgroup parameters. A program to generate point data in the resolved resonance region has been written and used to prepare data for Na, Fe, Cr and Ni. Methods suitable for the unresolved resonance region are to be developed. A large number of subsidiary programs necessary to prepare the new library have been written. An AUS library containing ENDFB derived data for most of the important isotopes and data from the GYMEA library for other isotopes will be available shortly.

The Fast Spectrum Code MURAL

The MURAL code which calculates a detailed flux distribution within a fast reactor lattice cell has been obtained from Britain and commissioned on the site computer. The 2000 group data library FGL5U containing unadjusted

TABLE 4.1

COMPARISON OF RESONANCE CAPTURES IN ^{238}U

Radius in cm		PEARLS	MIRANDA Error %	PEARLS	MIRANDA Error %
Fuel	Moderator				
Metal Fuel		D_2O Moderator		Graphite Moderator	
0.5	1	0.6229	+0.2	0.9556	+0.4
0.5	2	0.2168	+0.1	0.5256	+0.8
0.5	4	0.05882	0.0	0.16667	+0.3
0.5	8	0.01493	0.0	0.04408	+0.1
0.5	16	0.003742	0.0	0.01117	+0.1
0.5	32	0.000936	+0.1	0.002802	0.0
1	2	0.5710	+0.3	0.9287	+0.7
1	4	0.1729	+0.0	0.4366	+0.8
1	8	0.04467	-0.1	0.12814	+0.2
1	16	0.01123	-0.1	0.03329	-0.1
1	32	0.002813	-0.2	0.008402	-0.1
2	4	0.5027	+0.6	0.8818	+1.0
2	8	0.1356	+0.2	0.3546	+0.8
2	16	0.03416	+0.0	0.09896	+0.2
2	32	0.008554	+0.0	0.02541	0.0
4	8	0.4236	+1.4	0.8103	+1.4
4	16	0.1054	+1.1	0.2840	+1.5
4	32	0.02620	+1.0	0.07647	+1.1
Oxide Fuel		H_2O Moderator			
0.5	0.7071	0.24660	-0.5		
0.5	1.0	0.10296	-0.4		
0.5	1.4142	0.04604	-0.3		

cross sections was also provided. The code supplied was an interim version. A detailed study of many sections of the code was therefore made and a revised version written. The cross section output from the code was also made compatible with the AUS modular scheme. The resultant code has been tested on a range of clean critical experiments on the ZPR3 facility. The results obtained were quite satisfactory. In particular, the discrepancies in k_{eff} were less than 2 per cent which is about the expected accuracy with this data.

4.2 REACTOR CALCULATIONS (B. McGregor, B. Harrington)

Three computer codes were compared to determine their usefulness in analysing a pulsed neutron experiment. The codes involved were a Monte Carlo code, MORSE, a diffusion kinetics code, POW, and a time dependent SN code, TDA.

A series of three test problems were devised to progressively model the experiment. All problems assumed a spherical system with an isotropic source. The first problem had a single energy group source for the first nanosecond only; the second problem had a multigroup energy source, still for the first nanosecond only; the third problem had a time and energy group dependent source.

POW and MORSE were shown to be in good agreement with significant differences only occurring at times when the system did not correspond with the approximations made in POW.

Our version of the TDA code did not handle a time dependent source. There was also a tendency for the results beyond 50 ns to be higher than the other two codes for the problems with a source constant over one time interval.

Time Dependent Spectra in Thorium Stack

The MORSE Monte Carlo code with combinational geometry has been used to look at the geometrical and other effects which can not be treated in simple analyses of the pulsed neutron experiments. Essentially two systems are being studied with MORSE. In the simple system the experiment is represented as a solid sphere with a symmetric source and with neutron scattering treated as P0 with a transport approximation. In the complex system the experiment is treated as a cube with a cylindrical hole through the centre. The source is asymmetric and neutron scattering is treated with a P3 approximation. The detectors are located at the correct orientation to the axis of the source deuterons.

Monte Carlo Codes

KENO, a Monte Carlo criticality code, has been used for calculations of critical facility configurations. An interesting discrepancy was found between KENO and POW (2-dimensional diffusion) calculations of the MOATA mockup. The KENO calculated k_{eff} was about 1.5 per cent higher than the diffusion theory result with a standard deviation of about 0.5 per cent. Differences of a few per cent in the volume averaged fluxes were also observed. A more detailed comparison is being undertaken for the POW calculations of the planned second critical configuration. The AUS transport theory module AUAUSN will be included in the comparison.

While running the comparisons with POW a problem with the use of albedos in KENO occurred. Help has been sought from the code authors at ORNL.

4.3 MULTIGROUP DATA

Condensation of Multigroup Cross Section Data Sets (I. J. Donnelly)

Several 100 group neutron cross section data sets suitable for shielding calculations are available at AAEC. However, for many calculations, fewer groups are required because of computing considerations, so the 100 groups are condensed to a fewer group structure. The condensation procedure usually consists of taking a weighted average of the cross sections over the new group structure and the accuracy of this procedure depends on the weighting function chosen.

The following program has been set up to investigate several possible condensation procedures. The quantity evaluated was the neutron penetration through thick slabs of water and iron. A fission source of neutrons was assumed on the left hand side (at x = 0) of the slab and the neutron dose through the slab was calculated using the transport code ANISN and the 104 neutron groups of the cross section library DLC-9. These cross sections were then condensed to 29 neutron groups using the following flux spectra as weighting functions:

1. ϕ_A, the flux arising from an infinite homogeneous fission source in the slab material.
2. ϕ_B, the flux near the fission source in the slab.
3. ϕ_C, the flux halfway through the slab, at x = 50 cm in water and x = 30 cm in iron.

These condensed cross section sets were used to calculate the neutron dose through the slab and the results were compared with the 104 group values.

For water, ϕ_A and ϕ_B have similar spectra and give doses which are about 15 per cent too low at a distance of 100 cm from the source, at which point the dose had decreased by a factor of about 10^6. It should be noted that this 15 per cent difference can be caused by a change of only 1 per cent in the total cross section of water. Flux ϕ_C gives condensed cross sections which evaluate the dose at x = 100 cm within 1 per cent, although the dose at x = 50 cm is 5 per cent too high. This accurate result is obtained because ϕ_C is an approximate average of the flux spectrum across the slab and hence leads to slab averaged values of the cross sections.

Similar results have been obtained for the iron slab, although in this case ϕ_C gives no better results than ϕ_A, both predicting the dose to within 8 per cent at x = 50 cm. In both the water and iron slabs, the flux spectra ϕ_A and ϕ_C differ considerably and so the insensitivity of the dose to the weighting spectrum used for group condensation indicates that the 29 group structure is fine enough to give accurate results as long as a reasonable flux spectrum is used for group condensation. As ϕ_A is most easily calculated, this is the flux suggested for group condensation.

Cross Section Data Sets for Shielding Calculations

(I. J. Donnelly and B. J. McGregor)

There are two prerequisites for a shielding calculation. First of all adequate neutron and gamma ray cross section data must be available; secondly a suitable particle transport computer code is needed. Throughout the world and particularly at Oak Ridge National Laboratory, considerable effort is being expended on the measurement and analysis of cross sections important for shielding, and on the generation of cross section data sets to be used with transport codes. This cross section data is available both as basic point cross sections on the ENDF/B data file and also in the form of multigroup cross section data sets which have been condensed from the ENDF/B data. We have obtained several of these data sets as well as a copy of AMPX, the modular code system developed by ORNL for the editing of ENDF/B data into a multigroup format. As the manpower necessary to obtain a full understanding of the AMPX system and make it operational at AAEC is prohibitive, we have decided to use the multigroup data sets which are continually being developed and disseminated by ORNL. This policy has the advantage that the data sets are used by many organisations, hence any shortcomings are rapidly discovered.

The AMPX system will probably only be used here if we wish to review some of the basic cross section averaging procedures.

The multigroup data sets typically have 100 neutron groups and up to 18 gamma ray groups. This group structure is fine enough to make the cross sections relatively independent of the flux spectrum which has been used in their evaluation. However, this number of groups is too large for convenience in many claculations and must be reduced. Several codes for achieving this have been obtained from ORNL and made operational at AAEC.

We have obtained the following data library sets and appropriate processing codes from the Radiation Shielding Information Center:

DLC-9	104 neutron-18 gamma P8 coupled library for 9 shielding elements present in concrete.	1969 data
DLC-2D	100 neutron ENDF/B version III data for 60 elements with P8 scattering.	1968 data
DLC-2B	Similar to DLC-2D but version I data.	1973 data
DLC-23	CASK 22 neutron-18 gamma coupled P3 data for 20 elements. Processed from VII and VIII data.	

At present an investigation is being made of the use of benchmark problems to test new data sets as they become available.

The European Shielding Information Service (ESIS) is organising benchmark experiments, publication and calculations which should be useful for checking codes and data sets. Experiment I is on neutron propagation in laminated iron-water shields, while Experiment II treats neutron propagation in iron.

4.4 REACTOR DATA (J. L. Cook, A. R. Musgrove, G. D. Trimble)

Fission Mass Yields

The mass yield curves for some 70 fissile nuclides have been studied on the basis of the three mode hypothesis and good agreement has been obtained for all processes except the spontaneous fission of ^{248}Cm which appears to require at least five modes. The energy dependence of the eight parameters required for the fit has been studied and systematic relationships between them and the energy above the fission barrier have been found. The weights assigned to each Gaussian mode, which are essentially partial cross sections,

appear to resonate. In particular, the most asymmetric mode seems to have a resonance at the position of the giant dipole resonance observed in photo-fission cross sections.

The systematics of the parameters in relation to the periodic table are also under investigation. As yet, the positions and widths of the Gaussian modes cannot be predicted reliably, but they appear to be related to the minima in the potential energy surface for highly distorted nuclei. The distribution of the peaks appears to be correlated strongly with the neutron number of the parent isotope, though as yet the significance of each value is not known.

The model works well for isotopes ranging from ^{210}Po to ^{258}Fm with the above noted exception and future studies will centre around the problem of predicting unmeasured yield curves with some degree of reliability, particularly the curves for ^{240}Pu, ^{241}Pu and ^{242}Pu, for which the data is scant.

Fission Product Cross Sections

Programs for calculating fission product cross sections based on a Monte Carlo method have been written. It is proposed that by a sampling technique, cross sections for some 80 nuclides for which only thermal cross sections and resonance integrals have been measured, will be determined. By further restricted random sampling, errors will be attached to each cross section point so that uncertainties in fission product worths can be determined. A library of these nuclides will be made available to overseas users in a standard ENDF/B format.

AUS Interactive Input and Output (J. Pollard, G. Trimble)

The commissioning of the Division's GT40-PDP-11/05 computer for remote job entry via an attached card reader has greatly facilitated normal job submission. In addition, the computer has interactive graphics capability which is to be developed for input and output to the AUS scheme. Presently, a FOCAL-VT system has been written as a means of trying out ideas using the mini-computer.

Calculation of Direct and Cumulative Fission Product Yields

(A. R. Musgrove)

Over the past year we have been interested in some of the problems associated with the calculation of fission product direct yields in some of the more common fissionable isotopes. Owing to lack of time, our review paper at Bologna ('Prediction of Unmeasured Fission Product Yields', Panel on Fission Product Nuclear Data, Bologna, November 1973), presented some rather hurried fits to experimental yields which nevertheless showed that a simple 'universal' prescription for calculation in various fission nuclei would not be adequate. The Gaussian fits to mass yield curves are now so well advanced that we turn once again to this complex problem. Here we set down some of the ideas which we are pursuing.

The first step is to calculate the most probably Z value for each post neutron emission mass A, $Z_p(A)$. This is conveniently (but not necessarily) referred back to the pre-neutron emission situation because this is necessarily symmetrical about $A_F/2$ where A_F = fissioning nucleus mass number:

$$Z_p(A) = \rho A' - \Delta Z(A)$$

where

$$A' = A + \nu(A)$$

and $\nu(A)$ is the average number of neutrons which were released when the beta decay chain of mass A was formed. This approach is at once less than satisfactory because ν will depend on N and Z particularly their evenness or oddness.

$\rho = Z_F/A_F$ and corresponds to a knife cut of the fissioning nucleus and $\Delta Z(A)$ is the all important correction which is negative for heavy mass chains and roughly 0.5 charge units.

Looking at experimental plots of $Z_p(A)$ we can differentiate at least 3 regions. The first around $A_F/2$ where ΔZ is roughly zero up to mass A_1. A second region for $A > A_2$ (heavy mass) can be roughly described by a straight line with $\Delta Z \simeq 0.5$ charge units and a transition region typically occurring near Z = 50 (or N = 82) between A_1 and A_2.

We are attempting such a schematic fit to the $Z_p(A)$ function with a tri-linear shape in which the object is to obtain A_1, A_2 and the slope and intercept of the line for $A > A_2$.

We have re-evaluated our recommended $\nu(A)$ values for ^{235}U only at present using Terrell's method* and the new Meek and Rider** yield compilation and evaluation. The new values are slightly changed from the ones we presented at Bologna.

In the next stage we define a fractional independent 'normal' yield by

$$FINY(Z,A) = \int_{Z-\frac{1}{2}}^{Z+\frac{1}{2}} P(Z)dZ$$

$$P(Z) = \frac{1}{\sqrt{2\pi\sigma^2}} \exp\left(-(Z-Z_p)^2/2\sigma^2\right)$$

where σ is <u>assumed</u> constant for all A.

The calculated fractional independent yield is then defined as

$$FIY(Z,A) = \left(1 + C(Z) + D(N)\right)FINY(Z,A)$$

where C(Z) is positive for Z even and negative for Z odd and at present <u>assumed</u> constant in magnitude. D(N) we hope will be zero for post neutron emission products due to a washing out of primary even N-odd N effects, however it looks certain that at least D(82) and possibly also D(50) will be required due to smaller $\nu(A)$ near these mass numbers and also due to secondary buildup, as neutron emission probably prefers to end at these magic numbers.

As hinted in the Bologna paper, the fine structure in the mass yield curve is intimately linked with the underlying odd-even fluctuations in FIY(Z,A). This is now demonstrated quite dramatically in our Gaussian fits to the mass yield curves. Of course, the fitting procedure in that case does not know about fine structure and the fits to ^{235}U + n at thermal, fission neutron and 14 MeV energies are shown in figures 4.1 to 4. . In the lower section of each figure the ratio of experimental cumulative yield to the calculated one is shown. The vertical lines give rough guides to the position of even Z fragments in the <u>primary</u> mass distribution and also N = 50 and 82.

---

*Terrell, J. (1962) - Phys. Rev. 127, 880.

**Meek, M. and Rider, B. F. (1974) - NEDO-12154-1

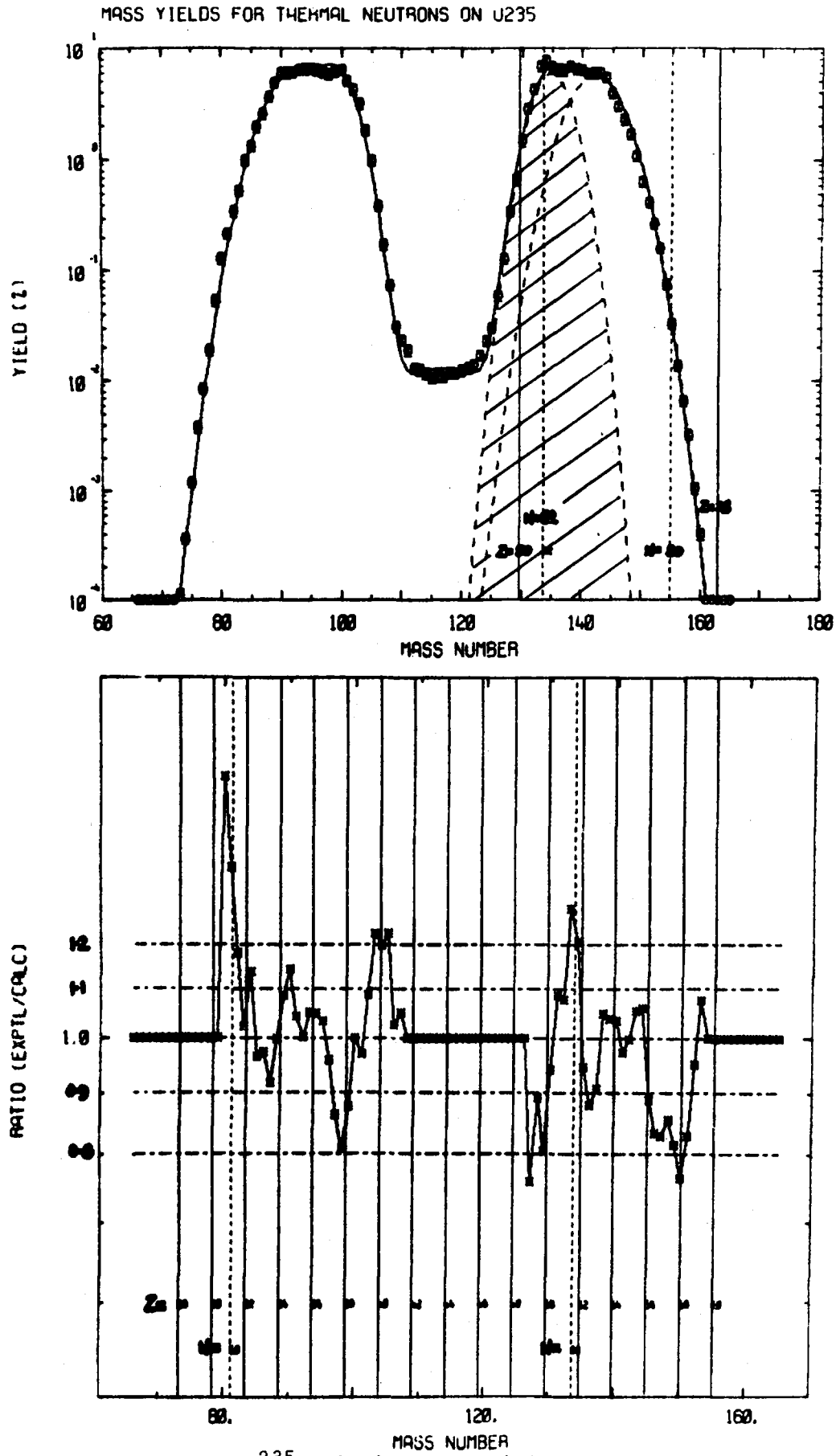

FIGURE 4.1 ^{235}U fission mass yields: thermal neutrons

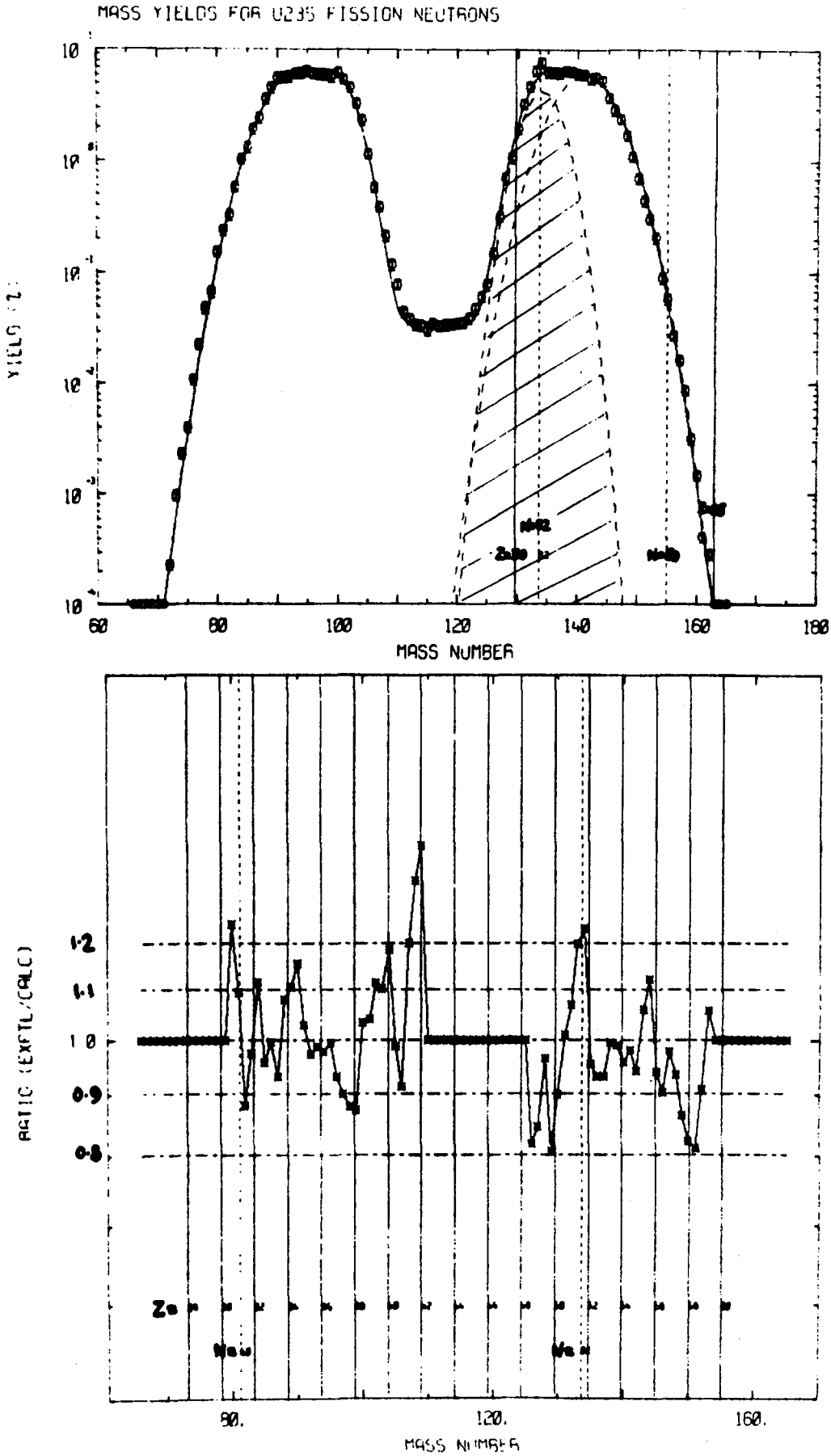

FIGURE 4.2 ^{235}U fission mass yields: fission neutrons

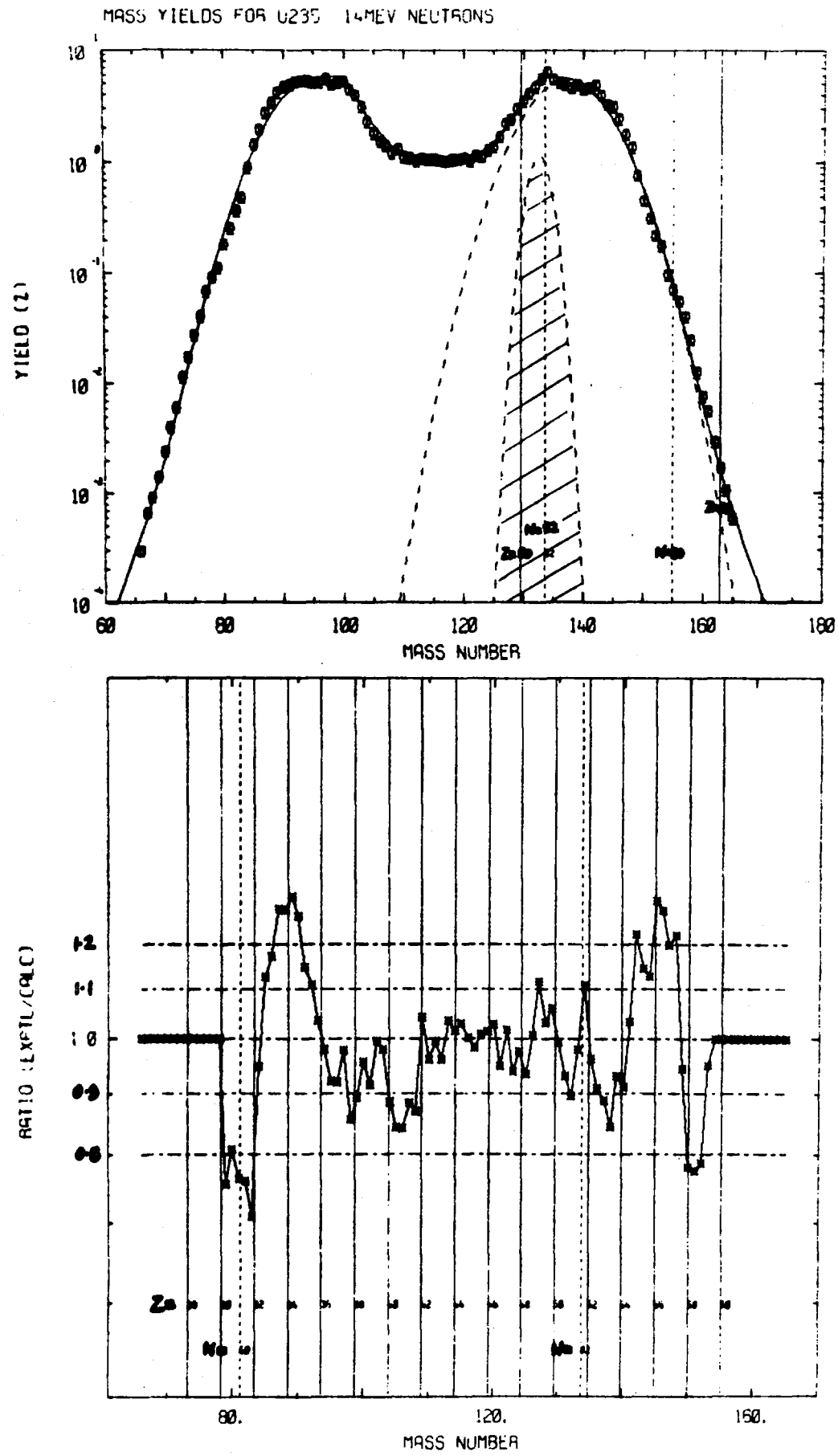

FIGURE 4.3 ^{235}U fission mass yields; 14 MeV neutrons

The fractional cumulative yield at mass A is given by

$$FCY(A) = \sum_{Z} FIY(Z,A)$$

and we can see that in general, this will not sum to 1. If we assume that the Gaussian fits give some approximation to a defined cumulative 'normal' yield then we can also fit the ratio experiment/calculation from these plots to C(Z) and D(N) as well as all the fractional independent and cumulative yield data.

It is perhaps evident from the figures that C(Z) and D(N) will decrease (as expected) with increasing neutron energy and we feel that this is also manifested in the different values of C(Z) which we presented at Bologna.

Investigation of Surface Impurities (D. W. Lang)

Zirconium metal is usually associated with an oxygen surface impurity. Fluorine used to etch the surface penetrates the oxygen but does not diffuse appreciably into the metal. The reaction $^{19}F(p,\alpha,\gamma)^{16}O$ has a resonance for (centre of mass) energy 0.875 MeV. A fluoride layer on an exposed surface thus interacts with a beam of 0.921 MeV protons, as can be detected by the resulting gammas. The same energy protons can interact deeper in the layer, but the proton beam must be produced at a higher energy to compensate for the energy lost in reaching the given depth.

Using the known cross section for the reaction as a function of energy and given the fluorine concentration at various depths, it would be possible to predict a yield curve to be obtained by varying the energy of a proton beam. Given the series of points from the yield curve and the associated errors, it is possible to reverse the prediction process and obtain the fluoride density at various depths in the oxygen. A program has been produced and shown to be effective for this purpose. The technique used involves finding as smooth a concentration profile as can be consistent with the data.

Pulsed Time of Flight Spectra

A program described earlier (AAEC/PR39-P), section 4.5) gave excellent results in unfolding time of flight spectra associated with beam pulses of considerable duration (pulse within order of magnitude of its maximum for 10 or more timing channels). When applied to pulses of lesser duration, problems developed in fitting the data with an acceptable value of chi square. The problem appears to be associated with considerable variation in the beam profile over one timing channel.

To minimise the difficulty it was decided to allow the computer to calculate as if three times as many channels had been used. Each channel of the beam profile was split into three and the computer was permitted to share the available beam between the three with the single provision that each share should be positive. The neutron spectrum was similarly free, but for output the neutron spectrum channels were grouped into the corresponding trio and only the totals were taken. The fit to the data was improved, but the value of chi square was still beyond the bounds set for simpler statistical error. More encouragingly, the neutron spectrum output (groups of three channels) stopped varying noticeably in a very few iterations. The present program assumes that the proton beam of the accelerator has the same energy profile at all points of its time profile. Further changes in the program should wait on a measurement to verify this assumption.

Resolution Matrices obtained by Measurement

It is desirable to be able to unfold data even when the resolution functions involved, as well as the data to be unfolded, must be obtained by experiment. Response functions of scintillation counters for beams of mono-energetic neutrons are being used as a test case. A program is being constructed to take advantage of such measurements. Given values of the response function at a network of points, it is possible to interpolate and obtain the response function at any other convenient set of points and hence the resolution matrix required for a given set of measurements. It is being assumed, in writing the programs involved, that the response functions are smoothly varying. A program has therefore been written to smooth the measured response functions in a manner consistent with their statistical errors.

5. RUM JUNGLE ENVIRONMENTAL STUDIES (B. Clancy, W. Bertram, I. Ritchie)

With large strip mining operations in semi-tropical areas it is possible that local pollution can be caused by heavy metals leached out of the overburden heaps following heavy rainfalls. A mechanism postulated is the bacterial oxidation of natural sulphide ores in the presence of water and oxygen. It is certain that adequate assessment of proposed anti-pollution measures can only be made if it is known where within the heaps such oxidation will occur and how quickly the polluting metal can migrate out of the heaps. It thus becomes necessary to know with some confidence the distribution of water and oxygen within the heaps during the course of a season.

Investigations of the flow of polluted water from the overburden heaps can be separated into two parts:

(i) the flow of water in the heaps,

(ii) the interaction of bacteria, ore and water.

The basic physics of water flow through homogeneous porous beds is understood and the fundamental problem (in a mathematical sense) is to solve a Laplace equation with imposed boundary conditions.

Equations have been set up which describe the position of the water table and the water movement in the heaps, which are assumed to take the form of truncated pyramids. Some trial calculations, using the AAEC neutron diffusion code POW, have shown that computation of solutions to realistic problems is feasible and a special purpose computer program is being developed to perform water flow calculations in homogeneous heaps. The basic numerics and solution strategy of the program were tested against a simple experiment and found to be good.

Extension of the program to the cylindrical geometry of the heap model is well advanced and there is confidence that water table movement in the heaps can be predicted. There is also confidence that the code will predict the movementof water layers due to rainfall through the top layers of the heap. Prediction of this water layer movement and the movement of the water table should allow estimates to be made of the rate at which air is pumped into the heaps during the wet season.

Analysis of the 1969-70 data on run-off and spring water from the heap indicates that within an order of magnitude the metal ion concentrations do

not vary over different parts of the heap or over different times in the wet season. This means that seasonally averaged figures for the central run-off metal ion concentrations, for which a number of measurements exist, provide a reasonable basis on which to estimate total amounts of metal (e.g. Cu, Mn) produced, metal ion consumed and oxygen used in a season. These estimates have allowed the following conclusions to be drawn.

1. Sufficient oxygen cannot be supplied dissolved in rain water, as the oxygen solubility in water is about three orders of magnitude lower than the oxygen concentrations required. For the same reason, little of the oxidation process is likely to take place below the water table.

2. If the oxidation is assumed to take place in the stack as a whole, then the air in the pore spaces must be turned over about 2 to 4 times a season in order to supply enough oxygen to explain the metal ion concentrations in the run-off. The metal ion content would be decreased by a negligible amount.

3. If the oxidation is assumed to take place in the top 30 cm or so of the heap, then this volume must be turned over approximately 100 to 200 times a season in order to supply the required oxygen. The ion content of this top layer would be exhausted in approximately 8 to 10 years.

4. If the oxidation were confined to a thin layer which is assumed to be exhausted of metal ion each season, then the layer would have to be only 2 to 3 cm thick.

These points allow the following tentative conclusions to be drawn about where in the heap the oxidation may take place.

(a) The oxidation process could take place in the entire volume of the stack provided pumping mechanisms exist to change the air in the stack two to three times a season.

(b) The oxidation could be confined to a thin surface layer provided a mechanism exists for exposing a new surface every season.

(c) The oxidation process could be a combination of (a) and (b).

(d) The oxidation is unlikely to be confined to a volume ~30 cm in from the top surface as a reduction in metal ion content and hence metal ion concentration in the run-off would be noticeable in a comparatively short period (~3 to 4 years).

6.1 PUBLICATIONS

Papers

Bertram, W. K. and Cook, J. L. (1974) - The role of unitarity in resonance theory. Aust. J. Phys. 28, 1. (in press)

Bird, J. R., Campbell, B. L. and Price, P. B. (1974) - Prompt nuclear analysis. Atomic Energy Review, Vol. 12, No. 2.

Rose, E. K., Cook, J. L. and Bertram, W. K. (1974) - Statistics for Adler-Adler resonance parameters. Aust. J. Phys. 27, 1.

Reports

Bertram, W. K., Clancy, B. E., Cook, J. L. and Rose, E. K. (1974) - The statistical distribution functions for products of variables with a Gaussian distribution with zero mean. AAEC/E313.

Cook, J. L. (1974) - A statistical model for compound nucleus formation. AAEC/E315.

McGregor, B. J. and Mynatt, F. R. (1973) - Effects of air-density perturbations on the transport of gamma rays produced by point gamma ray sources. ORNL-TM-4266.

Musgrove, A. R. de L. (1974) - Investigation of the energetics of binary and ternary fission in ^{252}Cf and ^{236}U. AAEC/E304.

Rose, E. K. and Cook, J. L. (1974) - The statistical distribution function for product ratios. AAEC/E316.

Ritchie, A. I. M., Rainbow, M. T. and Moo, S. P. (1974) - Time dependent ^{237}Np, ^{235}U and ^{239}Pu fission rates in a thorium assembly during the interval 0-200 ns using a pulsed $^{9}Be(d,n)$ source. Part II: Theory. AAEC/E295.

Conference Papers

National Soviet Conference on Neutron Physics, Kiev, May 28-June 2, 1973:

Allen, B. J., Kenny, M. J., Bray, K. H., Barrett, R., Carlson, L. E. - Neutron capture by ^{56}Fe for neutron energies to 460 keV.

Allen, B. J., Mcsgrove, A. R. de L., Chan, D. M. A., Macklin, R. L. - Neutron capture cross sections of the Ca and Ba isotopes.

Boldeman, J. W. - Prompt neutron yield from the spontaneous fission of ^{252}Cf.

Boldeman, J. W. - Recent relative $\bar{\nu}_p$ measurements.

Conference Papers (cont'd)

Boldeman, J. W. and Walsh, R. L. - Energy dependence of the average total fission fragment kinetic energy in the neutron fission of ^{233}U.

2nd International Symposium on Neutron Capture Gamma Ray Spectroscopy and Related Topics, Sept. 2-6, 1974, Petten:

Allen, B. J. - Fast neutron capture gamma ray spectra in Fe.

Bird, J. R. and Hille, F. - Single particle states in neutron capture.

Bird, J. R., Russell, L. H. and Bubb, I. F. - Isotopic analysis facility using neutron capture.

Pe, Hla - Energy dependence of partial p-wave capture cross sections.

Hogg, G. R. and Tendys, J. - X-ray spectral measurements of the dense plasma focus. Aust. Inst. of Physics National Congress, Adelaide, May 1974.

Turner, W. J. and Trimble, G. D. - Simulation of transient two-phase compressible flow. SIMSIG Conf., AINSE, Lucas Heights, May 13, 1974.

DISTRIBUTION LIST

AAEC/PR40-P

1.	Chairman	
2.	Deputy Chairman	
3.	Commissioner (Sir Lenox Hewitt)	
4.	Commissioner (K. F. Alder)	
5.	Program Manager, Nuclear Science and Applications	
6.	Program Manager, Power and Energy	
7.	Program Manager, Uranium Fuel Cycle	
8.	Site Manager	
9.	Chief, Materials Division	
10.	Chief, Physics Division	
11.	Chief, Engineering Research Division	
12.	Chief, Chemical Technology Division	
13.	Chief, Instrumentation and Control Division	
14.	Chief, Environmental and Public Health Division	
15.	Chief, Isotope Division	
16.	Head, Applied Mathematics and Computing Section	
17.	Head, Mechanical Development Section	
18.	Head, Regulatory and External Relations Branch	
19.	Secretary	
20.	Assistant Secretary	Head Office
21.	Director, Information Services	
22.	Library	
23.	Director, Nuclear Plant Safety Unit, Mascot	
24.	Head, Nuclear Studies Group	
25.	Mascot Library	
26.	Professor Sir Sidney Sunderland, Dean, Faculty of Medicine, University of Melbourne	Safety Review Committee
27.	Dr. C. J. Cummins, Director, NSW Department of Health	
28.	Mr. D. J. Stevens, Director ARL	
29.	Controller, Site Information Services	
30.	Controller, Site Administration	
31.	Controller, Site Operations	
32.	Controller, Engineering Services	
33.	Controller, Site Planning	
34.	Manager, Commercial Applications	
35.	Nuclear Materials Officer	
36.	ASNT	
37.	Executive Officer, AINSE	
38.		
39.	RE Library	
40.		
41.	Washington Office	
42.		
43.	London Office	
44.	Vienna Office	
45.	Tokyo Office	
46.	Head, Experimental Reactor Physics Section	
47.	Head, Neutron Physics Section	
48.	Head, Theoretical Physics Section	

DISTRIBUTION LIST (cont'd)

49. Head, Reactor Performance Section
50. Head, Engineering Physics Section
51. Head, Chemical Physics Section
52. Head, Applied Physics Section
53. Head, Health Physics Research Section
54. Head, Radioisotope Services Branch
55. Head, Pharmaceutical & Chemical Products Section
56. Head, Irradiation Research Section
57. Head, Reactor Operations Section
58-98. W. Gemmell for INDC and Bilateral Agreement correspondents
99. B. Allen
100. J. Boldeman
101. J. Connolly
102. J. Cook
103. P. Duerden
104. G. Durance
105. J. Harries
106. G. Hogg
107. M. Kenny
108. D. Lang
109. B. McGregor
110. A. Musgrove
111. J. Pollard
112. M. Rainbow
113. I. Ritchie
114. J. Tendys
115. W. Turner
116-146. J. R. Bird (for special distribution)
147. D. Byers (University of Canterbury, N.Z.)
148. V. Deniz (BARC, India)
149. S. Kapoor (BARC, India)
150-170. Bilateral Agreements (UKAEA 5, USAEC 11, AECL 5) via H.O.
171-180. Spares